PHENOTYPIC SPECTRUM: CHARACTERIZING THE ROOT DIVERSITY IN COMMON BEAN

by

LIMENG XIE

(Under the Direction of Alexander Bucksch)

ABSTRACT

Plant roots display a wide range of architectural types, each with unique spatial arrangement and shape characteristics. Traditional theoretical models don't fully capture this root architectural variation, often attributing it to genetic (G) and environmental (E) variation or the G by E interaction. Addressing this, we developed Dirt-Pop, a computational pipeline, designed to cluster the root architectural variations of a single genotype into multiple root architecture types. This pipeline employs the DS-curve as a shape descriptor, integrates the K-means++ clustering algorithm, an outlier removal strategy, and the Fréchet similarity metric. Applying this pipeline, three common bean (*Phaseolus vulgaris* L.) genotypes (DOR364, L8857 and SEQ7) exhibited five distinct root architecture types, with their composition varying under different water conditions. Validating DOR364 and SEQ7 in a mesocosm system, where water distribution was monitored by soil moisture sensors, both genotypes repeatedly displayed these five root architecture types. Moreover, the composition of SEQ7's five root architecture types changed across developmental stages and water conditions. By linking these root architecture types to published simulation models, each root architecture type observed can be assumed with a specific function in water and nutrients (Phosphorus and Nitrogen) uptake. We further

investigated how root architecture types and biomass allocation impact fitness outcome in both monoculture and mixture of SEQ7 and DOR364 under water-limited (WL) and non-limiting conditions to explore plant-plant interactions through the lens of resource partitioning and kin selection theories. The study reveals that mixtures of these two genotypes exhibited greater population fitness than monocultures. SEQ7 showed a significant increase in population fitness in mixtures, attributed to its tendency to maintain or reduce root biomass allocation, especially under WL conditions, and a strategic shift towards more deep root architecture types, enhancing water acquisition. In contrast, DOR364 increased root allocation for belowground resources acquisition in mixtures, but this did not confer a fitness benefit. These results underline the complexity of plant interactions, showing that neither kin selection nor niche partitioning theories fully explain the observed trait expression and fitness outcome.

INDEX WORDS: Phaseolus vulgaris L., root architecture, phenotypic spectrum, drought

PHENOTYPIC SPECTRUM: CHARACTERIZING THE ROOT ARCHITECTURE DIVERSITY IN COMMON BEAN

by

LIMENG XIE

BS, China Agricultural University, P. R. China, 2014

MS, Texas A&M University, USA, 2016

A Dissertation Submitted to the Graduate Faculty of The University of Georgia in Partial

Fulfillment of the Requirements for the Degree

DOCTOR OF PHILOSOPHY

ATHENS, GEORGIA

2024

© 2024

Limeng Xie

All Rights Reserved

PHENOTYPIC SPECTRUM: CHARACTERIZING THE ROOT DIVERSITY IN COMMON BEAN

by

LIMENG XIE

Major Professor: Alexander Bucksch Committee: Jim Leebens-Mack

Jim Leebens-Mack Megan DeMarche Maria Monteros

Electronic Version Approved:

Ron Walcott Vice Provost for Graduate Education and Dean of the Graduate School The University of Georgia May 2024

DEDICATION

I dedicate this dissertation to my beloved parents, Yuxia Ji and Xueru Xie, for enduring the continuous 1783 days and nights of my absence.

ACKNOWLEDGEMENTS

First, I want to thank Dr. Alexander Bucksch for his oversight, guidance and support of my Ph.D. research. His mentorship has been important in navigating the challenges of this academic journey, shaping my professional and personal growth.

I am grateful to my committee members, Dr. Jim Leebens-Mack, Dr. Megan Demarche and Dr. Maria Monteros, for their constructive feedback and unwavering support throughout this journey. A sincere thank you to Dr. Maria Monteros who showed me a great example of women leader in ag industry during the summer of 2022.

A big shout out to Dr. Shumei Chang, Dr. Wolfgang Lukowitz and Dr. John Burke, for their multifaceted support, especially during my time alone at UGA. Your kindness and assistance have been invaluable.

I would also like to thank our all the lab members in computational plant science lab for their friendship and help. Special thanks go to Peter Pietrzyk for helping build the mesocosm system, Wes Bonelli for keeping DIRT running on Cyverse and creating DIRT-2D and DIRT-Pop Docker containers for using locally. Thank you Jitrana Kengana and Sydney Page for helping root harvest and data collection. Thank you Suxing Liu for the friendship outside of the lab. Besides, I would like to thank Changyeon Kim for installing the soil moisture sensors in the mesocosm system. To Mike Boyd and Greg Cousins, thank you both of you for helping with all the greenhouse stuff and trying to keep my plants pest free.

I would like to express the appreciation for my writing buddies, Youngjee Ko and Ariel Hart, for our weekly writing gatherings at UGA and my remote writing buddies Hua Xin and

Joyce Wang for their company when I was writing this dissertation. A special thank you to Dr. Judy Milton for coordinating writing sessions and the emerging leader program for graduate students (and those delicious snacks and coffee!). Thank you, Aarum Youn-Heil, the UGA presentation practicum trainer, for her patience in helping me practice my presentation before every big conference.

I'm lucky to have my friends, Rachel Xu, Yalian Pei, Longwen Xu, Dianyi Liu, and Siwen Deng, during this journey. Your companionship, understanding, and constant encouragement were a beacon of hope during every tough moment when I almost quit. A heartfelt thanks to my friend Li Wang and her lovely son, Dylan, who provided comforting light during the dark period after my miscarriage. There are so many wonderful people I've encountered when I was at UGA whom I haven't named here, but please know that your kindness and encouragement have meant the world to me.

To my husband, Huang Chen: Your support has been my anchor throughout this Ph.D. I cannot thank you enough for your help with the data collection in early mornings and late nights for my experiment during the summer of 2023. Thank you for your financial support for the last two semesters to alleviate my burdens. By taking on most of our family obligations, you gave me the peace of mind needed to dedicate myself to writing this dissertation. Thank you for being the safety net beneath my every leap in this endeavor. I hope to be as strong a safety net for you as you have been for me.

To my beloved parents: Being thousands of miles far away from you for almost 6 years has been one of the toughest parts. Every challenge I faced, your words and love got me back on track. I can't wait to be back home to hug you both after such a long time.

To everyone who has been a part of this Ph.D. journey: each of you has played an irreplaceable role in bringing this to fruition. This experience has profoundly taught me the importance of self-care, both physically and mentally, as well as the value of having a supporting system and not be afraid to reach out for help. It has also instilled in me the courage to keep going on. I am committed to extending the kindness and support I've received from you to others for the rest of my life.

This dissertation research is funded by NSF CAREER grant 1845760 "The phenotypic spectrum: Quantifying new patterns of architecture variation in crop roots" to Dr. Alexander Bucksch, UGA Plant Biology Department and the UGA Graduate School. Credit is also due to ChatGPT for assistance with grammar and language checking only. However, it is important to note that no original content was generated by ChatGPT or any other AI-based tools. These tools did not produce any data, texts, literature reviews, or background sections, either with or without references in this dissertation.

TABLE OF CONTENTS

	Page
ACKNOWLEDGEMENTS	V
LIST OF TABLES	xi
LIST OF FIGURES	xiii
CHAPTER 1	1
INTRODUCTION	1
Root Architecture	1
Measurement of Root Architecture	2
Sampling Strategy and Framework for Study the Root Architecture Variation Across	
Environment	3
Sources of Root Architectural Variation of One Genotype	4
Two Theories Help Understand Population Fitness Outcome of Plant Interaction	5
The Necessity to Develop Controlled Growth Systems to Mimic Field Conditions	7
Overview of the Dissertation	7
Reference	9
CHAPTER 2	16
DEVELOPING A COMPUTATIONAL PIPELINE TO QUANTIFY ROOT ARCHITEC	TURE
DIVERSITY IN SINGLE GENOTYPES	16

Introduction	16
Materials and Methods	18
Results	23
Acknowledgements	30
References	30
Figures	37
CHAPTER 3	51
FROM OUTDOOR TO INDOOR FIELD: THE ROOT ARCHITECTURE TYPES	AND THEIR
CHANGE OVER THE DEVELOPMENTAL STAGES IN COMMON BEAN	51
Introduction	51
Materials and Methods	55
Results	60
Discussion	63
Acknowledgements	69
References	70
Figures	74
Appendix B	84
CHAPTER 4	96
EVALUATION OF POPULATION FITNESS OF COMMON BEAN MONOCULT	URE AND
MIXTURE	96

Introduction	96
Materials and Methods	98
Results	100
Discussion	101
Acknowledgements	102
Reference	106
Figures	110
Appendix C	118
CHAPTER 5	
SUMMARY	121
Reference	126
Figures	128

LIST OF TABLES

Page
Table S2.1: Sample size of common bean genotypes DOR364, L8857 and SEQ7 grown under non-
limiting (NL) and water-limited (WL) condition in the 2015 and 2016 field experiment at Willcox,
AZ47
Table S2.2: The value of mean curve of each root architecture types among three genotypes
DOR364, L8857, and SEQ7
Table S2.3: The summary statistics of aboveground shoot biomass among root architecture types
of three common bean genotypes between conditions in 2016
Table S2.4 The summary statistics of aboveground shoot biomass among three common bean
genotypes between conditions in 2016. 50
Table S3.1: Sample sizes across different root architecture types of SEQ7 during various growth
stages and DOR364 at mature stage under each water condition.
Table S3.2: The mean DS curve of SEQ7 is listed across growth stages and conditions 90
Table S3.3: The value of mean DS curve of DOR364 is listed under non-limiting (NL) and water-
limited (WL) conditions
Table S3.4: Chi-square test of homogeneity for comparing compositions of root architecture types
between growth stages and conditions.
Table S3.5: The summary statistics for shoot biomass, root biomass and shoot/root ratio of SEQ7
over growth stages and conditions. 93

Table S3.6: Geometric mean values of D1 and D2 for each alignment of the mean DS	curve at 42
DAS for observed root architecture types and simulated root architecture models	94
Table S4.1 Sample sizes across different root architecture types of DOR364 and S	EQ7 under
various planting scenarios and conditions.	119
Table S4.2 Summary statistics of seed number per plant and root-shoot ratio of DOR364	and SEQ7
over planting scenarios and conditions.	120

LIST OF FIGURES

Page
Figure 2.1: Clear architectural differences were observed among the excavated roots of
neighboring DOR364 plants of DOR364 from a plot in 2016 (Willcox, AZ)
Figure 2.2: The Dirt-Pop pipeline computes the root architecture types of a single genotype 38
Figure 2.3: Five root architecture types of DOR364 (n=822), L8857 (n=1663), and SEQ7
(n=845) were observed across years (2015 and 2016) under non-limiting (NL) and water-limited
(WL) conditions. 39
Figure 2.4: The heatmap of Fréchet distance matrix among mean curve of each root architecture
type of three genotypes DOR364, L8857 and SEQ7
Figure 2.5: The composition of root architecture types in DOR364 (n=797), L8857 (n=1772),
and SEQ7 (n=768) under non-limiting (NL) and water-limited (WL) conditions in 2015 and
2016
Figure 2.6: Aboveground shoot biomass of root architecture types in three genotypes DOR364
(n=401), L8857 (n=578), SEQ7 (n=490) under non-limiting (NL) and water-limited (WL)
conditions in 2016
Figure 3.1: Five root architecture types of SEQ7 were observed across developmental stages and
conditions
Figure 3.2: The heatmap of Fréchet distance matrix confirmed that while AT1 through AT5 were
distinct, each showed consistent internal similarity across varying growth stages and conditions.
76

Figure 3.3: Five root architecture types of DOR364 were observed at mature stage (R8-R9, 84
days of sowing) under nonlimiting (NL, $n=143$) and water-limited (WL, $n=118$) conditions 77
Figure 3.4 The heatmap of Fréchet distance matrix showed that five root architecture types were
similar between SEQ7 and DOR364 at mature stages (R8-R9)
Figure 3.5: The composition of root architecture types of SEQ7 changed over growth stages and
conditions 79
Figure 3.6: Shoot biomass, root biomass and root-shoot ratio were mostly not correlated with
root architecture types (AT) but with growth stages
Figure 3.7: The closest matched simulated root architecture model with root architecture types
observed at 42 days of sowing (DAS).
Figure 4.1: Seed number per plant of mixture of DOR364 and SEQ7 were higher than
monoculture of DOR364 and SEQ7. 110
Figure 4.2: Seed number per plant of DOR364 (A) and SEQ7 (B) were different between mixture
and monoculture planting scenarios under between non-limiting (NL) and water-limited (WL)
conditions
Figure 4.3: Comparison of root-shoot ratio of DOR364 (A) and SEQ7 (B) between mixture and
monoculture planting scenarios under non-limiting (NL) and water-limited (WL) conditions.112
Figure 4.4: Five root architecture types of SEQ7 and DOR364 were observed across planting
scenarios (monoculture and mixture)
Figure 4.5: The heatmap of Fréchet distance matrix confirmed that while AT1 through AT5 were
distinct, each showed consistent internal similarity across both monoculture and mixture for
DOR364 (panel A) and SEO7 (panel B)

Figure 4.6: The composition of root architecture types of DOR364 (panel A) and SEQ7 (panel B)
between planting scenarios (Mix: mixture and Mono: monoculture) and conditions (WL: Water-
limited and NL: Non-limiting)
Figure 4.7: Percentage change in root architecture categories for SEQ7 and DOR364 when
comparing mixtures to monocultures
Figure 5.1: The comparison of phenotypic plasticity framework and phenotypic spectrum
framework. 128
Figure 5.2: Radar plots illustrating the different patterns of both macronutrients and
micronutrients in seeds among root architecture types of SEQ7 under water-limited (WL) and
non-limiting (NL) conditions. 129
Figure 5.3: Boxplot of both macronutrients and micronutrients in seeds among root architecture
types (ATs) of SEQ7 under water-limited (WL) and non-limiting (NL) conditions
Figure S2.1: The weather information of Willcox, AZ. The dash line is for 2016, and the solid line
is for 2015
Figure S2.2: Illustration of magnitude and shape outliers in an example cluster
Figure S2.3: The mean DS-curves of five root architecture types of three genotypes DOR364,
L8857 and SEQ7 under non-limiting and water-limited condition in 2015 and 2016 45
Figure S2.4: Shoot biomass of three genotypes DOR364 (n=401), L8857(n=578), SEQ7 (n=490)
under non-limiting (NL) and water-limited (WL) conditions in 2016
Figure S3.1: Top view schematic of the mesocosm system.
Figure S3.2: The time-series experiment of SEQ7 in the mesocosm system. 85
Figure S3.3: The daily mean volumetric water content (vwc) across all growth stages and
conditions86

Figure S3.4: The five root architecture types of SEQ7 (Panel A) and DOR364 (Panel B) are	
presented from both field and mesocosm settings.	87
Figure S3.5: DS curves derived from 12 simulated root architecture models.	88
Figure S4.1: The daily mean volumetric water content (vwc) across planting scenarios	118

CHAPTER 1

INTRODUCTION

Root Architecture

Plant growth is fundamentally limited by the availability of resources, including water and nutrients. The root system plays a critical role in capturing these soil resources. To improve plant resilience, yield and efficiency, considerable effort has been invested to study the plant root system and to explain how they acquire resources from soil^{1,2}. One important aspect that determines the plant productivity is the root architecture. Since the nutrients are distributed at different levels in the soil, for example, leached nitrate in the subsoil and phosphorus in the topsoil, not to mention other nutrients highly heterogeneous spatial distributions³. As root architecture is the spatial arrangement of the root system³, it determines how effectively a plant exploit the soil resources. In general, root architecture includes two main components: geometric properties, such as length, angle, and distribution of a root system, and topological structure, which characterizes how individual root segments connect and organize within a root system⁴⁻⁶. Root architecture is a complex biological structure that can be quantified by various combinations of specific root traits. For example, the root architecture of a common bean (*Phaseolus vulgaris* L.) plant is the summation of the number, angle, elongation and branch pattern of adventitious, basal, tap root and lateral roots and other axial roots that develop from these three main root classes⁷.

Measurement of Root Architecture

Despite the importance of root architecture, it poses a considerable challenge to study. One obstacle is that roots are hidden belowground, making them difficult to measure directly. To address this, researchers have developed various root phenotyping platforms. Techniques such as magnetic resonance imaging (MRI)⁸ and X-ray⁹ computed tomography have been employed for non-destructive phenotyping of root systems in laboratory settings. More recently, low field magnetic resonance imaging (LF-MRI) has been implemented for non-destructively phenotyping root systems under field soil conditions^{10,11}. Although these platforms have the potential to provide more accurate representations of root architecture without causing the damage of the root system, their high costs and low throughput make them impractical for largescale studies, particularly in field conditions. Another challenge is the complexity of root architecture, which displays vast variations both within and among genotypes, and even within a single root system, making it hard to quantify¹². Early efforts to measure root architecture manually concentrated on simple parameters like root length and depth^{13,14}. This not only oversimplified the complex nature of root architecture but was also labor-intensive. The commercial software, WinRhizo, (Regent Instrument Inc., Ville de Québec, QC Canada) has facilitated the analysis by measuring traits like root surface area, average diameter, and some topological traits. However, its application is restricted to younger roots due to the constraints of paired scanner size^{15–17}.

To address these limitations, Shovelomics protocols have been developed, specifically to measure the root architecture for mature maize and legume plants in the field^{7,18}. This method involves excavating roots at the shovel-length radius and depth around the hypocotyl^{7,18}. After

soil removal, the roots are positioned on a phenotyping board where dominant root angles are determined using a protractor^{7,18}. Shovelomics focuses on phenotyping excavated root crowns, which represent the top portion of the root system. It is an efficient method for measuring the root architecture of mature roots in the field^{18,19}. Bucksch et al. (2014)²⁰ further enhanced Shovelomics by introducing an automated image-processing algorithm, increasing both the speed of analysis and the number of root architecture traits measured. Accompanied with automatic digital image root imaging (DIRT) platform, researchers can obtain 79 topological and geometric root traits, respectively^{20,21}. Bucksch et al. (2014) firstly introduced the shape descriptor DS values that describe the rate of root width accumulation over rooting depth²⁰. The curve connecting DS values over the 10%-90% depth range serves as an effective way to characterize the overall shape of root architecture. Thus, Shovelomics with DIRT computational platform is a powerful tool for detailed phenotyping of hundreds of mature roots of a single genotype and capturing architectural variations within individuals and populations.

Sampling Strategy and Framework to Study the Root Architecture Variation Across Environment

Current sampling strategies in plant phenotyping research primarily focus on capturing variation between genotypes, often operating under the assumption that a single genotype, in a given environment, exhibits a homogenous phenotype. As a result, researchers tend to seek an "average" phenotype representation for each genotype in that environment. Taking root studies for instance, researchers typically sample a small number of plant roots (usually range from 5 to 20) and measure compound or local root traits, such as root area, maximum width or depth^{15–17}. Such sampling strategy and measurement not only overlooks a substantial architectural variation

per genotype and but also ignores the whole root architectural organization. Moreover, when studying the root architecture of individual genotypes at a population scale across varied environments, the phenotypic plasticity framework is often employed^{12,22,23}. This framework primarily uses a reaction norm to analyze how the average trait changes in response to different environments. However, the reaction norm is not sufficient for analyzing how the hierarchical organization of the whole root system changes in response to these environmental changes. To bridge this knowledge gap, there's a need to increase the sample size and to a new framework that captures the architectural variations of roots within populations across different environments.

Sources of Root Architectural Variation of One Genotype

Accessing and interpreting root architectural variation is challenging, as roots grow in complex soil environments involving spatial and temporal dynamics of soil resources and interactions with neighboring plants and soil microorganisms²⁴. Root architectural variations in roots can be broadly attributed to the environmental variation, the genetic variation, and the interactions between these two.

Numerous studies have shown that environmental stress can significantly alter the root architecture of a single genotype²⁵. This variation in root architecture, induced by environmental change, is primarily associated with genotype-environment interactions, which are considered a major source of observed variation in root architecture. For example, common beans tend to develop shallower basal roots in phosphorous-limited environments, whereas they grow deeper roots in water-limited environments^{7,26,27}. Similarly, maize changes the root top angle and root

crown number based on the availability of nitrogen and water^{28–30}. Rice is also known to develop narrower root angles and deeper roots if grown in water-limited environments³¹.

Root-root interactions also contribute to the observed variation in root architecture within a single genotype. These interactions can be competition or avoidance (avoid competition) among individuals of the same genotype, through resources driven or chemical signaling mechanism^{32,33}. The resource-driven mechanism involves plant roots detecting the availability of surrounding resources, like water and nutrients, and responding to the presence of neighboring roots competing for these same resources³⁴. Direct chemical interactions involve the release of either toxic chemicals that can inhibit the growth of neighboring roots or non-toxic chemicals that facilitate recognition and thus alter root growth responses³⁵.

The response of plants to their neighbors varies depending on the identity of those neighbors, with plants capable of discerning the relatedness of neighboring plants and modifying their responses accordingly³⁶. For example, the sea rocket (*Cakile edentula*) had less root allocation when planted with kin-groups than with strangers³⁷. Some species also may avoid each other belowground by reducing root branching intensity and specific root length in response to kin neighbor rather than strangers³⁸. Such kin recognition often require soluble chemical signaling mediated by root exudates³⁹. Thus, the variation in root architecture within a single genotype is a complex interplay of environmental conditions, genetic factors, and complex interactions with neighboring plants.

Two Theories Help Understand Population Fitness Outcome of Plant Interaction

The interaction between neighboring plants in an agricultural system is essential to understand the performance of plants. The intensity of these interactions can significantly

influence crop yields, with negative interactions potentially leading to reduced yields, while positive interaction might enhance productivity⁴⁰. Two foundational theories in ecology are proposed to understand such plant interactions.

Resource partitioning theory that individuals of the same species or genotype, sharing similar phenotypes, compete more intensely for the same resources compared to those of different genotypes^{41–43}. This intensified competition within more genetically related populations can diminish overall fitness and productivity. Physiological and agronomic studies have suggested that avoidance between genetically distinct plants, leveraging their differing traits and resource needs, can lead to increased combined yields^{44–46}. For example, the intercrop of squash, common bean, and maize, which exploits the complementarity in root architecture and spatial segregation to achieve synergistic resource utilization and enhanced yield⁴⁷

Kin selection theory, on the other hand, suggests that plants can recognize the genetic relatedness of their neighbors and can modulate their competitive behavior accordingly^{37,48,49}. It implies that interactions with genetically similar individuals are characterized by reduced competition, leading to increased group fitness⁵⁰. This theory is supported by ecological evidence indicating that closely related plants exhibit less competitive traits (e.g., decreased root allocation and nutrient uptake) when interacting with each other, compared to their interactions with genetically distant individuals^{37,38,51,52}. Such behaviors suggest that populations comprised of closely related individuals may achieve higher overall fitness than those with genetically distant individuals.

The Necessity to Develop Controlled Growth Systems to Mimic Field Conditions

Root studies conducted in controlled environments typically use containers such as rhizotrons, pots, or small-scale mesocosm systems such as PVC tubes or Rhizoboxes^{53–57}. While these systems are invaluable for plant research, they have several limitations that hinder the translation of the results to the crops grown in the field. One issue is that the size and shape of these containers can influence the root growth of plants⁵⁶. Specifically, large plants confined to small containers tend to develop a relatively large fraction of roots growing close to, or even touching the pot edges^{56,58}, potentially altering the root architecture. Thus, researchers use these systems to study young roots before root growth is constrained by the pot dimensions. However, this brings another issue: the root architectural traits measured at the early stages of growth might not be consistent with those measured in fully mature plants, as root architecture tends to change as plants develop²⁴. Another limitation is the common practice of planting only one plant per container, which excludes the possibility of inter-plant interactions. The isolated growing conditions diverge significantly from field conditions, where crops are grown in proximity to allow for root-root interaction. Consequently, the root architecture observed under such isolated conditions may not replicate the root architecture within a population in fields. To address these limitations and enhance the transferability of controlled environment studies to field conditions, it is important to develop growing systems that allow for root interactions and unrestricted root growth.

Overview of the Dissertation

The overall goal of this dissertation is to study the root architectural variation within a plant population. By leveraging both field studies and controlled environment experiments, this

dissertation quantifies root architectural variation within homogeneous populations under different water conditions and across different growth stages. Further exploration focuses on how root architecture variation affects plant interactions and then the overall fitness of the population in monoculture and mixture, to provide implications for agricultural yield applications.

Specifically, Chapter 2 aims to develop a computational pipeline to cluster root architectures of homogeneous populations into distinguishable root architecture types, using root data from three common bean genotypes (DOR364, L8857 and SEQ7) under water-limited (WL) and non-limiting (NL) conditions in 2015 and 2016. This chapter examines how many root architecture types exist in each genotype and the change in the composition of root architecture types under different water conditions. Additionally, it investigates differences in aboveground biomass among the identified root architecture types.

Chapter3 validates the five root architecture types observed under field conditions by replicating two genotypes (SEQ7 and DOR364) in a controlled mesocosm system. The goal is to determine if these root architecture types persist despite the considerable environmental variation encountered in the field. This chapter also explores changes in the composition of SEQ7's root architecture types throughout developmental stages and links identified root architecture types with existing public root simulation models to infer their functions.

Chapter4 quantifies the overall fitness outcomes in monoculture and mixture planting scenarios using DOR364 and SEQ7 genotypes. This involves understanding the differences in plant interaction when interacting with either genetically identical or different neighbors of the same genotype. This chapter also investigates changes in the composition of root architecture

types and root biomass allocation between the monoculture and mixture under both WL and NL conditions.

In summary, this dissertation proposes the phenotypic spectrum as a new framework to explore root architecture types within plant populations, their environmental acclimatization, and response in monoculture and mixture.

Reference

- 1. Lynch, J. P. Root phenotypes for improved nutrient capture: an underexploited opportunity for global agriculture. *New Phytol.* **223**, 548–564 (2019).
- 2. Lynch, J. P. Rightsizing root phenotypes for drought resistance. *J. Exp. Bot.* **69**, 3279–3292 (2018).
- 3. Lynch, J. P. Root Architecture and Plant Productivity. *Plant Physiol.* **109**, 7–13 (1995).
- 4. Beidler, K. V. *et al.* Changes in root architecture under elevated concentrations of CO2 and nitrogen reflect alternate soil exploration strategies. *New Phytol.* **205**, 1153–1163 (2015).
- 5. Jung, J. K. H. & McCouch, S. Getting to the roots of it: Genetic and hormonal control of root architecture. *Front. Plant Sci.* **4**, 465–474 (2013).
- 6. Balduzzi, M. *et al.* Reshaping plant biology: Qualitative and quantitative descriptors for plant morphology. *Front. Plant Sci.* **8**, 117 (2017).
- 7. Burridge, J., Jochua, C. N., Bucksch, A. & Lynch, J. P. Legume shovelomics: High-Throughput phenotyping of common bean (*Phaseolus vulgaris* L.) and cowpea (*Vigna unguiculata* subsp, *unguiculata*) root architecture in the field. *Field Crops Res.* **192**, 21–32 (2016).

- 8. van Dusschoten, D. *et al.* Quantitative 3D Analysis of Plant Roots Growing in Soil Using Magnetic Resonance Imaging. *Plant Physiology* **170**, 1176–1188 (2016).
- 9. Herrero-Huerta, M. *et al.* 4D Structural root architecture modeling from digital twins by X-Ray Computed Tomography. *Plant Methods* **17**, 123 (2021).
- 10. Bagnall, G. C. *et al.* Low-field magnetic resonance imaging of roots in intact clayey and silty soils. *Geoderma* **370**, 114356 (2020).
- 11. Bagnall, G. C. *et al.* Design and demonstration of a low-field magnetic resonance imaging rhizotron for in-field imaging of energy sorghum roots. *Plant Phenome J.* **5**, e20038 (2022).
- 12. Schneider, H. M. & Lynch, J. P. Should Root Plasticity Be a Crop Breeding Target? *Front. Plant Sci.* **11**, (2020).
- 13. Schnepf, A. *et al.* Statistical Characterization of the Root System Architecture Model CRootBox. *Vadose Zone J.* **17**, 170212 (2018).
- Zhang, H. & Forde, B. G. An Arabidopsis MADS Box Gene That Controls Nutrient-Induced Changes in Root Architecture. *Science* 279, 407–409 (1998).
- 15. Cichy, K. A., Snapp, S. S. & Blair, M. W. Plant growth habit, root architecture traits and tolerance to low soil phosphorus in an Andean bean population. *Euphytica* **165**, 257–268 (2009).
- 16. Wang, X., Pan, Q., Chen, F., Yan, X. & Liao, H. Effects of co-inoculation with arbuscular mycorrhizal fungi and rhizobia on soybean growth as related to root architecture and availability of N and P. *Mycorrhiza* **21**, 173–181 (2011).
- 17. Manavalan, L. P. *et al.* Identification of Novel QTL Governing Root Architectural Traits in an Interspecific Soybean Population. *PLOS ONE* **10**, e0120490 (2015).

- 18. Trachsel, S., Kaeppler, S. M., Brown, K. M. & Lynch, J. P. Shovelomics: High throughput phenotyping of maize (Zea mays L.) root architecture in the field. *Plant Soil* **341**, 75–87 (2011).
- 19. Le Marié, C. A. *et al.* Shovelomics root traits assessed on the EURoot maize panel are highly heritable across environments but show low genotype-by-nitrogen interaction. *Euphytica* **215**, (2019).
- 20. Bucksch, A. *et al.* Image-Based High-Throughput Field Phenotyping of Crop Roots. *Plant Physiol.* **166**, 470–486 (2014).
- 21. Das, A. *et al.* Digital imaging of root traits (DIRT): A high-throughput computing and collaboration platform for field-based root phenomics. *Plant Methods* **11**, 1–12 (2015).
- 22. Lobet, G. *et al.* Demystifying roots: A need for clarification and extended concepts in root phenotyping. *Plant Sci.* **282**, 11–13 (2019).
- 23. Schneider, H. M. Characterization, costs, cues and future perspectives of phenotypic plasticity. *Ann. Bot.* **130**, 131–148 (2022).
- 24. Rich, S. M., Christopher, J., Richards, R. & Watt, M. Root phenotypes of young wheat plants grown in controlled environments show inconsistent correlation with mature root traits in the field. *J. Exp. Bot.* **71**, 4751–4762 (2020).
- 25. Lynch, J. P. Root phenes for enhanced soil exploration and phosphorus acquisition: Tools for future crops. *Plant Physiol.* **156**, 1041–1049 (2011).
- 26. Berny Mier Y Teran, J. C. *et al.* Root and shoot variation in relation to potential intermittent drought adaptation of Mesoamerican wild common bean (*Phaseolus vulgaris* L.). *Ann. Bot.* 124, 917–932 (2019).

- Polania, J., Poschenrieder, C., Rao, I. & Beebe, S. Root traits and their potential links to plant ideotypes to improve drought resistance in common bean. *Theor. Exp. Plant Physiol.* 143–154 (2017).
- 28. Mi, G. *et al.* Ideotype root architecture for efficient nitrogen acquisition by maize in intensive cropping systems. *Sci. China Life Sci.* **53**, 1369–1373 (2010).
- 29. York, L. M., Galindo-Castañeda, T., Schussler, J. R. & Lynch, J. P. Evolution of US maize (*Zea mays* L.) root architectural and anatomical phenes over the past 100 years corresponds to increased tolerance of nitrogen stress. *J. Exp. Bot.* **66**, 2347–2358 (2015).
- 30. Saengwilai, P., Tian, X. & Lynch, J. P. Low crown root number enhances nitrogen acquisition from low-nitrogen soils in maize. *Plant Physiol.* **166**, 581–589 (2014).
- 31. Uga, Y. *et al.* Control of root system architecture by DEEPER ROOTING 1 increases rice yield under drought conditions. *Nat. Genet.* **45**, 1097–1102 (2013).
- 32. Yoneyama, K. & Bennett, T. Whispers in the dark: Signals regulating underground plant—plant interactions. *Curr. Opin. Plant Biol.* **77**, 102456 (2024).
- 33. Wang, N.-Q., Kong, C.-H., Wang, P. & Meiners, S. J. Root exudate signals in plant–plant interactions. *Plant Cell Environ.* **44**, 1044–1058 (2021).
- 34. de Kroon, H., Mommer, L. & Nishiwaki, A. Root Competition: Towards a Mechanistic Understanding. in *Root Ecology* (eds. de Kroon, H. & Visser, E. J. W.) 215–234 (Springer, Berlin, Heidelberg, 2003).
- 35. Schenk, H. J., Callaway, R. M. & Mahall, B. E. Spatial Root Segregation: Are Plants

 Territorial? in *Advances in Ecological Research* (eds. Fitter, A. H. & Raffaelli, D.) vol. 28

 145–180 (Academic Press, 1999).

- 36. Biedrzycki, M. L. & Bais, H. P. Kin recognition: Another biological function for root secretions. *Plant Signal. Behav.* **5**, 401–402 (2010).
- 37. Dudley, S. A. & File, A. L. Kin recognition in an annual plant. *Biol. Lett.* **3**, 435–438 (2007).
- 38. Semchenko, M., Saar, S. & Lepik, A. Plant root exudates mediate neighbour recognition and trigger complex behavioural changes. *New Phytol.* **204**, 631–637 (2014).
- 39. Biedrzycki, M. L., Jilany, T. A., Dudley, S. A. & Bais, H. P. Root exudates mediate kin recognition in plants. *Commun. Integr. Biol.* **3**, 28–35 (2010).
- 40. Deng, J. *et al.* Models and tests of optimal density and maximal yield for crop plants. *Proc. Natl. Acad. Sci. U. S. A.* **109**, 15823–15828 (2012).
- 41. Ashton, I. W., Miller, A. E., Bowman, W. D. & Suding, K. N. Niche complementarity due to plasticity in resource use: plant partitioning of chemical N forms. *Ecology* **91**, 3252–3260 (2010).
- 42. Fajardo, A. & McIntire, E. J. B. Under strong niche overlap conspecifics do not compete but help each other to survive: facilitation at the intraspecific level. *J. Ecol.* **99**, 642–650 (2011).
- 43. Silvertown, J. Plant coexistence and the niche. Trends Ecol. Evol. 19, 605–611 (2004).
- 44. Brooker, R. W. *et al.* Improving intercropping: a synthesis of research in agronomy, plant physiology and ecology. *New Phytol.* **206**, 107–117 (2015).
- 45. Demie, D. T. *et al.* Mixture × Genotype Effects in Cereal/Legume Intercropping. *Front. Plant Sci.* **13**, (2022).
- 46. Li, L., Tilman, D., Lambers, H. & Zhang, F. S. Plant diversity and overyielding: Insights from belowground facilitation of intercropping in agriculture. *New Phytol.* **203**, 63–69 (2014).

- 47. Zhang, C., Postma, J. A., York, L. M. & Lynch, J. P. Root foraging elicits niche complementarity-dependent yield advantage in the ancient 'three sisters' (maize/bean/squash) polyculture. *Ann. Bot.* **114**, 1719–1733 (2014).
- 48. Bais, H. P. Shedding light on kin recognition response in plants. *New Phytol.* **205**, 4–6 (2015).
- 49. Yang, X.-F., Li, L.-L., Xu, Y. & Kong, C.-H. Kin recognition in rice (*Oryza sativa*) lines. *New Phytol.* **220**, 567–578 (2018).
- 50. West, S. A., Pen, I. & Griffin, A. S. Cooperation and competition between relatives. *Science* **296**, 72–75 (2002).
- 51. Zhang, L., Liu, Q., Tian, Y., Xu, X. & Ouyang, H. Kin selection or resource partitioning for growing with siblings: implications from measurements of nitrogen uptake. *Plant Soil* **398**, 79–86 (2016).
- 52. Takigahira, H. & Yamawo, A. Competitive responses based on kin-discrimination underlie variations in leaf functional traits in Japanese beech (*Fagus crenata*) seedlings. *Evol. Ecol.* **33**, 521–531 (2019).
- 53. Clark, R. T. *et al.* Three-Dimensional Root Phenotyping with a Novel Imaging and Software Platform. *Plant Physiol.* **156**, 455–465 (2011).
- 54. Rinehart, B., Poffenbarger, H., Lau, D. & McNear, D. A method for phenotyping roots of large plants. *Plant Phenome J.* **5**, e20041 (2022).
- 55. Martins, S. M. *et al.* PhenoRoots: an inexpensive non-invasive phenotyping system to assess the variability of the root system architecture. *Sci. Agric.* 77, e20180420 (2019).

- 56. Poorter, H., Bühler, J., Van Dusschoten, D., Climent, J. & Postma, J. A. Pot size matters: A meta-analysis of the effects of rooting volume on plant growth. *Funct. Plant Biol.* **39**, 839–850 (2012).
- 57. Wu, J. *et al.* RhizoChamber-Monitor: a robotic platform and software enabling characterization of root growth. *Plant Methods 2018 141* **14**, 1–15 (2018).
- 58. Herold, A. & McNeil, P. H. Restoration of Photosynthesis in Pot-Bound Tobacco Plants. *J. Exp. Bot.* **30**, 1187–1194 (1979).

CHAPTER 2

DEVELOPING A COMPUTATIONAL PIPELINE TO QUANTIFY ROOT ARCHITECTURE DIVERSITY IN SINGLE GENOTYPES

Introduction

Root architecture, the spatial arrangement of root systems in the soil, is crucial to determine how effectively plants can acquire water and nutrients, thereby significantly impacting plant productivity^{1,2}. For example, root systems with steeper angles are more effective in accessing deep soil resources and better at tolerating drought stress, which can lead to improved yields under drought conditions^{3–6}. Root architecture can be described by specific root traits, which vary among genotypes and species. These traits include geometric (such as length, depth and angle) or topological (such as branch density, branch structure and the number of root tips) characteristics, or one can derive a shape descriptor from the whole root system or a specific part of the root system of interest^{7–11}.

Current concepts to quantify these root architectural variations operate under the assumption of homogenous phenotype for a specific genotype^{12–14}.

- 1. Sampling strategies are designed to capture phenotypic variation only between genotypes or focus solely on the average trait of one genotype.
- 2. Single traits are measured on the plant without quantifying the hierarchical organization of the root system.

This sampling strategy and measurement disregards the considerable architectural variation exhibited by each genotype and ignores the hierarchical organization of the root

system. Contrary to this common assumption, we have observed clear architectural variation among neighboring plants' root systems in our field experiments (Figure 2.1). This observation suggests current assumptions and measurements maybe insufficient in capturing this architectural variation.

Hence, in Chapter 2, we tackle the coverage problem of phenotypes with the highthroughput phenotyping platform Digital Imaging of Root Traits (DIRT)^{7,15}. DIRT provides a shape descriptor DS curve to summarize the excavated root system as a function derived from the width profile over the excavated root depth. Thus, capturing the spatial arrangement of the whole root architecture shape, instead of locally measured root traits. Previous studies on root architectures of cowpea⁷, common bean¹⁵, maize⁷, and cassava¹⁶ demonstrated the capability of DS-curves in distinguishing root architectures among genotypes, thereby effectively describing the entire root system. Therefore, it is possible to develop a computational pipeline that automatically distinguishes previously observed architecture types in field experiments from 2015 and 2016. The primary goal of this chapter is to quantify root architectural variation within a single genotype in a large scale of agricultural experiments. As a result, we developed a rigorous computing pipeline Dirt-Pop to cluster the root architectural variation within one genotype into different root architecture types. Dirt-Pop used Kmeans++ clustering to cluster DS-curves of excavated root images, eliminated excavation-induced outliers, and computed similarities between average DS-curves describing each root architecture type across genotypes. The pipeline was applied to three common bean (*Phaseolus vulgaris* L.) genotypes DOR364, L8857 and SEQ7 collected over two years 2015 and 2016 under water-limited (WL) and nonlimiting (NL) conditions.

The specific objectives of this chapter are:

- 1. To identify how many root architecture types are present for each genotype.
- 2. To investigate how the composition of root architecture types change between different years and conditions for each genotype.
- 3. To test the difference in aboveground biomass among the identified root architecture types for each genotype under each condition across both years.

Materials and Methods

Plant material and growth conditions

We chose the three common bean genotypes DOR364, L8857 and SEQ7 for this study because they represent different genetic backgrounds and morphologies. DOR364, originating from the Mesoamerican panel⁴, is a deep-rooted and phosphorus-inefficient genotype^{17,18}. This genotype, known for its small red seeds, is widely cultivated in Central America¹⁹. L8857, a recombinant inbred line derived from the drought-resistant B98311 line and phosphorous-tolerant TLP19 line, carries a genetic lineage from Mesoamerican panel²⁰. This black-seeded cultivar exhibits a shallow root system, optimizing phosphorous uptake efficiency in topsoil^{21,22}. The SEQ7 is a drought-tolerant cultivar from Andean panel²³. The root of SEQ7 has two basal root whorls²⁴ and has a dimorphic architecture that optimize resource uptake in the topsoil and deep soil (personal communication between A. Bucksch and J.P. Lynch).

Field experiments were conducted at the Apache Root Biology Center in Willcox, AZ (32° 15′ 9.25″ N, 109° 49′ 56.93″ W) under NL and WL conditions in 2015 and 2016. The planting site's soil type was a loam soil type (coarse-loamy, mixed, thermic Typic Torrifluvents). The plants were grown from May through August, a period which saw maximum temperatures fluctuating from 20.60 °C to 41.10 °C in 2015, and from 21.70 °C to 44.40 °C in 2016. The

minimum temperatures during these periods ranged from -0.6 °C to 23.90 °C in 2015 and from 3.3 °C to 23.90 °C in 2016^{25} .

We planted three genotypes DOR364, L8857 and SEQ7 in plots with an in-row distance of 10 cm and an out-row distance of 36 cm. Each plot exclusively was planted with a single genotype. The sample size of each genotype grown under NL and WL conditions in 2015 and 2016 are listed in Table S2.1. The cumulative precipitation during these growing periods was markedly different between the two years, with a total rainfall of 98.1 mm in 2015, increasing to 195.1 mm in 2016. To simulate the water-limited condition, irrigation was suspended during the final two weeks of the growing period. It was noted that minor rainfall events occurred during this period in both experimental years (Figure S2.1). Apart from the variation in water supply, the same agricultural management practices, including routine fertilization and pest control, were applied under both conditions.

We excavated the mature roots at ten weeks in the field using a specifically developed legume Shovelomics method¹⁵. Following excavation, we captured images of the roots using the DIRT root imaging protocol to determine 2D root architecture traits. In addition to obtaining the root images, a subset of samples from the 2016 experiment were dried at 60°C for 72 hours, after which each shoot's weight was measured to determine dry shoot biomass.

Customized DIRT-Pop pipeline for clustering DS-curves into root architecture types

We developed a customized DIRT-Pop pipeline to cluster DS-curves into several root architecture types (Figure 2.2). The specific steps are described below:

Step 1: Image processing and DS-value extraction. Initially, the raw root images were uploaded and processed in the DIRT online platform²⁶. During this process, each image was manually checked to ensure correct segmentation and accurate root identification. The DIRT

algorithm primarily identifies roots by focusing on the most foreground pixels. This occasionally results in the misidentification of sample labels, which are larger than the roots, as roots themselves. To correct such errors, we used the GIMP image processing software to mask the sample labels with a black background color. Subsequently, we extracted nine sample points from the DS-curve²⁷. We collected all the DS-curves of one genotype across WL and NL conditions during the year 2015 and 2016.

Step 2: K-means++ clustering with outlier removal. Clustering algorithms, in general, aim to partition a dataset into clusters where items within the same cluster share greater similarity with each other than with those in different clusters²⁸. Given the assumption that different genotypes may have different number of root architecture types, we chose to apply Kmeans ++ clustering method at the genotype level. The K-means++ algorithm was chosen because it adopts an improved probability-weighted strategy for assigning initial cluster centroids. This algorithm significantly reduces the likelihood of the algorithm converging to suboptimal local minima, ensuring more consistent and better clustering results²⁹. We used scikit-learn Python package³⁰ to perform the K-means++ clustering algorithm, which aims to minimize the within-cluster variation, commonly referred to as the inertia value. Since Kmeans++ is an unsupervised learning algorithm, specifying the number of clusters as input is needed. To determine this optimal cluster number, we used Python package kneed³¹ to implements the Kneedle algorithm³². The Kneedle algorithm identifies a balance point, either an 'elbow' or 'knee', where adding one more cluster results in a slower reduction of inertia compared to not adding an extra cluster³³. Within the Step 2, we also used the R package Roahd³⁴ to identify outliers within clusters based on two defined criteria: magnitude and shape. Here, magnitude outliers describe the DS curves that contain atypical high or low values³⁵, which

mostly indicating the shape deformation resulting from unintended damage to the roots during excavation. Shape outliers describe the DS curves that exhibit a different shape than the rest DS curves within the same cluster³⁵. For detailed visuals and statistics on these two types of outliers, please see Figure S2.2. The outlined process for K-means++ clustering, optimal cluster number determination, and outlier removal can be summarized as:

- 1. Execute K-means++ algorithm i times for each k value, where we denote the number of iterations i=1...1000 and k denotes the number of clusters k=1...25.
- 2. Apply the Kneedle algorithm to each iteration to compute the elbow/knee. The most frequently occurring knee/elbow point is selected as the optimal cluster number *k* through a majority voting approach.
- 3. Perform K-means++ algorithm 1000 times using the optimal k value and return the result exhibiting the lowest inertia as the optimal solution.
- 4. Using the optimal solution from the previous step, apply the shape and magnitude outlier algorithm to detect if there are any outliers.
- 5. If outliers are detected, remove them, and return to the first step. If no outliers are present, finalize the current optimal solution as the output.

Each cluster is denoted as one root architecture type. Given that shape and magnitude outliers have been removed, it is appropriate to represent each root architecture type using the mean curve of a cluster.

Step 3: Assessing shape similarity of root architecture types among genotypes.

Following the clustering of each genotype, we computed the Fréchet distance as a metric of shape similarity between the mean DS-curves of the three genotypes. The Fréchet distance can be thought of as the shortest leash length needed to allow two travelers to traverse each curve

from start to finish, possibly at different speeds³⁶. The Fréchet distance was chosen to compute the shape similarity because it considers both the location and the ordering of the points along the curves. This offers a more comprehensive measure of similarity compared to other metrics that might only focus on point-wise distance without considering the sequence of points^{36,37}, such as the Euclidean and Manhattan distances. Specifically, we computed the pairwise Fréchet distance matrix of the mean DS-curve of each root architecture type across the genotypes using the python package, similaritymeasures^{38,39}. We then visualized Fréchet distance matrix by creating a hierarchically-clustered heatmap using the python package, Seaborn with Ward's method⁴⁰.

The Dirt-Pop pipeline used in our study can be found in the GitHub repository: https://github.com/Computational-Plant-Science/DIRT-Pop.v1

Statistical analysis

After obtaining the clustering results for each genotype, to determine whether the frequency of each genotype's root architecture types was evenly distributed across conditions, we performed a pairwise Chi-square test of homogeneity between conditions. We visualized the frequency distribution of these root architecture types using bar plots, which were created with the ggplot2 package⁴¹. To analyze the difference in aboveground shoot biomass among root architecture types in 2016 under each condition, we applied the non-parametric Kruskal-Wallis test for each genotype. If the Kruskal-Wallis test indicated significance at a P-value < 0.05, we then used the Wilcoxon rank sum test to identify which specific root architecture types had higher or lower aboveground shoot biomass. The same tests were used to compare the aboveground shoot biomass among genotypes under each condition. All statistical analyses were conducted using R (v 4.2.0)⁴².

Results

Each genotype showed five different root architecture types across two years and two water conditions.

The DIRT-Pop pipeline identified five distinct root architecture types (AT1 through AT5) for DOR364, L8857 and SEQ7 across both WL and NL conditions during the years 2015 and 2016 (Figure 2.3). According to Fréchet distance matrix, AT1, AT2, AT3 and AT4 were similar, but AT5 was slightly different across the three genotypes (Figure 2.3, Figure 2.4 and Figure S2.3). The peak of DS curve indicates the depth at which most width accumulation change occurs, while the curve's angle or rate quantifies the pace of width accumulation over depth. By examining the mean curve value (Table S2.2), AT1 reached the maximum width accumulation at 70% excavated rooting depth (Figure 2.3). In comparison, AT2 accumulated width at an almost steady rate over the excavated depth. AT3 reached the maximum width accumulation at 60% depth (Figure 2.3). On the other hand, AT3 achieved its maximal width at 60% depth, though with a higher rate of width accumulation compared to AT1 (Figure 2.3). AT4's width accumulation peaked at approximately 40% depth, gradually decreasing slowly until 90% excavated rooting depth (Figure 2.3). Interestingly, AT5, which was observed in DOR364 was different from AT5 in SEQ7 and L8857. While AT5 in DOR364 peaked in width at 40% depth, AT5 in both SEQ7 and L8857 reached maximal width at 60% of the depth.

The composition of root architecture types in three common bean genotypes changed between different water conditions.

DOR364 population had significant differences in root architecture type composition under both NL and WL conditions across two consecutive years (Chi-squared test; P = 0.032 in 2015; P = 0.042 in 2016; Figure 2.5a). In 2015, under WL condition, DOR364 reduced AT2 by

11.07% while increasing AT3 and AT4 by 6.74% and 8.20%, respectively, in comparison to the NL condition (AT2: 37.77% NL vs. 26.70% WL; AT3: 10.31% NL vs. 17.05% WL; AT4: 19.28% NL vs. 27.84% WL; Figure 2.5a). In 2016, DOR364 showed a similar pattern as observed in 2015: a decrease in AT2 by 4.96% and an increase in AT3 and AT4 by 8.16% and 5.76%, respectively. However, there was a decrease of 9.58% in AT1 when comparing NL to WL conditions (AT1: 33.69% NL vs. 24.11% WL; AT2: 32.62% NL vs. 27.66% WL; AT3: 11.70% NL vs. 19.86% WL; AT4: 17.73% NL vs. 23.40% WL; Figure 2.5a).

L8857 showed a significant difference in the composition of root architecture types for between WL and NL conditions over two years (Chi-squared test; P = 0.0005 in 2015; P = 0.015 in 2016; Figure 2.5b). In 2015, under WL conditions, L8857 showed reductions of 7.70% in AT1 and 4.66% in AT4, while AT3 saw an increase of 7.10% compared to the NL condition (AT1: 27.44% NL vs. 19.74% WL; AT3: 21.64% NL vs. 28.74% WL; AT4: 21.64% NL vs. 16.98% WL; Figure 2.5b). In 2016, a decrease of 10.95% was observed in AT2 under the WL condition, alongside a 7.01% increase in AT3 (AT2: 26.60% NL vs. 15.65% WL; AT3: 22.70% NL vs. 29.71% WL; Figure 2.5b). Notably, despite changes in other root architecture type composition, AT5 consistently represented approximately 10% of the population across both conditions and years (Figure 2.5b).

In 2015, SEQ7 underwent significant changes in the composition of root architecture types under varied water conditions (Chi-squared test, P = 0.0005; Figure 2.5c). Specifically, under the WL condition, the proportions of AT2 and AT4 decreased by 13.74% and 11.98%, respectively (AT2: 35.94% NL vs. 22.02% WL; AT4: 31.25% NL vs. 19.27% WL; Figure 2.5c). Conversely, AT1, AT3, and AT5 exhibited increases of 10.64%, 10.08%, and 4.22%, respectively (AT1: 21.09% NL vs. 30.73% WL; AT3: 8.59% NL vs. 20.64% WL; AT5: 3.12%

NL vs. 7.34% WL; Figure 2.5c). However, in 2016, the composition of root architecture types of SEQ7 showed no statistically significant differences between the conditions (Chi-squared test, P = 0.37; Figure 2.4c). Despite no significant overall change in root architecture type composition, there were observable shifts in the proportions of specific root architecture types when comparing WL and NL conditions. AT1 and AT3 decreased by 4.99% and 4.48%, respectively, while AT4 increased by 5.40% under the WL condition compared to the NL condition (AT1: 33.06% NL vs. 28.07% WL; AT3: 24.00% NL vs. 19.52% WL; AT4: 18.40% NL vs. 23.80% WL; Figure 2.4c). The changes in root architecture type composition observed in 2016 were opposite from those observed in 2015.

Variation in root architecture is not correlated with variation in aboveground shoot biomass.

Three genotypes had significant differences in aboveground shoot biomass under each condition (Figure S2.4). However, for individual genotypes, there was generally no significant difference in root architecture types (Figure 2.6 & Figure S2.4). At the population level, the aboveground biomass of genotype SEQ7 (mean=27.03) was significantly lower than that of DOR364 (mean=29.53, Wilcoxon rank-sum test, P <0.01) and L8857 (mean=29.53, Wilcoxon rank-sum test, P <0.01) under the WL condition (Figure S2.4). While, when under the NL condition, SEQ7 (mean=23.97) showed significantly greater aboveground shoot biomass than L8857 (mean=21.82, Wilcoxon rank-sum test, P <0.01) and DOR364 (mean=19.76, Wilcoxon rank-sum test, P <0.01; Figure S2.4). A detailed examination within genotypes revealed no significant differences among root architecture types in DOR364 under either condition (Figure 2.6). For L8857, no significant difference in aboveground shoot biomass was observed under the WL condition. However, under the NL condition, AT2 of L8857 exhibited significantly higher aboveground shoot biomass compared to the other four root architecture types (Wilcox rank sum

test, P < 0.05, Figure 2.6, Table S2.3). In the case of SEQ7, no significant difference in aboveground shoot biomass was found under the NL condition. Yet, under the WL condition, the aboveground shoot biomass of AT3 (mean=24.36) and AT5 (mean=25.58) in SEQ7 was significantly lower than AT1 (mean=29.29) and AT2 (mean=26.85, Wilcox rank sum test, P < 0.05; Figure 2.6).

Discussion

The DIRT-Pop pipeline quantifies the diverse root architectures within common bean genotypes.

The primary objective of this chapter was to develop the DIRT-Pop computational pipeline (Figure 2.1) as a tool to characterize the root architectural variations into root architecture types within three common bean genotypes (DOR364, L8857 and SEQ7). The pipeline uses the DS-curve shape descriptor, to capture the architectural organization of root width over the rooting depth, focusing on the whole root system's shape rather than single or localized root traits. Therefore, The DIRT-Pop pipeline provides an alternative approach to quantify root architectural variation in comparison to combining single or local root traits into integrated root phenotypes^{43,44}. Two features of DIRT -Pop pipeline enhance the quality of data analysis. First, the incorporation of the Kneed algorithm³², combined with a majority voting strategy, facilitates the objective, automatic determination of the optimal number of root architecture types (k) for the Kmeans++ clustering algorithm. This feature eliminates the need for subjectively selecting k beforehand. Second, the pipeline employs an outlier removal strategy that excludes damaged root samples during manual extraction and removes shape outliers within root architecture types. Therefore, with these enhancements, the DIRT-Pop pipeline improves the robustness and reliability in characterization of root architecture variations.

By analyzing over 800 replicates per genotype, DIRT-Pop pipeline has identified five distinct root architectural types for each of three common bean genotypes. The result provides quantitative evidence against the general assumption that a single genotype has only one common root architecture type within a given environment. It also underscores the limitations of the current sampling strategy missing extensive variation in root architecture that exists within one genotype. As such, we hypothesize that each genotype may exhibit a specific number of root architecture types.

The varied composition of root architecture types in common bean populations suggests acclimatization strategies to different water conditions.

Understanding the root architectural traits of a single genotype across different environments is crucial for enhancing crop resilience and productivity. Typically, researchers use the framework of phenotypic plasticity to investigate how these traits change in response to environmental conditions^{45–47}. Phenotypic plasticity refers to the ability of a single genotype to exhibit varied phenotypic responses under different environmental conditions^{48–50}. It is commonly analyzed by using reaction norms that represent on how average traits vary across environmental gradients^{45,51–53}. In this study, we adopted a different approach by analyzing changes in the composition of identified root architecture types by the DIRT-Pop pipeline within each genotype's population under differing water conditions, rather than comparing average trait values – the average DS curve. This method provides a deeper understanding of root architectural acclimatization at the population level. Three common bean genotypes showed different responses under two water conditions, as evidenced by shifts in the compositions of root architecture types. In 2015 and 2016, both DOR364 and L8857 exhibited significant shifts in their root architecture type compositions under two different water conditions (Figure 2.5).

SEQ7, however, only showed a significant change in 2015, but not in 2016 (Figure 2.5). The reason might be that in 2016, there was standing water left in the SEQ7 plot, which may not induce water stress under WL condition. Notably, the percentage of which specific root architecture types were changed varied among DOR364, L8857, and SEQ7. For example, under WL conditions, DOR364 increased the proportion of AT4 and AT2 types, whereas L8857 and SEQ7 increased the proportion of AT3 compared to NL conditions. This variability in response among the genotypes suggests that acclimatization strategies may be genotype specific. Therefore, we hypothesize that different common bean populations may exhibit different root architecture acclimatization strategies in response to varying water conditions.

Diverse root architecture types in a single genotype showed minimal effect on aboveground shoot biomass.

Another goal of this chapter was to explore the relationship between different root architecture types and aboveground shoot biomass in three common bean genotypes: SEQ7, DOR364, and L8857. Interestingly, the result revealed no significant differences in aboveground shoot biomass among most root architecture types within each genotype under both water conditions, except the AT2 in L8857 under NL conditions and the AT1 and AT2 types in SEQ7 under WL conditions (Figure 2.6). Lynch has previously proposed three root architecture ideotypes, typically categorized as deep, intermediate, and shallow root systems, each having distinct capabilities in water and nutrient uptake^{1,54,55}. Thus, it was anticipated that different root architecture types would correlate with varying levels of plant productivity, as indicated by aboveground shoot biomass in this study, particularly given the known association between deep root systems and drought resistance in various crops^{3,56}. However, the finding did not show a significant variation in aboveground shoot biomass associated with each root architecture type.

Several reasons could explain this observation: First, as highlighted by Fitter (1994), alterations in root architecture do not necessarily lead changes in root biomass⁵⁷, which might not alter biomass partitioning. Therefore, the shoot biomass associated with each root architecture type might remain unchanged. Supporting evidence from a previous study in Salix miygbeana showed no correlation between aboveground biomass and root architectural traits⁵⁸. Instead, it suggested aboveground shoot biomass was influenced by external environmental factors, such as the soil type, rather than by root architecture⁵⁸. Second, in the experimental setup, the common bean plants were grown in proximity, allowing for root interaction among neighboring plants. However, the specific impact of such interactions on shoot biomass remains unclear. For example, a plant with a deep root architecture ideotype may increase competition in water uptake from a neighboring plant with a similar deep root architecture ideotype, as opposed to one with a shallow root architecture ideotype. This is because shallow root systems exploits surface soil resources, whereas deep root systems capture subsoil resources, potentially reducing direct competition for water^{1,54,55}. Thus, the advantages typically associated with deep root systems for water uptake under water-limited conditions might not necessarily lead to higher shoot biomass, as it also depends on the root architecture types of neighboring plants. We identified five distinct root architecture types co-existing within a single common bean genotype under one water condition, suggesting more complex interactions beyond a binary deep vs shallow root system interaction. There are multiple combinations of interactions among different root architecture types. A particular root architecture type could interact not only with identical types but also with up to four other types within the genotype. Nevertheless, the interactions between these diverse root architecture types and their impact on shoot biomass remain unexplored. Third, the specific functions of these five root architecture types in terms of water and nutrient uptake are not yet

fully understood. Without a comprehensive understanding of these roles in resource uptake, it is challenging to establish a direct association between root architecture type and their shoot biomass. Therefore, further research is essential to elucidate the specific resource uptake functions of the identified root architecture types and to understand their effects on plant productivity, when plants interact with each other.

Acknowledgements

We thank Nicholas Klepp and John Miller for initially implementing Kmeans++ algorithm in Scala as the first tool investigate the phenotypic spectrum in 2016. We also thank Natalie Busener for annotating the sample label in the excel file and James Burridge for helping to plant and collect the field data at Willcox, AZ.

References

- 1. Lynch, J. P. Root phenotypes for improved nutrient capture: an underexploited opportunity for global agriculture. *New Phytol.* **223**, 548–564 (2019).
- 2. Burridge, J. D., Rangarajan, H. & Lynch, J. P. Comparative phenomics of annual grain legume root architecture. *Crop Science* **60**, 2574–2593 (2020).
- 3. Uga, Y. *et al.* Control of root system architecture by DEEPER ROOTING 1 increases rice yield under drought conditions. *Nat Genet* **45**, 1097–1102 (2013).
- 4. Ho, M. D., Rosas, J. C., Brown, K. M. & Lynch, J. P. Root architectural tradeoffs for water and phosphorus acquisition. *Funct. Plant Biol.* **32**, 737–748 (2005).
- 5. Trachsel, S., Kaeppler, S. M., Brown, K. M. & Lynch, J. P. Shovelomics: High throughput phenotyping of maize (*Zea mays* L.) root architecture in the field. *Plant Soil* **341**, 75–87 (2011).

- Manschadi, A. M., Christopher, J. T., Hammer, G. L. & Devoil, P. Experimental and modelling studies of drought-adaptive root architectural traits in wheat (*Triticum aestivum* L.). *Plant Biosyst. Int. J. Deal. Asp. Plant Biol.* 144, 458–462 (2010).
- 7. Bucksch, A. *et al.* Image-Based High-Throughput Field Phenotyping of Crop Roots. *Plant Physiol.* **166**, 470–486 (2014).
- 8. Berntson, G. M. Topological scaling and plant root system architecture: developmental and functional hierarchies. *New Phytol* **135**, 621–634 (1997).
- 9. Falk, K. G. *et al.* Computer vision and machine learning enabled soybean root phenotyping pipeline. *Plant Methods* **16**, 5 (2020).
- Falk, K. G. *et al.* Soybean Root System Architecture Trait Study through Genotypic,
 Phenotypic, and Shape-Based Clusters. *Plant Phenomics* 2020, (2020).
- 11. de Dorlodot, S. *et al.* Root system architecture: opportunities and constraints for genetic improvement of crops. *Trends Plant Sci.* **12**, 474–481 (2007).
- 12. Cichy, K. A., Snapp, S. S. & Blair, M. W. Plant growth habit, root architecture traits and tolerance to low soil phosphorus in an Andean bean population. *Euphytica* **165**, 257–268 (2009).
- 13. Wang, X., Pan, Q., Chen, F., Yan, X. & Liao, H. Effects of co-inoculation with arbuscular mycorrhizal fungi and rhizobia on soybean growth as related to root architecture and availability of N and P. *Mycorrhiza*. **21**, 173–181 (2010).
- 14. Manavalan, L. P. *et al.* Identification of Novel QTL Governing Root Architectural Traits in an Interspecific Soybean Population. *PLOS ONE* **10**, e0120490 (2015).
- 15. Burridge, J., Jochua, C. N., Bucksch, A. & Lynch, J. P. Legume shovelomics: High-Throughput phenotyping of common bean (*Phaseolus vulgaris* L.) and cowpea (*Vigna*

- *unguiculata* subsp, *unguiculata*) root architecture in the field. *Field Crops Res.* **192**, 21–32 (2016).
- Busener, N., Kengkanna, J., Saengwilai, P. J. & Bucksch, A. Image-based root phenotyping links root architecture to micronutrient concentration in cassava. *PLANTS, PEOPLE, PLANET* 2, 678–687 (2020).
- 17. Liao, H. *et al.* Effect of phosphorus availability on basal root shallowness in common bean. *Plant Soil* **232**, 69–79 (2001).
- 18. Basu, P. & Pal, A. Spatio-temporal analysis of development of basal roots of common bean (*Phaseolus vulgaris* L.). *Plant Signal. Behav.* **6**, 982–985 (2011).
- 19. Asfaw, A., Blair, M. W. & Struik, P. C. Multienvironment Quantitative Trait Loci Analysis for Photosynthate Acquisition, Accumulation, and Remobilization Traits in Common Bean Under Drought Stress. *G3 GenesGenomesGenetics* **2**, 579–595 (2012).
- 20. Frahm, M. A. *et al.* Breeding beans for resistance to terminal drought in the Lowland tropics. *Euphytica* **136**, 223–232 (2004).
- 21. Burridge, J. D. *et al.* A case study on the efficacy of root phenotypic selection for edaphic stress tolerance in low-input agriculture: Common bean breeding in Mozambique. *Field Crops Res.* **244**, 107612 (2019).
- 22. Henry, A., Rosas, J. C., Beaver, J. S. & Lynch, J. P. Multiple stress response and belowground competition in multilines of common bean (*Phaseolus vulgaris* L.). *Field Crops Res.* **117**, 209–218 (2010).
- CIAT. Annual Report 2008: Outcome Line SBA-1: Improved Beans for the Developing World. (2009).

- 24. Miguel, M. A., Widrig, A., Vieira, R. F., Brown, K. M. & Lynch, J. P. Basal root whorl number: a modulator of phosphorus acquisition in common bean (*Phaseolus vulgaris*). *Ann. Bot.* **112**, 973–982 (2013).
- 25. NOAA. Datasets | Climate Data Online (CDO) | National Climatic Data Center (NCDC). https://www.ncei.noaa.gov/cdo-web/datasets.
- 26. Das, A. *et al.* Digital imaging of root traits (DIRT): A high-throughput computing and collaboration platform for field-based root phenomics. *Plant Methods* **11**, 1–12 (2015).
- 27. The GIMP Development Team. GIMP. (2019). https://www.gimp.org/
- 28. Wang, H., Wang, W., Yang, J. & Yu, P. S. Clustering by pattern similarity in large data sets. in *Proceedings of the 2002 ACM SIGMOD international conference on Management of data* 394–405 (Association for Computing Machinery, New York, NY, USA, 2002).
- 29. Arthur, D. & Vassilvitskii, S. k-means++: the advantages of careful seeding. in *Proceedings* of the eighteenth annual ACM-SIAM symposium on Discrete algorithms 1027–1035 (Society for Industrial and Applied Mathematics, USA, 2007).
- 30. Pedregosa, F. *et al.* Scikit-learn: Machine Learning in Python. *Journal of Machine Learning Research* **12**, 2825–2830 (2011).
- 31. Arvai, K. kneed: Knee-point detection in Python. *Github Repository*, (2023). https://github.com/arvkevi/kneed
- 32. Satopää, V., Albrecht, J., Irwin, D. & Raghavan, B. Finding a 'kneedle' in a haystack:

 Detecting knee points in system behavior. in *Proceedings International Conference on Distributed Computing Systems* 166–171 (2011).
- 33. Bholowalia, P. & Kumar, A. EBK-Means: A Clustering Technique based on Elbow Method and K-Means in WSN. *International Journal of Computer Applications* **105**, 17–24 (2014).

- 34. Ieva, F., Paganoni, A. M., Romo, J. & Tarabelloni, N. Roahd Package: Robust Analysis of High Dimensional Data. *R Journal* **11**, 291–307 (2019).
- 35. Arribas-Gil, A. & Romo, J. Shape outlier detection and visualization for functional data: the outliergram. *Biostatistics* **15**, 603–619 (2014).
- 36. Eiter, T. & Mannila, H. Computing Discrete Fréchet Distance. *Technical Report*, (1994).
- 37. Driemel, A., Har-Peled, S. & Wenk, C. Approximating the Fréchet Distance for Realistic Curves in Near Linear Time. *Discrete Comput. Geom.* **48**, 94–127 (2012).
- 38. Jekel, C. similaritymeasures: Quantify the difference between two arbitrary curves in space. *Github Repository*, (2023). https://github.com/cjekel/similarity_measures
- 39. Jekel, C. F., Venter, G., Venter, M. P., Stander, N. & Haftka, R. T. Similarity measures for identifying material parameters from hysteresis loops using inverse analysis. *Int. J. Mater. Form.* **12**, 355–378 (2019).
- 40. Waskom, M. seaborn: statistical data visualization. J. Open Source Softw. 6, 3021 (2021).
- 41. Wickham, H. ggplot2: Elegant Graphics for Data Analysis. Springer-Verlag New York (2016).
- 42. R Core Team. R: A Language and Environment for Statistical Computing. (2022).
- 43. Klein, S. P., Schneider, H. M., Perkins, A. C., Brown, K. M. & Lynch, J. P. Multiple Integrated Root Phenotypes Are Associated with Improved Drought Tolerance. *Plant Physiol.* **183**, 1011–1025 (2020).
- 44. York, L. M., Nord, E. A. & Lynch, J. P. Integration of root phenes for soil resource acquisition. *Front. Plant Sci.* **4**, 355 (2013).

- 45. Schneider, H. M. & Lynch, J. P. Should Root Plasticity Be a Crop Breeding Target? *Front. Plant Sci.* **11**, 546 (2020).
- 46. Lobet, G. *et al.* Demystifying roots: A need for clarification and extended concepts in root phenotyping. *Plant Sci.* **282**, 11–13 (2019).
- 47. Schneider, H. M. Characterization, costs, cues and future perspectives of phenotypic plasticity. *Ann. Bot.* **130**, 131–148 (2022).
- 48. Forsman, A. Rethinking phenotypic plasticity and its consequences for individuals, populations and species. *Heredity* **115**, 276–284 (2015).
- 49. Pigliucci, M. Evolution of phenotypic plasticity: where are we going now? *Trends Ecol. Evol.* **20**, 481–486 (2005).
- 50. De Kroon, H., Huber, H., Stuefer, J. F. & Van Groenendael, J. M. A modular concept of phenotypic plasticity in plants. *New Phytol.* **166**, 73–82 (2005).
- 51. Dingemanse, N. J., Kazem, A. J. N., Réale, D. & Wright, J. Behavioural reaction norms: animal personality meets individual plasticity. *Trends Ecol. Evol.* **25**, 81–89 (2010).
- 52. Schlichting, C. D. & Pigliucci, M. *Phenotypic Evolution: A Reaction Norm Perspective*. (Sinauer Associates, 1998).
- 53. Gavrilets, S. & Scheiner, S. M. The genetics of phenotypic plasticity. V. Evolution of reaction norm shape. *J. Evol. Biol.* **6**, 31–48 (1993).
- 54. Lynch, J. P. Steep, cheap and deep: An ideotype to optimize water and N acquisition by maize root systems. *Ann. Bot.* **112**, 347–357 (2013).
- 55. Lynch, J. P. & Brown, K. M. Topsoil foraging an architectural adaptation of plants to low phosphorus availability. *Plant and Soil* **237**, 225–237 (2001).

- 56. Li, B. *et al.* Are crop deep roots always beneficial for combating drought: A review of root structure and function, regulation and phenotyping. *Agric. Water Manag.* **271**, 107781 (2022).
- 57. Fitter, A. H. Architecture and Biomass Allocation as Components of the Plastic Response of Root Systems to Soil Heterogeneity. in *Exploitation of environmental heterogeneity of plants* (Academic Press, New York, NY, USA, 1994).
- 58. Fontana, M., Collin, A., Courchesne, F., Labrecque, M. & Bélanger, N. Root System Architecture of *Salix miyabeana* "SX67" and Relationships with Aboveground Biomass Yields. *Bioenergy Res.* **13**, 183–196 (2020).
- 60. López-Pintado, S. & Romo, J. On the concept of depth for functional data. *J. Am. Stat. Assoc.* **104**, 718–734 (2009).
- 61. López-Pintado, S. & Romo, J. A half-region depth for functional data. *Comput. Stat. Data Anal.* 55, 1679–1695 (2011).

Figures

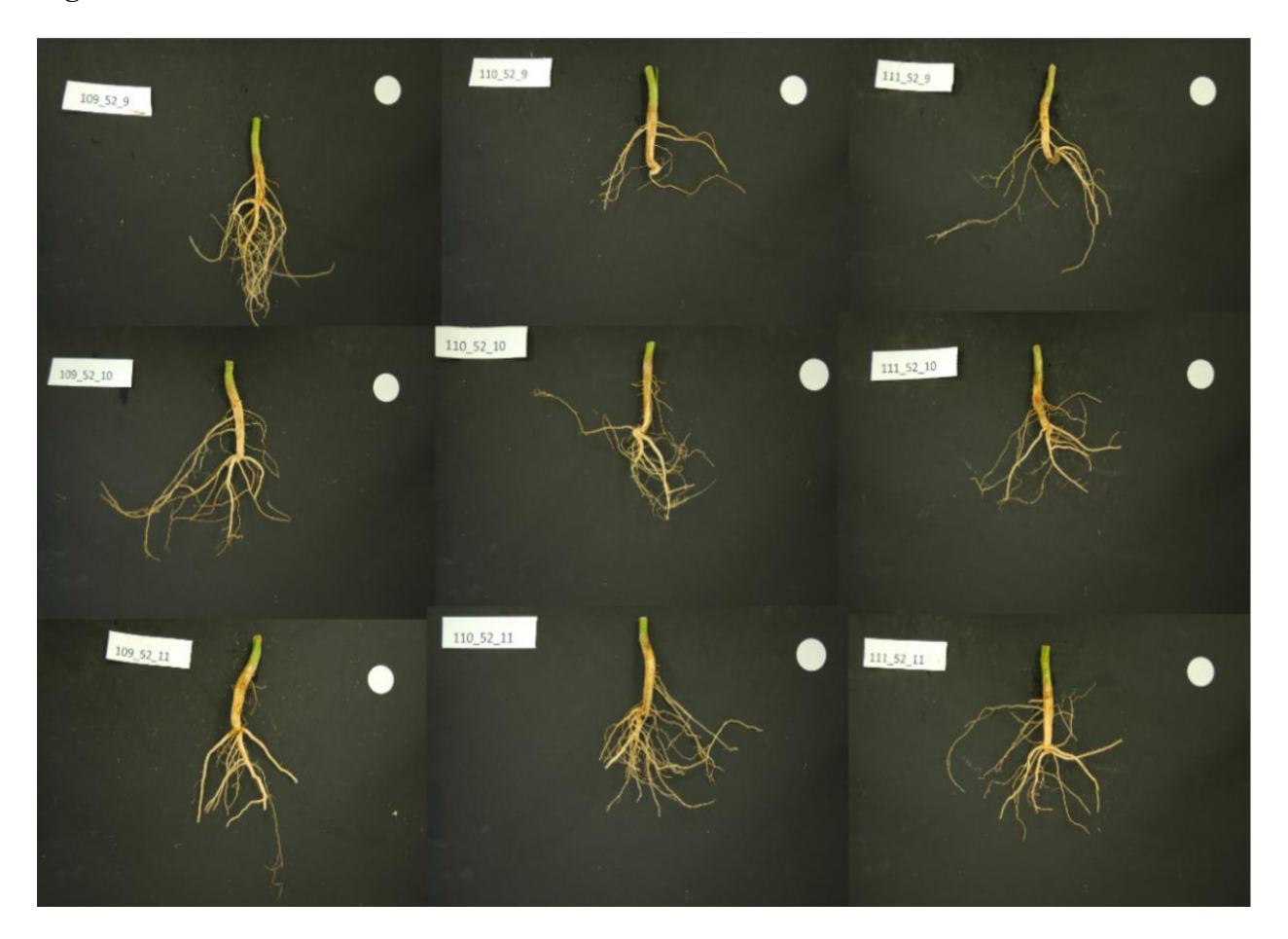


Figure 2.1: Clear architectural differences were observed among the excavated roots of neighboring DOR364 plants of DOR364 from a plot in 2016 (Willcox, AZ). These plants were excavated with Shovelomics. The tag in the picture is labelled as row-plot-column, such as root 111-52-9 is grown in 111th row and 9th column in the 52nd plot.

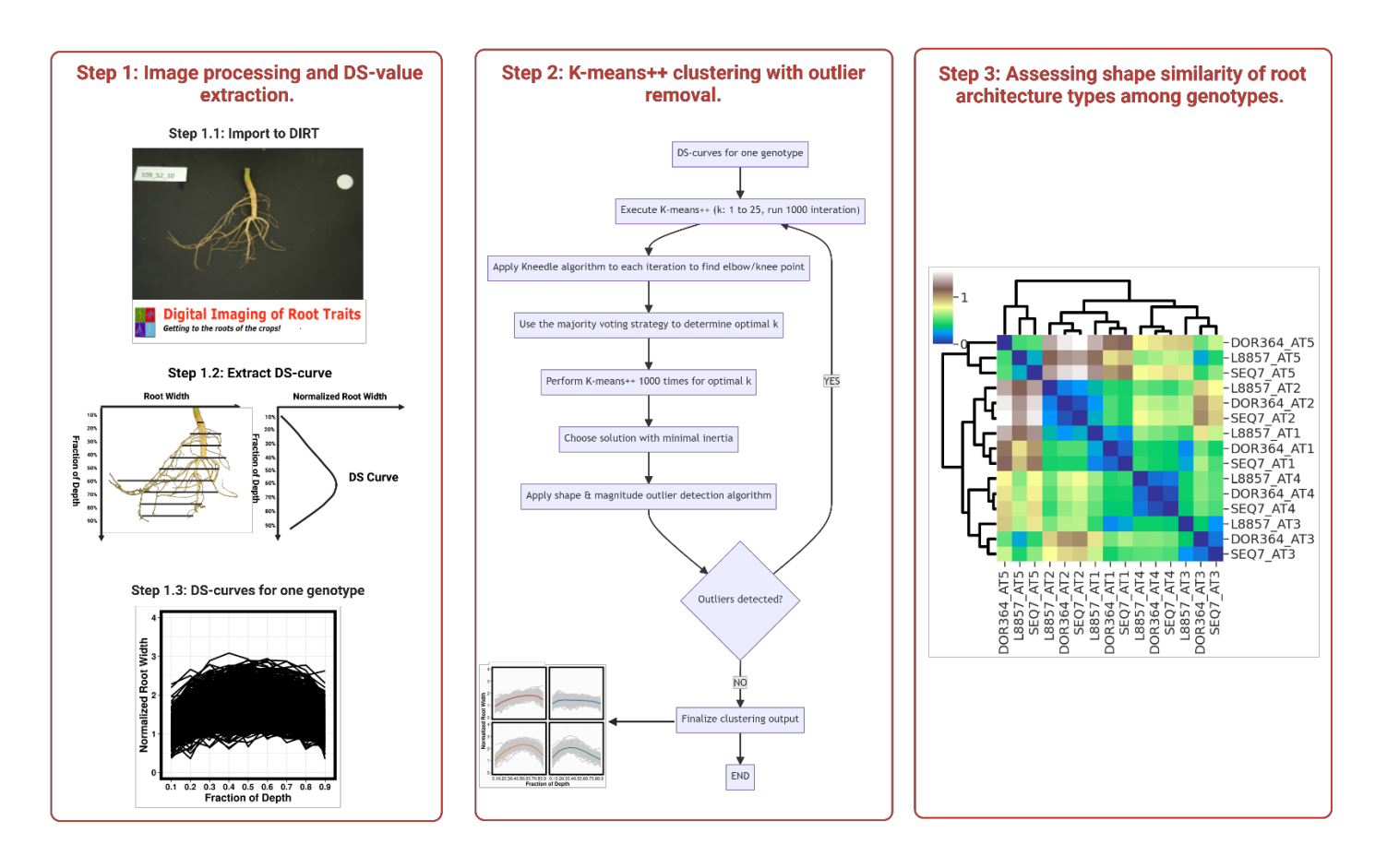


Figure 2.2: The Dirt-Pop pipeline computes the root architecture types of a single genotype. In Step 1: Root images are input into DIRT, leading to the extraction of the shape descriptor DS-curve for each genotype. In Step 2: The Kmeans++ clustering method, complemented by an outlier removal strategy, is used to cluster distinct root architecture types. In Step 3: The hierarchically clustered heatmap using a Fréchet distance matrix to assess the similarity of root architecture types across various genotypes.

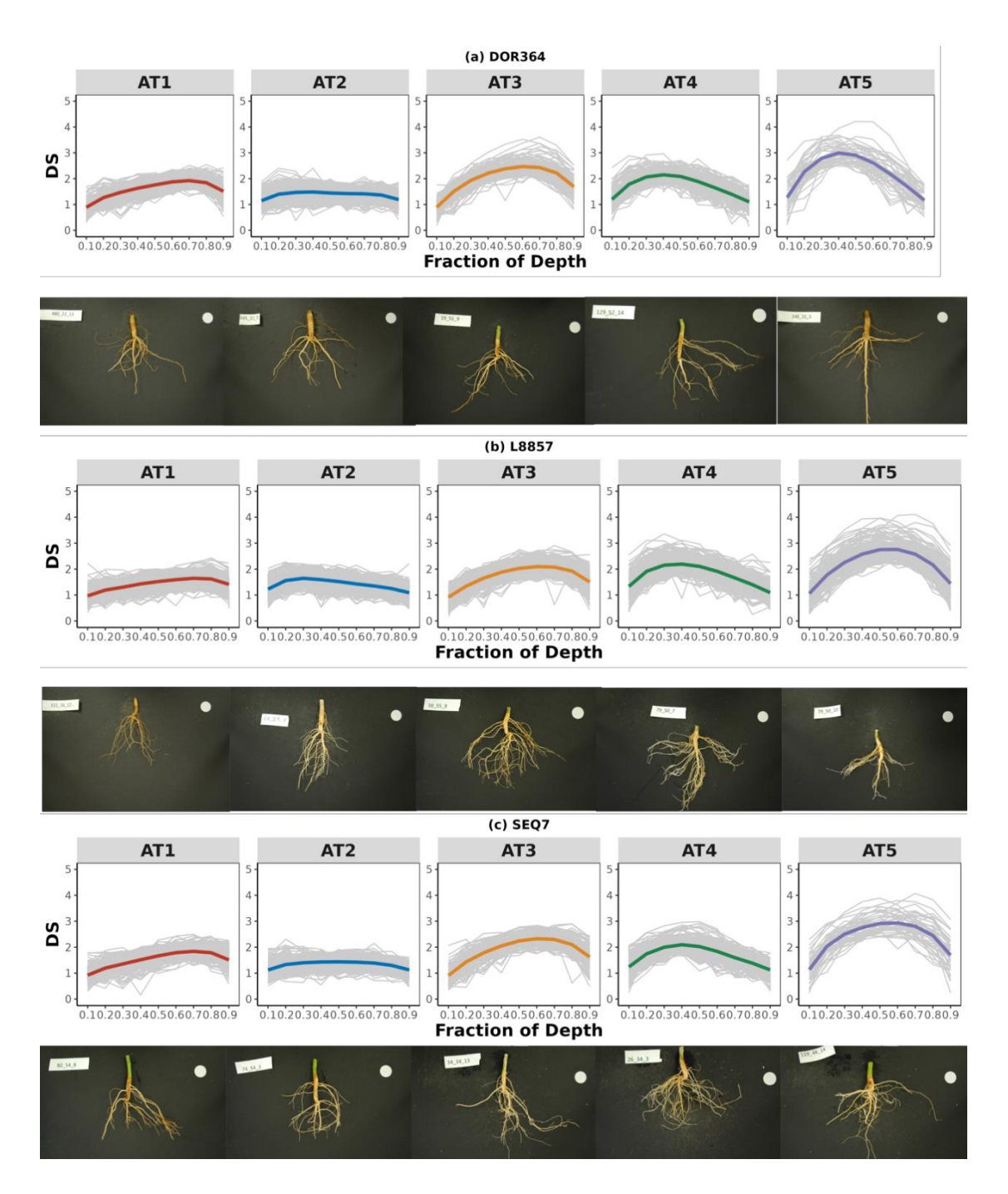


Figure 2.3: Five root architecture types of DOR364 (n=822), L8857 (n=1663), and SEQ7 (n=845) were observed across years (2015 and 2016) under non-limiting (NL) and water-limited (WL) conditions. We have graphed the mean DS curve corresponding to each root architecture type, with a representative root image displayed below. The reference marker measured 24.26 mm.

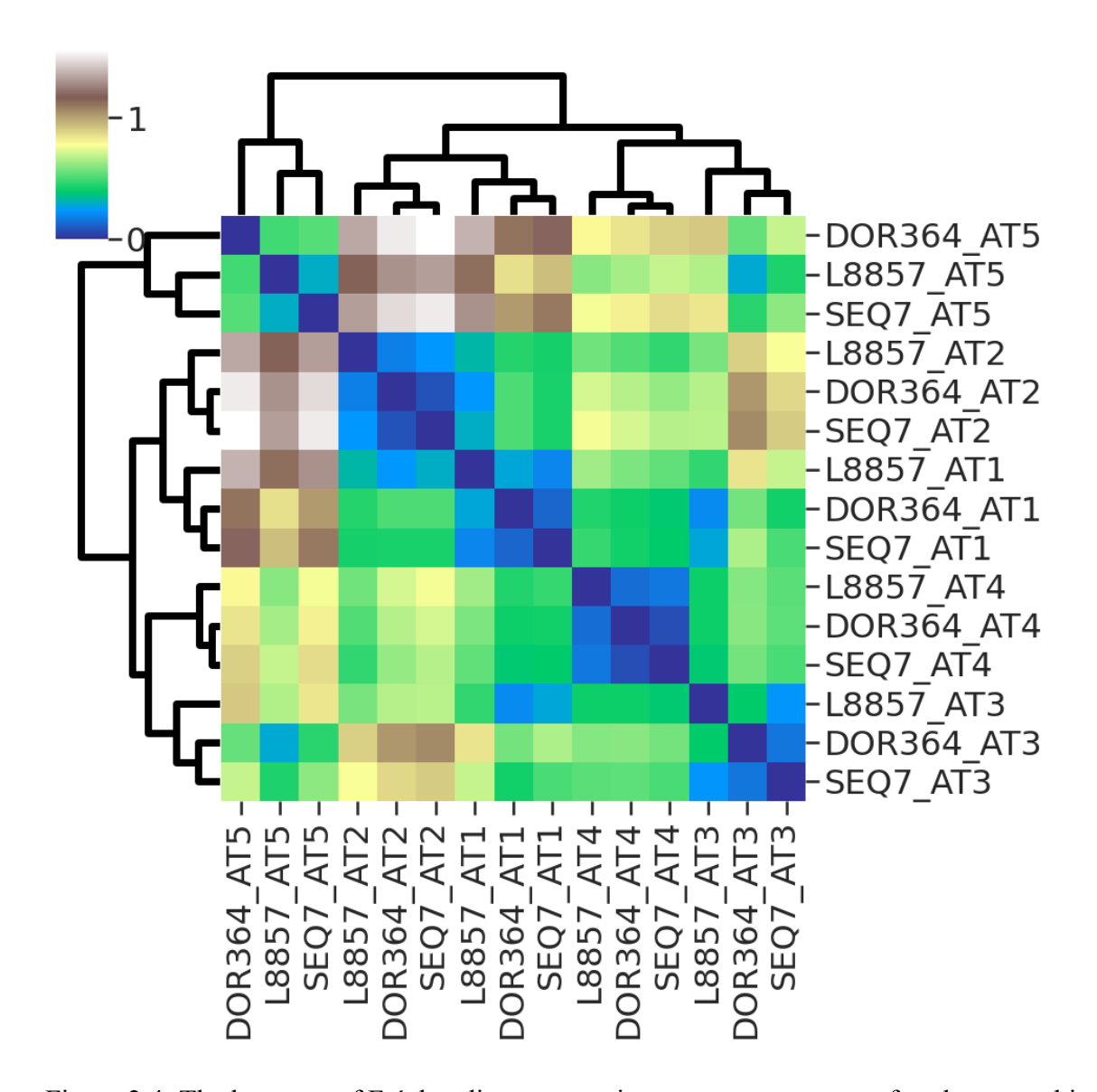


Figure 2.4: The heatmap of Fréchet distance matrix among mean curve of each root architecture type of three genotypes DOR364, L8857 and SEQ7. Each pixel's color in the heatmap corresponds to the Fréchet distance between two root architecture types, with blue representing higher similarity and brown denoting greater dissimilarity. The dendrograms on the axes represent the hierarchical clustering using wards method of the clusters based on their Fréchet distances.

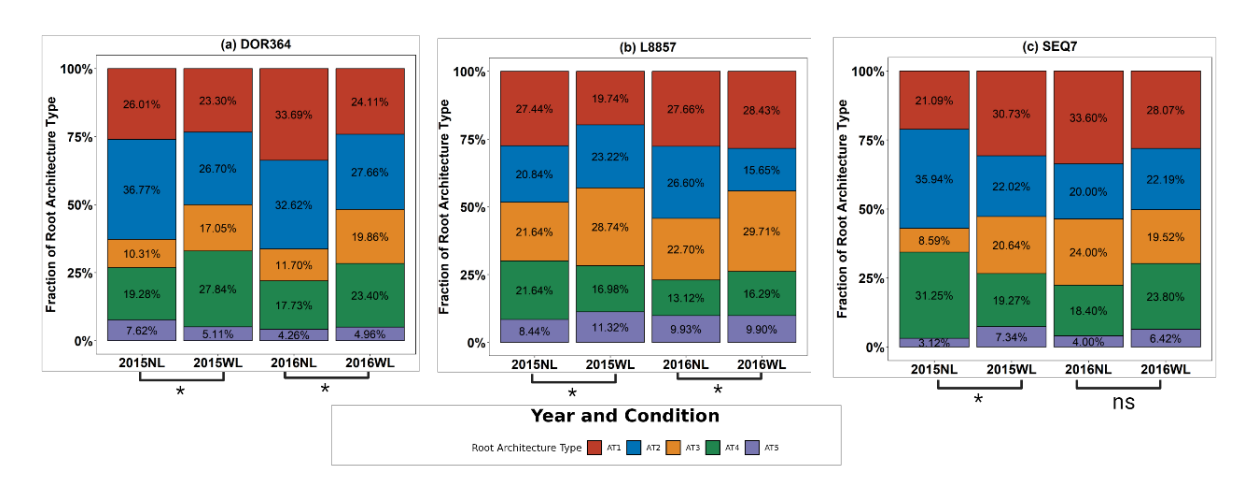


Figure 2.5: The composition of root architecture types in DOR364 (n=797), L8857 (n=1772), and SEQ7 (n=768) under non-limiting (NL) and water-limited (WL) conditions in 2015 and 2016. We used the Chi-squared test to compare the different ratios of root architecture types. The asterisk (*) denotes a significance level with a P < 0.05 while 'ns' indicates a non-significant level with a P > 0.05, as determined by a Chi-square test.

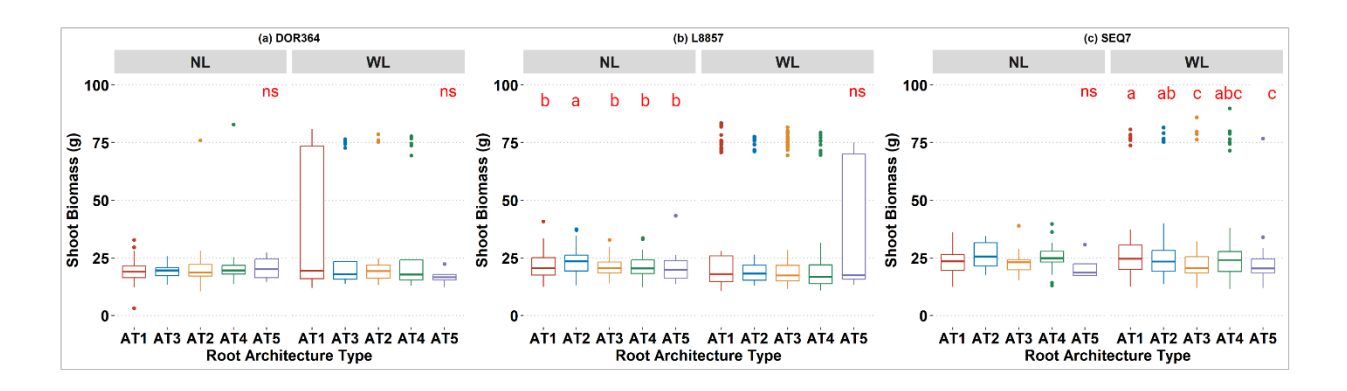


Figure 2.6: Aboveground shoot biomass of root architecture types in three genotypes DOR364 (n=401), L8857 (n=578), SEQ7 (n=490) under non-limiting (NL) and water-limited (WL) conditions in 2016. We applied Kruskal-Wallis's test and pairwise Wilcoxon rank sum test after to identify any significant differences in these traits among ATs. Different letters label ATs with significant differences, with a significance threshold set as P < 0.05. The notation ns refers not significant.

Appendix A

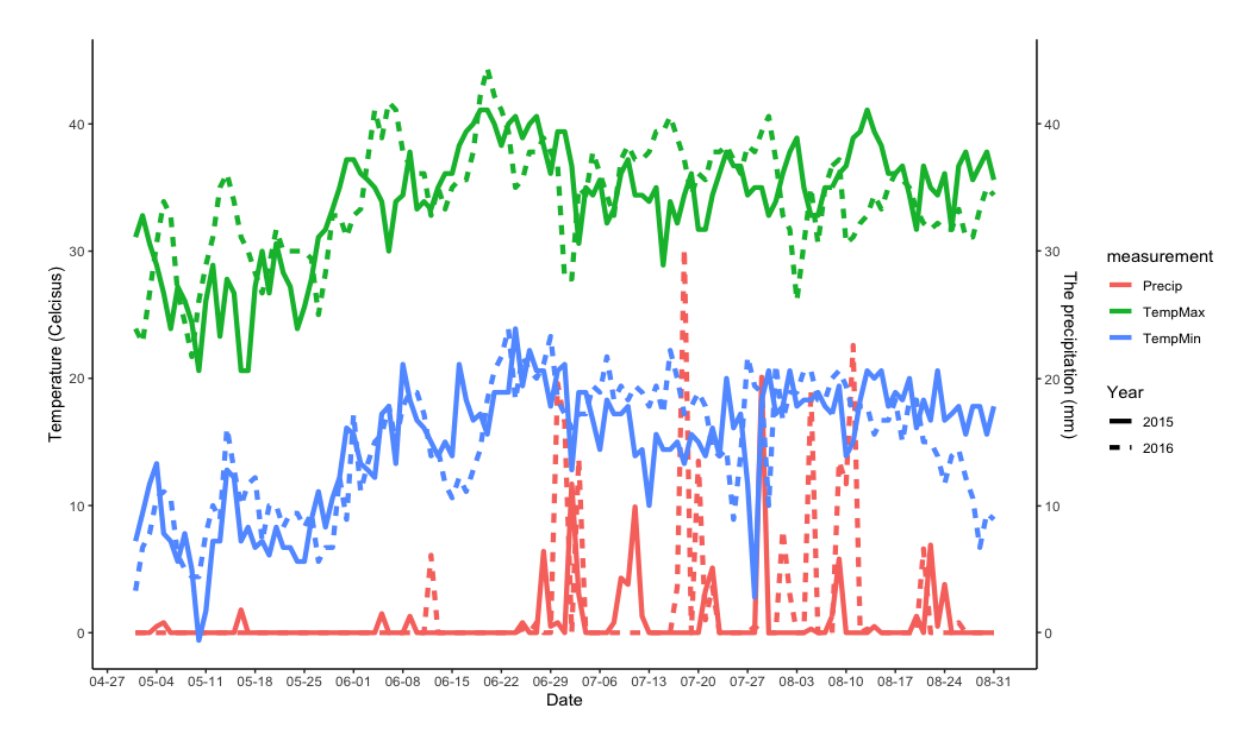


Figure S2.1: The weather information of Willcox, AZ. The dash line is for 2016, and the solid line is for 2015. The red line is the precipitation (mm), the green line is the maximum temperature of the day, and the blue line is the minimum temperature of the day.

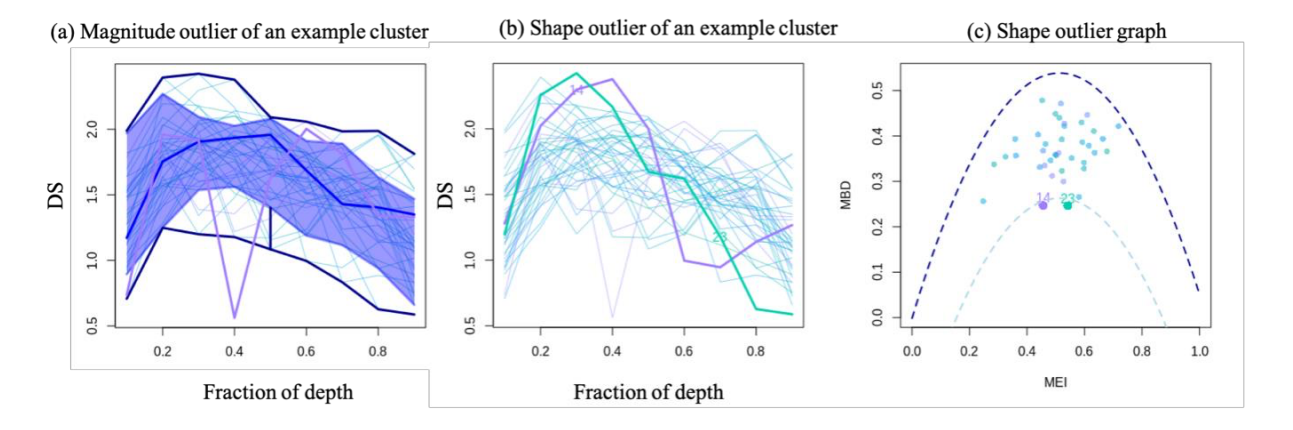


Figure S2.2: Illustration of magnitude and shape outliers in an example cluster. (a) A magnitude outlier (purple) identifies as a curve lying partially out of the 1.5 times of the central region (dark-blueish shadow band) of a univariate functional boxplot. The two board lines denote the range of maximum and minimum of DS values at each depth. (b) The two shape outliers (Dark green and purple curves) show different shapes from the rest curves. (c) The shape outlier graph detects outliers defined by MBD and MEI. Shape outliers are quantified using the modified band depth (MBD)⁶⁰ and the modified epigraph index (MEI)³¹. The MBD represents the mean probability that a DS curve lies within a band formed by two random sample curves in a single cluster⁶⁰. The MEI is an order statistic that measures a DS curve's location or centrality within a cluster^{35,61}. A shape outlier curve is identified when its distance to the parabola (the dash purple line) surpasses the third quartile plus one interquartile range³⁵.

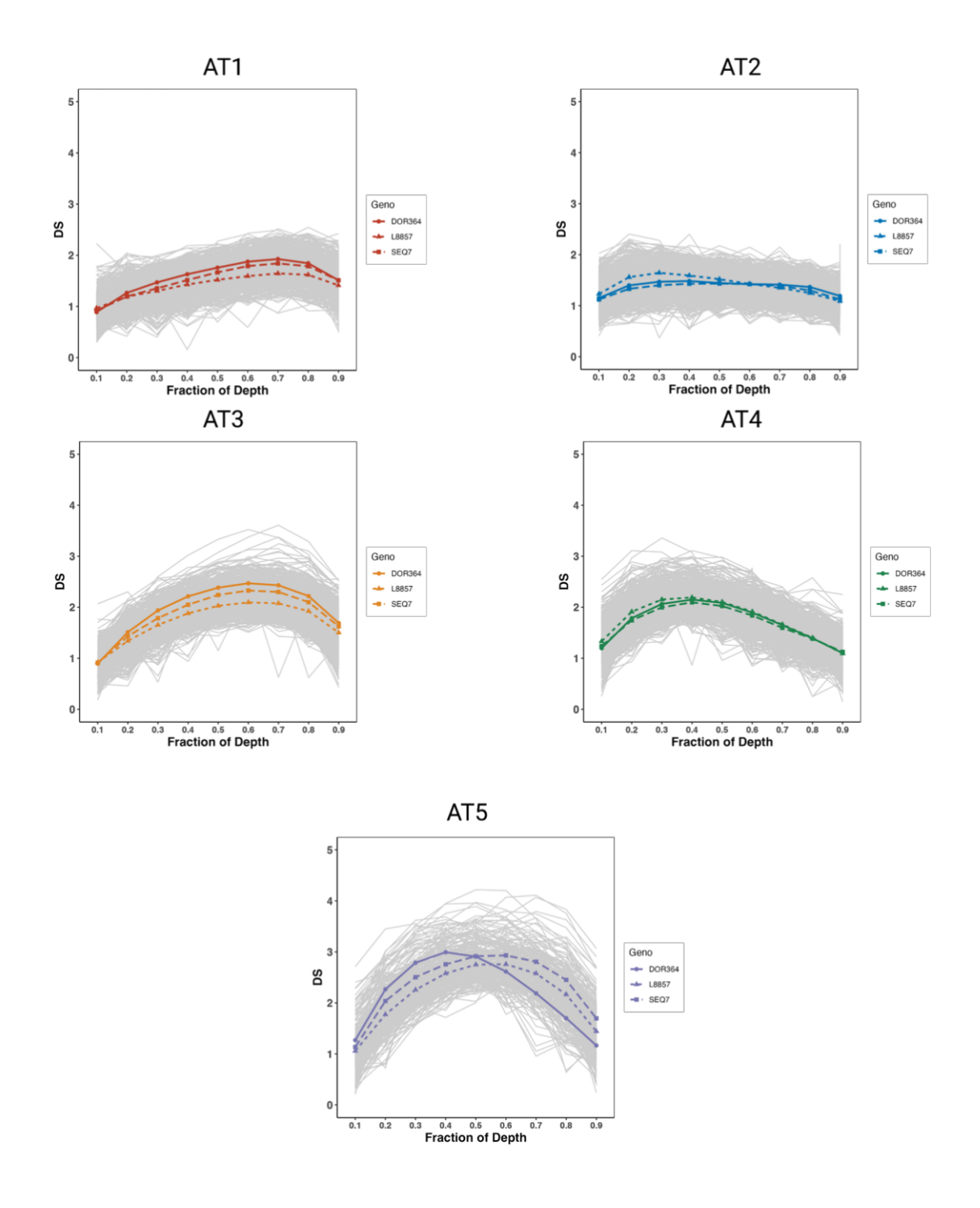


Figure S2.3: The mean DS-curves of five root architecture types of three genotypes DOR364, L8857 and SEQ7 under non-limiting and water-limited condition in 2015 and 2016.

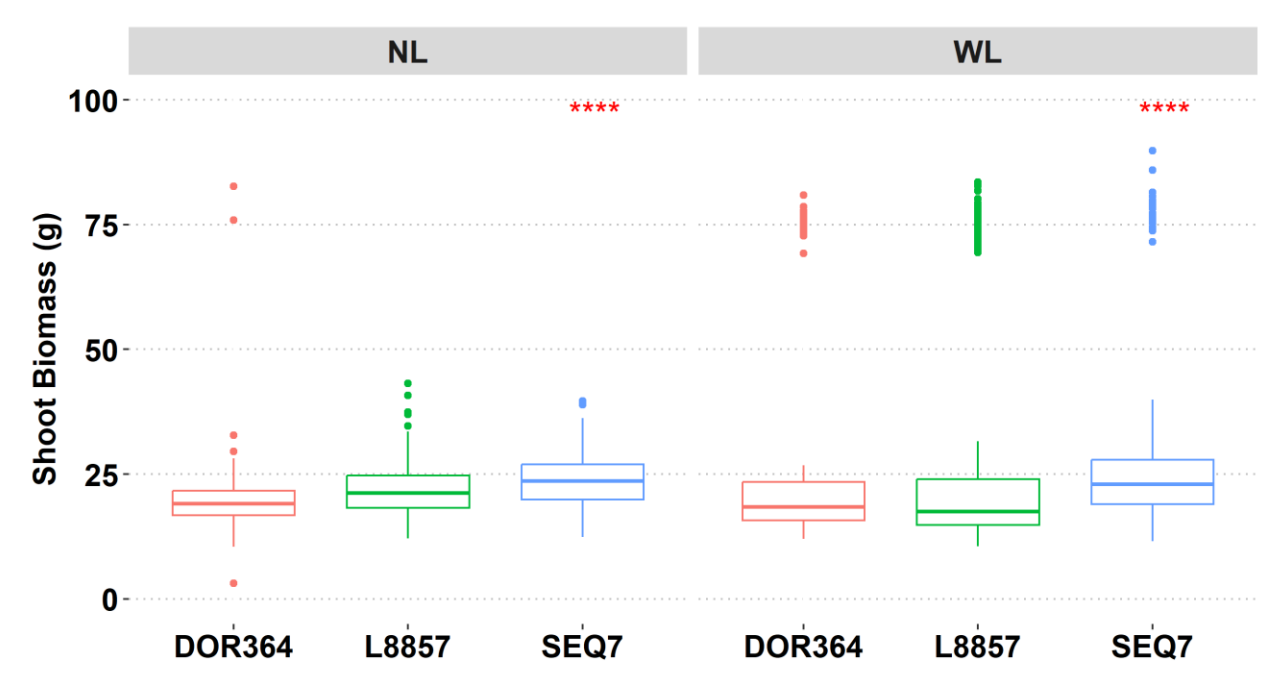


Figure S2.4: Shoot biomass of three genotypes DOR364 (n=401), L8857(n=578), SEQ7 (n=490) under non-limiting (NL) and water-limited (WL) conditions in 2016. The Kruskal-Wallis test was used to test any aboveground shoot biomass difference among genotypes under each condition. Statistical significance is denoted as: **** for P < 0.001; ** for P < 0.001; * for P < 0.05; and ns for not significant.

Table S2.1: Sample size of common bean genotypes DOR364, L8857 and SEQ7 grown under non-limiting (NL) and water-limited (WL) condition in the 2015 and 2016 field experiment at Willcox, AZ.

	DOR364	L8857	SEQ7
2015NL	258	423	135
2015WL	204	792	235
2016NL	315	311	138
2016WL	156	341	404
Total	933	1867	912

Table S2.2: The value of mean curve of each root architecture types among three genotypes DOR364, L8857 and SEQ7.

Genotype	AT	DS10	DS20	DS30	DS40	DS50	DS60	DS70	DS80	DS90
DOR364	AT1	0.89	1.26	1.47	1.63	1.76	1.87	1.93	1.84	1.51
L8857	AT1	0.97	1.19	1.30	1.43	1.52	1.59	1.65	1.62	1.41
SEQ7	AT1	0.92	1.19	1.35	1.51	1.67	1.79	1.84	1.79	1.51
DOR364	AT2	1.15	1.40	1.47	1.48	1.44	1.42	1.41	1.37	1.19
L8857	AT2	1.23	1.56	1.64	1.59	1.52	1.43	1.35	1.25	1.09
SEQ7	AT2	1.12	1.33	1.40	1.43	1.43	1.42	1.39	1.30	1.12
DOR364	AT3	0.89	1.51	1.94	2.21	2.38	2.47	2.43	2.22	1.69
L8857	AT3	0.92	1.34	1.65	1.88	2.03	2.09	2.08	1.92	1.50
SEQ7	AT3	0.91	1.43	1.79	2.05	2.24	2.33	2.30	2.10	1.62
DOR364	AT4	1.20	1.78	2.06	2.15	2.09	1.89	1.65	1.39	1.10
L8857	AT4	1.33	1.91	2.15	2.19	2.10	1.91	1.66	1.40	1.09
SEQ7	AT4	1.24	1.74	2.00	2.10	2.02	1.84	1.60	1.38	1.12
DOR364	AT5	1.27	2.27	2.79	2.99	2.91	2.62	2.19	1.70	1.16
L8857	AT5	1.06	1.77	2.26	2.58	2.75	2.76	2.58	2.17	1.44
SEQ7	AT5	1.14	2.04	2.50	2.76	2.91	2.93	2.81	2.45	1.70

Table S2.3: The summary statistics of aboveground shoot biomass among root architecture types of three common bean genotypes between conditions in 2016. 'NL' denotes non-limiting conditions and 'WL' denotes water-limited conditions.

Genotype	Condition	Root Architecture Type	Mean	Median	Interquartile Range (IQR)	Standard Deviation (SD)	Sample Size (N)
DOR364	2016 NL	AT1	19.09	18.97	5.10	4.34	91
DOR364	2016 WL	AT1	36.14	19.43	57.53	27.89	31
DOR364	2016 NL	AT2	19.93	18.64	5.08	7.09	87
DOR364	2016 WL	AT2	25.02	19.21	5.62	18.69	36
DOR364	2016 NL	AT3	19.29	19.53	3.39	3.03	31
DOR364	2016 WL	AT3	29.77	17.87	7.72	24.19	28
DOR364	2016 NL	AT4	20.91	19.51	3.77	9.51	48
DOR364	2016 WL	AT4	30.85	17.77	8.69	24.85	30
DOR364	2016 NL	AT5	20.36	20.17	8.03	4.33	12
DOR364	2016 WL	AT5	16.79	16.61	2.35	3.08	7
L8857	2016 NL	AT1	21.62	20.54	7.46	5.58	75
L8857	2016 WL	AT1	30.72	18.00	11.10	24.95	85
L8857	2016 NL	AT2	23.39	23.47	6.80	5.31	73
L8857	2016 WL	AT2	28.11	18.19	6.58	22.85	48
L8857	2016 NL	AT3	21.08	20.53	4.73	3.68	62
L8857	2016 WL	AT3	28.96	17.40	6.70	24.22	92
L8857	2016 NL	AT4	21.24	20.48	5.90	4.73	37
L8857	2016 WL	AT4	28.04	16.83	8.17	23.85	50
L8857	2016 NL	AT5	20.73	19.89	7.72	6.02	28
L8857	2016 WL	AT5	32.88	17.51	54.27	25.68	28
SEQ7	2016 NL	AT1	23.05	23.45	6.78	4.87	42
SEQ7	2016 WL	AT1	29.29	24.56	10.58	16.74	103
SEQ7	2016 NL	AT2	26.16	25.56	10.05	5.41	25
SEQ7	2016 WL	AT2	26.85	23.35	9.13	14.54	79
SEQ7	2016 NL	AT3	22.85	23.11	4.45	4.81	29
SEQ7	2016 WL	AT3	24.36	20.54	7.04	14.40	72
SEQ7	2016 NL	AT4	25.16	24.84	4.61	6.11	23
SEQ7	2016 WL	AT4	27.13	24.11	8.70	16.00	89
SEQ7	2016 NL	AT5	21.24	18.54	5.12	6.41	4
SEQ7	2016 WL	AT5	25.58	20.46	6.10	16.46	24

Table S2.4 The summary statistics of aboveground shoot biomass among three common bean genotypes between conditions in 2016. 'NL' denotes non-limiting conditions and 'WL' denotes water-limited conditions.

Genotype	Condition	Mean	Median	Interquartile Range (IQR)	Standard Deviation	Sample Size (N)
DOR364	NL	19.76	19.08	4.90	6.37	269
DOR364	WL	29.53	18.45	7.66	23.54	132
L8857	NL	21.82	21.20	6.55	5.13	275
L8857	WL	29.53	17.53	9.14	24.18	303
SEQ7	NL	23.97	23.59	7.05	5.37	123
SEQ7	WL	27.03	22.95	8.91	15.65	367

CHAPTER 3

FROM OUTDOOR TO INDOOR CONDITIONS: THE ROOT ARCHITECTURE TYPES AND THEIR CHANGE OVER THE DEVELOPMENTAL STAGES IN COMMON BEAN

Introduction

Plant roots display a wide range of architectural types, each with unique spatial organization and shape characteristics. Variation in root architecture is considerable both within and among genotypes in response to diverse environmental conditions. Chapter 2 presented DIRT-Pop, a computational pipeline to cluster these variations into distinct root architecture types. Notably, even one genotype of common bean with relatively similar genetic background, exhibited five distinctive root architecture types when grown in a common field. According to the quantitative genetic model, phenotypic variation can be assumed as the summation the variation of genetic (G) and environmental (E) variation, and their interaction¹⁻³. Hence, the five distinctive root architecture types observed from one common bean genotype under the one watering condition are commonly assumed from the variation within the environment, mainly due to the patchy soil conditions in fields^{4,5}. Numerous plant species modify their root systems in response to the heterogeneity in resources availability during development^{5,6}. Given this reason, one question this chapter seeks to address is: if environmental variation is reduced, will these diverse root architecture types still be observed in common bean populations?

When examining a population at the level of individual plants, the root architectural variation may stem from the root-root interactions and/or as a result of the genetics driving the developmental program of the root⁷. Such differences could be a result of the strategies plants

use for nutrient competition with their neighbors. Current research indicates that neighboring roots might alter their root architecture, either growing into the same space to increase competition or avoiding already occupied zones to avoid competition, depending on the identity of the neighboring roots^{8,9}. Plants can differentiate the relatedness of neighbors¹⁰ and alter their response to their neighbors. For example, that the sea rocket (Cakile edentula) had less root allocation when planted with kin-groups than with strangers¹¹. Some species also avoid belowground competition by reducing root branching intensity and specific root length in response to kin neighbor¹². Wuest et al (2022) even showed an allele with major effect on increased "cooperation" and productivity in high-density planting in Arabidopsis thaliana¹³. Such "cooperation" was quantified by reduced root allocation and a trade-off between group versus individual performance matrix¹³. As a result, plants change their root architecture according to their neighbors and have the genetic that detect and regulate the response to these neighboring plants. Thus, elucidating how these root architectural types change from the initial growth stages to full maturity, we can gain a deeper understanding how plants optimize resource uptake within population over time.

Root architecture is important for water and nutrients uptake and therefore can impact the plant productivity. Lynch (2019) first proposed three bean root architecture ideotypes for distinct nutrient uptake function under specific environmental conditions¹⁴:

1. "Steep, cheap, deep" (SCD) ideotype, optimized for deep soil exploration and mobile resources like water, leached nitrate (N) and sulfur (S). It has fewer basal root whorls, fewer adventitious roots, and a steep basal root growth angle.

- "Topsoil foraging" (TF) ideotype focuses on topsoil resources such as phosphorus
 (P), potassium (K), calcium (Ca), and magnesium (Mg). It is characterized by a shallow basal root angle and a higher number of adventitious roots.
- 3. The standard ideotype balances both deep and shallow soil exploration, with a medium basal root angle and average numbers of adventitious roots and basal whorls.

Greenhouse experiments confirmed that SCD ideotype in common beans showed superior performance under drought stress¹⁵. In contrast, the TF ideotype was more effective under phosphorus stress, while the standard ideotype showed resilience under both phosphorus and drought stress conditions¹⁵. A recent study provided detailed insights into root architecture phenotypes, by modeling 12 root architectures with variations in basal root whorl numbers (1-4 whorls) and growth angles (shallow, fan, deep), it was demonstrated that multiple root architecture phenotypes might be optimized for a specific environment rather than only one root ideotype optimized for one environment¹⁶. However, both greenhouse and simulation studies had limitations, primarily due to restricted sample sizes of 4 to 6 plants per genotype or root architecture phenotype^{15,16}. Specifically, the greenhouse study⁹ was performed in pots. Given that the pot size may restrict root growth and there's no interaction with neighboring plants, this could lead to biases when predicting biomass or plant productivity in field plots where plants grow in a population setting. Recognizing these limitations, optimizing for experimental setups that better replicate field conditions to accurately assess root architecture's impact on plant productivity are needed. This has led us to develop a mesocosm system that can accommodate larger sample sizes and allow for root interactions.

By using such a mesocosm system, we explore the relationship between root architecture and biomass allocation in plants, particularly focusing on how different root architecture types

influence shoot and root biomass under varying water conditions that grow in a population setting. Plants respond to environmental changes by modulating their biomass allocation and root architectural traits^{17,18}. A key area of interest is whether changes in root architecture leads to alterations in biomass allocation. For example, under drought stress, plants may not only develop deeper root systems (an architectural response) but also may increase biomass allocated to the roots (an allocation response) to access deeper water sources ^{19,20}. This interplay between root architecture and allocation also underscore potential trade-offs in biomass distribution between roots and shoots, where plants invest heavily in root biomass (allocation) to develop a particular root architecture (e.g., extensive lateral of roots for water acquisition) may limit the biomass available for shoot development 19,20. However, it is also important to point out that while root architectural changes can result in biomass allocation changes, they can also occur without changes in allocation, suggesting a level of independence between these two responses²¹. Through examining the influence of root architecture types on shoot and root biomass, as well as biomass allocation between these components across developmental stages, we seek to better understand how individual plants within a population holistically respond to different water conditions through root acclimatization.

To sum up, in Chapter 3, we built an indoor field, also a mesocosm system, which was filled with well-mixed homogenous growth medium and equipped with a sensor-regulated irrigation system, to achieve precisely controlled water distribution throughout the system. Using this setup, we can grow plants into mature stages without container restriction and allowing plants to interact with each other. By growing a time-series trial with genotype SEQ7 over different growth stages and genotype DOR364 at mature stage, we aim to answer the following questions:

- 1. Can we observe multiple root architecture types of DOR364 and SEQ7 in the mesocosm system?
- 2. How does the compositions of root architecture types of SEQ7 change across growth stages and under NL and WL conditions?
- 3. Are there differences in shoot biomass, root biomass and root-shoot ratio among root architecture types of SEQ7 throughout growth stages under WL and NL conditions?
- 4. Can we match observed root architecture types with a recent published 12-root architecture models¹⁶, thereby offering insights into nutrients uptake functions of these root architecture types?

Materials and Methods

The mesocosm system setup

We built a mesocosm system (W: 548.64 cm, L:670.56 cm, D: 55.88 cm) to mimic desert soil conditions in The University of Georgia campus in Athens, GA²². We first put one layer (~ 4 cm depth) of marble rocks (The Quikrete Companies, Atlanta, GA, USA) at the bottom. We then filled in with well-mixed growth medium, composed of the following compounds (by volume) 33.23% coarse A3 vermiculite (Palmetto Vermiculite, Woodruff, SC, USA), 44.30% fine grade pine bark (Fernacres Farms, Washington, GA, USA), 22.15% river bottom sand (L.C Curtis & Son, Watkinsville, GA, USA), 0.18% ground limestone (Austinville Limestone Company, Austinville, VA, USA), 0.0466% superphosphate (Voluntary Purchasing Groups, Inc., Bonham, TX, USA), 0.0223% calcium nitrate (Yara North America, Tampa, FL, USA), 0.0223 % potassium nitrate (Haifa Group, Altamonte Springs, FL, USA), 0.0223% calcium sulfate dihydrate (Performance Mineral Corps, Saint John, IN, USA), 0.0223% micronutrients (ICL

Fertilizers, Dublin, OH, USA). The mixed growth medium had an average pH of 5.6, and an average lime buffer capacity of 461.83.

To regulate the water distribution in the mesocosm system, we installed a sensor-based irrigation system comprising 64 sensors (EC-5; Decagon Devices, Pullman, WA, USA) placed at two soil depths of 15.24 cm and 38.10 cm. The sensors' horizontal locations are detailed in the Figure S3.1. All the sensors were connected to a datalogger (CR1000, Campbell Scientific, Logan, UT, USA) via two multiplexers (AM16/32B, Campbell Scientific, Logan, UT, USA). The output from the sensors, initially being in voltage, was converted into volumetric water content (vwc) using a growth-medium specific calibration equation (vwc = (voltage/1000) * 1.4377-0.4096, r²=0.995). The decision to initiate irrigation for each plot (4 plots in total) was based on the average vwc of its 16 sensors in each plot. When this average vwc dropped below a pre-set threshold, the irrigation system was activated for 10 seconds specifically for that plot. We also recorded the average vwc value from each sensor every 30 minutes.

Plant growth condition and experimental design

We conducted a time series trial with the common bean genotype SEQ7(Figure S3.2). This trial included growing the SEQ7 genotype at different stages: 7 (Unifoliate, VC), 14 (Trifoliate, V1), 21 (Second-third trifoliate leaf, V2-V3), 42 (Vine development, V8), 63 (50%-Full seeds, R6-R7), and 90 (Full maturity, R8-R9) days after sowing (DAS). For the 7, 14, 21, and 42 DAS, the threshold of vwc was set at 30% to simulate NL conditions. For the 63 and 90 DAS stages, two different water conditions were implemented: WL and NL conditions. For the WL condition, we initially maintained the irrigation threshold at an average 30% vwc, subsequently changed it to 20% vwc during the vine developmental stages, thereby limiting the

water supply for the remainder of the growth period. The daily average vwc over all the growth stages and conditions of SEQ7 were plotted in the Figure S3.3.

We also grew the genotype DOR364 until it reached full maturity (R8-R9), under two different water conditions: WL and NL conditions. This genotype took 84 days after sowing (DAS) to reach full maturity. For the WL condition, in alignment with the approach used in the SEQ7 experiments, the irrigation threshold for WL conditions was adjusted from 30% to 20% vwc during the vine development stage. For the NL condition, a constant irrigation threshold at 30% vwc was maintained throughout the growth cycle.

The SEQ7 and DOR364 seeds used in this experiment were self-fertilized and collected from multiple locations within the pods of plants that were grown in pots in a greenhouse. All plants were sown following a completely randomized design with an in-row spacing of 28.88 cm and an out-row spacing of 33.53 cm. To ensure sufficient nutrient supply, we applied 4.81 kg of Osmocote (18-6-12 NPK; ICL Specialty Fertilizer, Dublin, Ohio) evenly across the mesocosm system before each planting cycle. Alongside this, we applied routine pesticide treatment. We controlled the greenhouse temperature at 20 °C during the night and 25 °C during the day, with a photoperiod of 16 hours of artificial light and 8 hours of darkness.

Trait measurement

We used the legume Shovelomics method to excavate SEQ7 roots at each designated growth stage and DOR364 roots at mature stage. After excavation, we cleaned them with tap water to remove the growth medium. For roots older than 42 DAS (including 42 DAS), where the mature root phenotype can be observed²³, we used the standard DIRT imaging protocol^{24,25} for capturing root images. However, for younger roots (less than 42 DAS), we revised the imaging step of DIRT protocol. We placed these younger roots in a plastic tray filled with water

and we positioned LED lights around the tray to ensure even illumination. We captured images of these roots in a darkroom specifically to minimize the impact of overhead room light and its reflection on the water, which could compromise the quality of the images. The images were subsequently analyzed by DIRT^{24,25}. The shoot and root tissues dried in an oven in 60 °C degrees for at least 72 hours and weighed using a digital scale (Model CQT202, Readability 0.01g, Adam Equipment, Oxford, CT, USA).

Statistical analysis

We applied the DIRT-Pop pipeline, as developed in Chapter 2, for clustering root images from all developmental stages of SEQ7 and for the mature stages of DOR364. The DIRT-pop pipeline was run at the genotype level. The sample size of SEQ7 at each designated growth stage and DOR364 at mature stage is listed in Table S3.1. Following the identification of the root architecture types of SEQ7, we conducted statistical analyses in R (v 4.2.0)²⁶. Specifically, we applied the pairwise Chi-square test of homogeneity to investigate whether the distribution of root architecture types was uniform across various developmental stages and conditions. To analyze the differences in shoot biomass, root biomass, and root-shoot ratio among root architecture types, we used the Kruskal-Wallis test, followed by pairwise Wilcoxon rank-sum tests.

Matching simulated root architecture models and excavated root architecture type using anelastic registration approach

The elastic registration method using Fisher-Rao Riemannian metric^{27,28} was used to align the DS curves of simulated root architecture models¹⁶ with the mean DS curve of root architecture types observed at 42 DAS. Images of 12 simulated root architecture models, varying in three root angles (Shallow, Fan, Deep) and 4 basal whorl numbers¹⁶, were imported into DIRT

to obtain the DS curves. As the simulated root architecture models represented the non-destructive root system without the stem, and excavated root samples included the stem up to the first node and omitted the deepest root parts, we removed the DS90 from the DS curves of simulated root architecture models and DS10 from mean DS curve of root architecture types, retaining eight DS values for both curve types. Using the scikit-fda Python package²⁹, we performed the elastic registration on the DS curves from the 12 simulated root architecture models, aligning them to the mean DS curve of the observed root architecture type. For each alignment:

D1 was calculated as the Euclidean distance between the transformed DS curve of simulated root architecture and the mean DS curve of the observed root architecture type, representing a measure of alignment accuracy. A smaller D1 value indicates a closer resemblance of the transformed simulated DS curve to the mean DS curve of the root architecture type.

D2 was calculated as the Euclidean distance between the original and transformed DS curves of the simulated root architecture, thereby quantifying the extent of the transformation. A smaller D2 suggests less modification of the simulated root architecture's DS curve during registration.

To determine the most representative simulated root architecture model for each root architecture type, we examined the 12 alignments corresponding to each observed root architecture type. The model with the smallest geometric mean (G) of D1 and D2 was selected as the most representative of the observed root architecture type. This selection criterion implies that the selected simulated root architecture model underwent minimal transformation yet achieved the closest alignment with the observed root architecture type.

Results

S3.2)

Five root architecture types of SEQ7 and DOR364 were identified in the mesocosm system.

Five different root architecture types showed in the SEQ7 genotype throughout all the developmental stages (Figure 3.1). The sample sizes for each root architecture type at each growth stage and water condition are detailed in Table S3.1. The Fréchet distance matrix also confirmed that the five root architecture types AT1 through AT5, are distinct from each other (Figure 3.2). However, within each individual architecture type, a consistent similarity is observed across different growth stages and conditions (Figure 3.2). By examining the mean value of DS curve of each root architecture type in Table S3.2, AT1 had the maximum width accumulation at 60-80% excavated rooting depth (Table S3.2). AT2 accumulated width at an almost steady rate over the excavated rooting depth (Table S3.2). Meanwhile, AT3 achieved its maximal width at 60-80% depth, although with a higher rate of width accumulation compared to AT1 (Table S3.2). AT4's width accumulation peaked at approximately 40%-50% depth, gradually decreasing until 90% excavated rooting depth (Table

Similarly, DOR364 showed five root architecture types when at full mature stage (
Figure 3.3:). The five root architecture types showed in DOR364 were similar compared with SEQ7 (Figure 3.4). The analysis of the mean DS curve values (Table S3.3) revealed: AT1 had its maximum width accumulation at 80% excavated rooting depth (Table S3.3). AT2 maintained an almost uniform width accumulation over the excavated rooting depth (Table S3.3). AT3 achieved its maximal width at 70-80% depth, although with a higher rate of width accumulation compared to AT1 (Table S3.3). AT4's width accumulation peaked around 50-60% depth, then gradually decreased until 90% excavated rooting depth (Table S3.3). AT5 reached

maximal width at the mid-point (50%) of the depth, with a higher rate of width accumulation compared to the other root architecture types (Table S3.3).

The composition of root architecture types changed over developmental stages and between conditions.

SEQ7 showed significant shifts in the composition of root architecture type during certain growth stages and under varying water conditions (Figure 3.5 and Table S3.4). From 7 to 13 DAS, the composition of root architecture type did not differ significantly (Chi-squared Test, P=0.296), with AT2 representing the smallest portion of the population and AT3, the largest from 13 to 21 DAS (Figure 3.5 and Table S3.4). From 13 to 21 DAS, a significant shift was observed. At DAS 21, there was an increase in the compositions of AT1 and AT2, accompanied by a decrease in AT3 and AT5 (Chi-squared Test, P<0.001; Figure 3.5 and Table S3.4). From 21 DAS to 42 DAS, the composition of root architecture type did not exhibit significant changes (Chi-squared Test, P=0.271; Figure 3.5 and Table S3.4). Reduced water availability from 42 DAS did not significantly impact the transition in the composition of root architecture type from 42 to 63 DAS under WL conditions (Chi-square Test, P=0.776; Figure 3.5 and Table S3.4). Yet, further water reduction led to a significant shift in the composition of root architecture types from 63 DAS to 90 DAS, characterized by a decrease in AT4 and an increase in AT1 (Chisquared Test, P=0.0193; Figure 3.5 and Table S3.4). Under NL conditions, there was a significant shift in the composition of root architecture type from 42 to 63 NL DAS, evidenced by an increase in AT3 and a decrease in AT4 (Chi-squared Test, P=0.018; Figure 3.5 and Table S3.4). At 63 DAS and 90 DAS, the composition of root architecture types exhibited significant differences between NL and WL conditions (Chi-squared Test, P=0.017; Figure 3.5 and Table S3.4) and 90 DAS (Chi-squared Test, P=0.048; Figure 3.5 and Table S3.4).

Shoot biomass, root biomass and root-shoot ratio were changed over the developmental stages and conditions but not among root architecture types.

The shoot biomass of SEQ7 population increased over the growth stages in NL conditions (Figure 3.6 and Table S3.5). However, with a limited water supply after 42 DAS, the shoot biomass increased until 63 DAS, followed by a reduction towards 90 DAS (Figure 3.6 and Table S3.5). The root biomass of SEQ population showed a similar trend in both NL and WL conditions, with an increase until 63 DAS and subsequently decreased to 90 DAS (Figure 3.6 and Table S3.5). The root-shoot ratio of SEQ7 initially rose from 7 DAS to 13 DAS and then decreased throughout the remaining growth stages under NL condition (Figure 3.6 and Table S3.5). In contrast, after limiting water supply at 42 DAS, the root-shoot ratio decreased until 63 DAS and then increased at 90 DAS (Figure 3.6 and Table S3.5). Limitations in water supply led to significant decreases in shoot biomass, root biomass at 63 DAS and 90 DAS compared to NL conditions (Figure 3.6 and Table S3.5). Interestingly, the root-shoot ratio was higher at 63 DAS but lower at 90 DAS under WL conditions compared to NL (Figure 3.6 and Table S3.5).

Generally, no significant difference in shoot biomass, root biomass or root-shoot ratio was found among ATs throughout most developmental stages. However, there were some exceptions. Specifically at 7 DAS, AT5 had a significantly higher shoot biomass than AT1, AT2, AT3 (Wilcoxon rank-sum test, P <0.05; Figure 3.6). At 90 DAS under NL condition, AT2 showed a significantly higher shoot biomass than other four root architecture types (Wilcoxon rank-sum test, P <0.05; Figure 3.6). At 42 DAS, AT1 and AT2 had a significant higher root biomass than AT3, AT4, AT5 (Wilcoxon rank-sum test, P <0.05; Figure 3.6). AT2 had significant higher root biomass than AT1, AT3, AT4 at 90 DAS under NL condition (Wilcoxon

rank-sum test, P < 0.05; Figure 3.6). Regarding the root-shoot ratio, AT5 had a significantly lower ratio compared to AT1, AT3, and AT4 (Wilcoxon rank-sum test, P < 0.05; Figure 3.6). Root architecture type observed may link to root simulation models.

To help understand the potential functions of the identified root architecture types, we matched 12 simulated root architecture models (40 days old) with excavated root architecture types observed at 42 DAS. The alignment results were quantified by the metrics D1 (alignment accuracy) and D2 (transformation extent). Table S3.6 presented the alignment results for each simulated root architecture model across the five root architecture types. For AT1, model 5 (Fan angle, 1 whorl) showed the most accurate alignment (D1=0.134, D2=1.459, Figure 3.7; Figure S3.5; Table S3.6), resulting in the lowest geometric mean of 0.442. This indicates a high degree of resemblance to the observed root architecture type with minimal transformation required. In contrast, model 9 (Shallow angle, 1 whorl) showed a low match for AT1 (D1=0.382, D2=2.547, G = 0.986, Figure 3.7; Figure S3.5; Table S3.6), suggesting a significant transformation was needed for alignment. Moving to AT2, the closest match was with model 10 (Shallow, 2 whorls, D1=0.062, D2=0.500, G=0.176, Figure 3.7; Figure S3.5; Table S3.6), indicating a highly accurate alignment with the observed root architecture type. Conversely, model 9 (Shallow angle, 1 whorl) for AT2 showed a less precise alignment (D1=0.176, D2=3.372, G=0.770, Figure 3.7; Figure S3.5; Table S3.6). For AT3, model 3 (Deep angle, 3 whorls) aligned most accurately (D1=0.155, D2=2.641, G=0.639, Figure 3.7; Figure S3.5; Table S3.6), demonstrating a good balance between resemblance and transformation extent. On the other hand, model 12 (Shallow, 4 whorls) for AT3 had a higher geometric mean (D1=0.484, D2=2.909, G=1.187, Figure 3.7; Figure S3.5; Table S3.6). In the case of AT4, model 6 (Fan, 2 whorls) was the best match (D1=0.443, D2=1.898, G=0.917, Figure 3.7; Figure S3.5; Table S3.6), showing moderate

matching accuracy. However, model 1 (Deep angle, 1 whorl) for AT4 required a significant transformation for alignment (D1=1.106, D2=2.977, G=1.814, Figure 3.7; Figure S3.5; Table S3.6). Lastly, for AT5, model 9 (Shallow, 1 whorl) showed the most satisfactory alignment (D1=0.392, D2=1.015, G=0.631, Figure 3.7; Figure S3.5; Table S3.6). In contrast, model 12 (Shallow, 4 whorls) for AT5 indicated a considerable transformation for alignment (D1=0.780, D2=4.173, G=1.804, Figure 3.7; Figure S3.5; Table S3.6).

Discussion

Consistent five root architecture types were observed across the mesocosm and field conditions.

In the mesocosm system, we identified five distinct root architecture types of SEQ7 across all developmental stages and DOR364 at the fully mature stage (

Figure 3.3:). Although environmental variation was controlled by mixing the growth medium and precisely regulating soil moisture, these five root architecture types were consistently observed. We then compared the mean DS curves for each root architecture type of DOR364 and SEQ7 at the R8-R9 stage in the mesocosm system with the mean DS curves for each root architecture type of DOR364 and SEQ7 of field (Figure S3.4). Similar root architecture types across these two environments were observed (Figure S3.4). The rate of width accumulation was higher in the mesocosm than in the field. This difference could be attributed to varied planting space—28.88 cm in-row and 33.53 cm out-row spacing in the mesocosm, compared to 10 cm in-row and 36 cm out-row spacing in the field. The increased space between plants in the mesocosm likely allows bean roots grow wider than in the field. Nevertheless, the general patterns of mean DS curve of each root architecture types were similar between two environments (Figure S3.4). The consistent observation of root architecture types of SEQ7 and DOR364, suggests minimizing environmental variation does not alter the range of observable

root architecture types within these two genotypes. This implies a strong genetic control over these root architecture types, however, the precise molecular mechanisms regulating these root architecture types remain unclear and need further investigation. Those mechanisms that drive the spatial arrangement of root architectural traits could to some extent explain the observed variability in architecture types, such as root angle and lateral branch length. Currently, the observed variability is generally classified as plasticity response environmental gradients per measured trait. In maize, genetic components of such trait specific plasticity have been identified in water-stress and non-limiting environments³⁰. Similarly, common bean genotypes show a specific plasticity response to phosphorus stress by altering the basal angle³¹. The different environmental gradients in our field experiment could be induced by root-root interaction. However, the genetic basis for how root-root interaction within one genotype is still unknown and needs further study³².

The root architecture dynamics of the SEQ7 population are complex throughout the growth stages.

Five distinct root architecture types of SEQ7 emerged as early as 7 DAS (Figure 3.1 & Figure 3.5). These early root architectural variations may be attributed to variations in seed weight. Seeds originating from various locations within the pod or harvested at different times during the growing season exhibit variation in individual seed weight^{33,34}. Particularly, seeds from peduncular with lower individual weights tend to develop fewer basal roots and smaller taproot diameters compared to those from the stylar position³⁴. For this experiment, we used SEQ7 seeds that were self-fertilized and collected from multiple locations within the pods of plants grown in pots. Given that plant development at such an early stage heavily relies on the nutritional reserves from the seed, it is expected that variations in seed weight may impact the

root architecture. Another contributing factor to early root architectural variations might be the oscillatory growth patterns observed in basal roots³⁵. During the early stages, these patterns can lead to fluctuations in the basal root growth angle, further affecting root architectural variation³⁵.

Starting with the root architecture type composition observed at 7 DAS, this initial composition remained consistent until 13 DAS (Figure 3.5 & Table S3.4). However, there was a marked shift in the root architecture types between 13 DAS and 21 DAS (Figure 3.5 & Table S3.4). Several factors could account for this change. One possibility is that by this time, the common bean plants had depleted their seed reserves³⁶, start to acquire external nutrients existing in soils. This hypothesis is supported by the fact that cotyledon abscission typically occurs between the 14th and 18th day after planting³⁶. By the 18th day post-germination, the common bean's seed reserves are usually exhausted, leading to potential adjustments in root architecture types to more efficiently access resources from the soil³⁶. Another possibility is that roots might start physically interacting with one another during the 13 DAS and 21 DAS (personal observation). The composition of root architecture types observed at 21 DAS persisted through 42 DAS (Figure 3.5 & Table S3.4). After reducing the water supply post-42 DAS, this composition remained stable through 63 DAS but experienced a shift by 90 DAS (Figure 3.5 & Table S3.4). This indicates that the SEQ7 population might need additional time to adjust its root architecture in response to prolonged water stress. Conversely, under non-limiting water conditions, the composition of root architecture types altered at 63 DAS (Figure 3.5 & Table S3.4), suggesting that factors other than water availability can influence these shifts. After this change, the composition stabilized and remained consistent through 90 DAS (Figure 3.5 & Table S3.4). Comparing the composition of root architecture types under different water conditions at 63 DAS and 90 DAS (Figure 3.5 & Table S3.4) revealed a significant shift between WL and NL

conditions. This observation supports the hypothesis in Chapter 2: Plant populations may adjust their root architecture types as a strategy to acclimate in response to environmental changes.

Root architectural change may not result in change of shoot biomass, root biomass and biomass allocation.

One objective of this chapter is to explore the relationship between root architecture type and shoot biomass, root biomass, and root-shoot ratio within the SEQ7 population across various growth stages and water conditions. At the population level, limited water availability led to a decrease in both shoot and root biomass, while increasing root-shoot ratio at 90 DAS in the SEQ7 population (Figure 3.6). This observation aligns with findings from numerous other plant species³⁷. The change in biomass distribution underlines the plant's acclimatation strategy to allocate more resources towards root development to enhance water uptake under drought conditions^{20,38}. At the individual level, the result revealed in general no significant differences in shoot, root, and root-shoot ratio among these architecture types (Figure 3.6). The lack of significant variation in biomass distribution among different root architecture types suggests that, in the context of the SEQ7 population, root architecture type may be independent from shoot biomass, root biomass and their ratios. The observation is supported by field observations of common bean genotypes (DOR364, L8857 and SEQ7) in Chapter 2 and is further supported by a recent simulation study, which suggests that different root architecture models may exhibit similar aboveground performance in specific environments due to internal resource competition and trade-offs driven by external environmental factors and interactions with neighboring plants¹⁶. Furthermore, the DS curve serves as a shape descriptor that to quantify root architecture as a whole, designed as approximately invariant to transformations like translation, rotation, and scaling, while root biomass is size dependent that quantifies the magnitude of mass without

concerning shape or spatial arrangement. The difference of shape and mass measurement explains why no significant difference in root biomass among different root architecture types. The result also provides empirical evidence to support Fitter's hypothesis changes in geometric aspects of root architecture, such as branching angle, might not necessarily translate to changes in biomass allocation²¹.

Root architecture types may link to different nutrient uptake function.

The exploration of linking specific root architecture types to a root architectural model aimed to derive functional insights from the observed five root architecture types. Given that root architecture plays an important role in soil resources uptake and the fact that these resources are not uniformly distributed in the soil^{39,40}, we hypothesized that different root architecture types may have different nutrient and resource uptake strategies. Based on the elastic registration and matching analysis, along with N and P uptake efficiency simulation results of root architecture models discussed in the paper¹⁶, we inferred the P and N uptake function of five root architecture types under the NL condition as follows: For P uptake (mmol plant⁻¹), the ranking is: AT3 (Deep, 3 whorls) > AT2 (Shallow, 2 whorls) > AT4 (Fan, 2 whorls) > AT5 (Shallow, 1 whorl) > AT1 (Fan, 1 whorl). For N uptake (mmol plant⁻¹), the ranking is: AT3 > AT4 > AT1 > AT2 > AT5. The AT3 has both better P and N uptake than other root architecture types, that is because nutrient uptake improves with a greater number of basal roots. However, an increase in the number of basal roots, particularly beyond 3 whorls would decrease the aboveground shoot biomass, as more resources are allocated to produce more roots¹⁶. In the paper, the authors did not provide any information about the N and P uptake under WL conditions, so we could not infer functions of the root architecture types under such condition 16. From the simulation result,

the function of nutrients uptake of root architecture types would change under different environmental stress, such as N, P or combined stress of these two¹⁶.

It is important to point out the limitation of the inferences. First of all, the root architecture model in the published paper does not include variable of adventitious roots, whereas the excavated roots in the experiment having different number of adventitious roots. Second, the shape descriptor DS-curve does not capture the number of basal roots and lateral root branching density, thus in the Figure S3.5, some of the simulated root architecture models have very similar DS curves. Therefore, a better root architecture model and a more distinguishable shape descriptor need to be developed to describe the real-world roots more accurately.

Acknowledgements

We express our gratitude to the following individuals for their help in this chapter:

Changhyeon Kim for installing the soil moisture sensors in the mesocosm system and programming the controller and measurement software of the sensors. Michael Boyd and Gregory Cousins for building the mesocosm and irrigation systems, as well as for their contributions to routine pest control and greenhouse management. Peter Pietrzyk for his assistance in building the mesocosm system and taking root images of 7 DAS and 13 DAS experiments. Sydney Page for aiding in the root harvest for experiments at 7 DAS, 13 DAS, and 63 DAS; measuring biomass data for the 7, 13, 21, 42, 63 DAS experiments and conducting preliminary data analysis for seed nutrient content. Joslyn Mcklveen for assistance with the planting of the 42 DAS experiment. Jitrana Kengkanna for root harvest and image collection during the 7, 13, and 63 DAS experiments. William Lavoy for root harvest and image collection of the 21 DAS experiment. Suxing Liu for assisting with the planting of the 90 DAS experiments.

References

- 1. Bruijning, M., Metcalf, C. J. E., Jongejans, E. & Ayroles, J. F. The Evolution of Variance Control. *Trends Ecol. Evol.* **35**, 22–33 (2020).
- 2. Baron, E., Richirt, J., Villoutreix, R., Amsellem, L. & Roux, F. The genetics of intra- and interspecific competitive response and effect in a local population of an annual plant species. *Funct. Ecol.* **29**, 1361–1370 (2015).
- 3. Bernardo, R. N. *Breeding for Quantitative Traits in Plants*. (Stemma Press, Woodbury, Minnesota, 2020).
- 4. Hodge, A. Plastic plants and patchy soils. J. Exp. Bot. 57, 401–411 (2006).
- 5. Hodge, A. The plastic plant: root responses to heterogeneous supplies of nutrients. *New Phytol.* **162**, 9–24 (2004).
- 6. Lippold, E., Lucas, M., Fahrenkampf, T., Schlüter, S. & Vetterlein, D. Macroaggregates of loam in sandy soil show little influence on maize growth, due to local adaptations of root architecture to soil heterogeneity. *Plant Soil* **478**, 163–175 (2022).
- 7. Rich, S. M., Christopher, J., Richards, R. & Watt, M. Root phenotypes of young wheat plants grown in controlled environments show inconsistent correlation with mature root traits in the field. *J. Exp. Bot.* **71**, 4751–4762 (2020).
- 8. Dudley, S. A. Plant cooperation. *AoB Plants* 7, plv113 (2015).
- 9. Fang, S. *et al.* Genotypic recognition and spatial responses by rice roots. *Proc. Natl. Acad. Sci. U. S. A.* **110**, 2670–2675 (2013).
- 10. Biedrzycki, M. L. & Bais, H. P. Kin recognition: Another biological function for root secretions. *Plant Signal. Behav.* **5**, 401–402 (2010).
- 11. Dudley, S. A. & File, A. L. Kin recognition in an annual plant. *Biol. Lett.* **3**, 435–438 (2007).

- 12. Semchenko, M., Saar, S. & Lepik, A. Plant root exudates mediate neighbour recognition and trigger complex behavioural changes. *New Phytol.* **204**, 631–637 (2014).
- 13. Wuest, S. E. *et al.* Increasing plant group productivity through latent genetic variation for cooperation. *PLOS Biol.* **20**, e3001842 (2022).
- 14. Lynch, J. P. Root phenotypes for improved nutrient capture: an underexploited opportunity for global agriculture. *New Phytol.* **223**, 548–564 (2019).
- 15. Ho, M. D., Rosas, J. C., Brown, K. M. & Lynch, J. P. Root architectural tradeoffs for water and phosphorus acquisition. *Funct. Plant Biol.* **32**, 737–748 (2005).
- 16. Rangarajan, H., Postma, J. A. & Lynch, J. P. Co-optimization of axial root phenotypes for nitrogen and phosphorus acquisition in common bean. *Ann. Bot.* **122**, 485–499 (2018).
- 17. Chapin, F. S. Integrated Responses of Plants to Stress. *BioScience* 41, 29–36 (1991).
- 18. Nicotra, A. B. *et al.* Plant phenotypic plasticity in a changing climate. *Trends Plant Sci.* **15**, 684–692 (2010).
- 19. Poot, P. & Lambers, H. Shallow-soil endemics: adaptive advantages and constraints of a specialized root-system morphology. *New Phytol.* **178**, 371–381 (2008).
- 20. Comas, L., Becker, S., Cruz, V. M. V., Byrne, P. F. & Dierig, D. A. Root traits contributing to plant productivity under drought. *Front. Plant Sci.* **4**, (2013).
- 21. Fitter, A. H. Architecture and Biomass Allocation as Components of the Plastic Response of Root Systems to Soil Heterogeneity. in *Exploitation of environmental heterogeneity of plants* (Academic Press, New York, NY, USA, 1994).
- 22. Xie, L. *et al.* Indoor-Field: A macro-mesocosm system to study the field dynamics of phenotypic spectrum of common bean (*Phaseolus vulgaris* L.). (2022).

- 23. Burridge, J., Jochua, C. N., Bucksch, A. & Lynch, J. P. Legume shovelomics: High-Throughput phenotyping of common bean (*Phaseolus vulgaris* L.) and cowpea (*Vigna unguiculata* subsp, *unguiculata*) root architecture in the field. *Field Crops Res.* 192, 21–32 (2016).
- 24. Das, A. *et al.* Digital imaging of root traits (DIRT): A high-throughput computing and collaboration platform for field-based root phenomics. *Plant Methods* **11**, 1–12 (2015).
- 25. Bucksch, A. *et al.* Image-Based High-Throughput Field Phenotyping of Crop Roots. *Plant Physiol.* **166**, 470–486 (2014).
- 26. R Core Team. R: A Language and Environment for Statistical Computing. (2022).
- 27. Srivastava, A., Wu, W., Kurtek, S., Klassen, E. & Marron, J. S. Registration of Functional Data Using Fisher-Rao Metric. Preprint at http://arxiv.org/abs/1103.3817 (2011).
- 28. Srivastava, A. & Klassen, E. P. Functional Data and Elastic Registration. in *Functional and Shape Data Analysis* (eds. Srivastava, A. & Klassen, E. P.) 73–123 (Springer, New York, NY, 2016).
- Ramos-Carreño, C., Torrecilla, J. L., Carbajo-Berrocal, M., Marcos, P. & Suárez, A. scikit-fda: A Python Package for Functional Data Analysis. Preprint at https://doi.org/10.48550/arXiv.2211.02566 (2023).
- 30. Schneider, H. M. *et al.* Genetic control of root architectural plasticity in maize. *J. Exp. Bot.* **71**, 3185–3197 (2020).
- 31. Liao, H. *et al.* Effect of phosphorus availability on basal root shallowness in common bean. *Plant Soil* **232**, 69–79 (2001).
- 32. Anten, N. P. R. & Chen, B. J. W. Detect thy family: Mechanisms, ecology and agricultural aspects of kin recognition in plants. *Plant Cell Environ.* **44**, 1059–1071 (2021).

- 33. Nakamura, R. R. Seed Abortion and Seed Size Variation within Fruits of *Phaseolus vulgaris*: Pollen Donor and Resource Limitation Effects. *Am. J. Bot.* **75**, 1003–1010 (1988).
- 34. Lorts, C., Lynch, J. P. & Brown, K. M. Parental effects and provisioning under drought and low phosphorus stress in common bean. *Food Energy Secur.* **9**, e192 (2020).
- 35. Basu, P. & Pal, A. Spatio-temporal analysis of development of basal roots of common bean (*Phaseolus vulgaris* L.). *Plant Signal. Behav.* **6**, 982–985 (2011).
- 36. Cortelazzo, A., Coutinho, J. & Granjeiro, P. Storage and aging of frence beans (*Phaseolus vulgaris* L.): effect on seed viability and vigor. *Braz. J. Morphol. Sci.* **22**, 121–128 (2005).
- 37. Eziz, A. *et al.* Drought effect on plant biomass allocation: A meta-analysis. *Ecol. Evol.* **7**, 11002–11010 (2017).
- 38. Berny Mier y Teran, J. C. *et al.* Root and shoot variation in relation to potential intermittent drought adaptation of Mesoamerican wild common bean (*Phaseolus vulgaris* L.). *Ann. Bot.* **124**, 917–932 (2019).
- 39. Dathe, A., Postma, J. A. & Lynch, J. P. Modeling Resource Interactions Under Multiple Edaphic Stresses. in *Enhancing Understanding and Quantification of Soil–Root Growth Interactions* 273–294 (John Wiley & Sons, Ltd, 2013).
- 40. Lynch, J. P. & Wojciechowski, T. Opportunities and challenges in the subsoil: pathways to deeper rooted crops. *J. Exp. Bot.* **66**, 2199–2210 (2015).

Figures

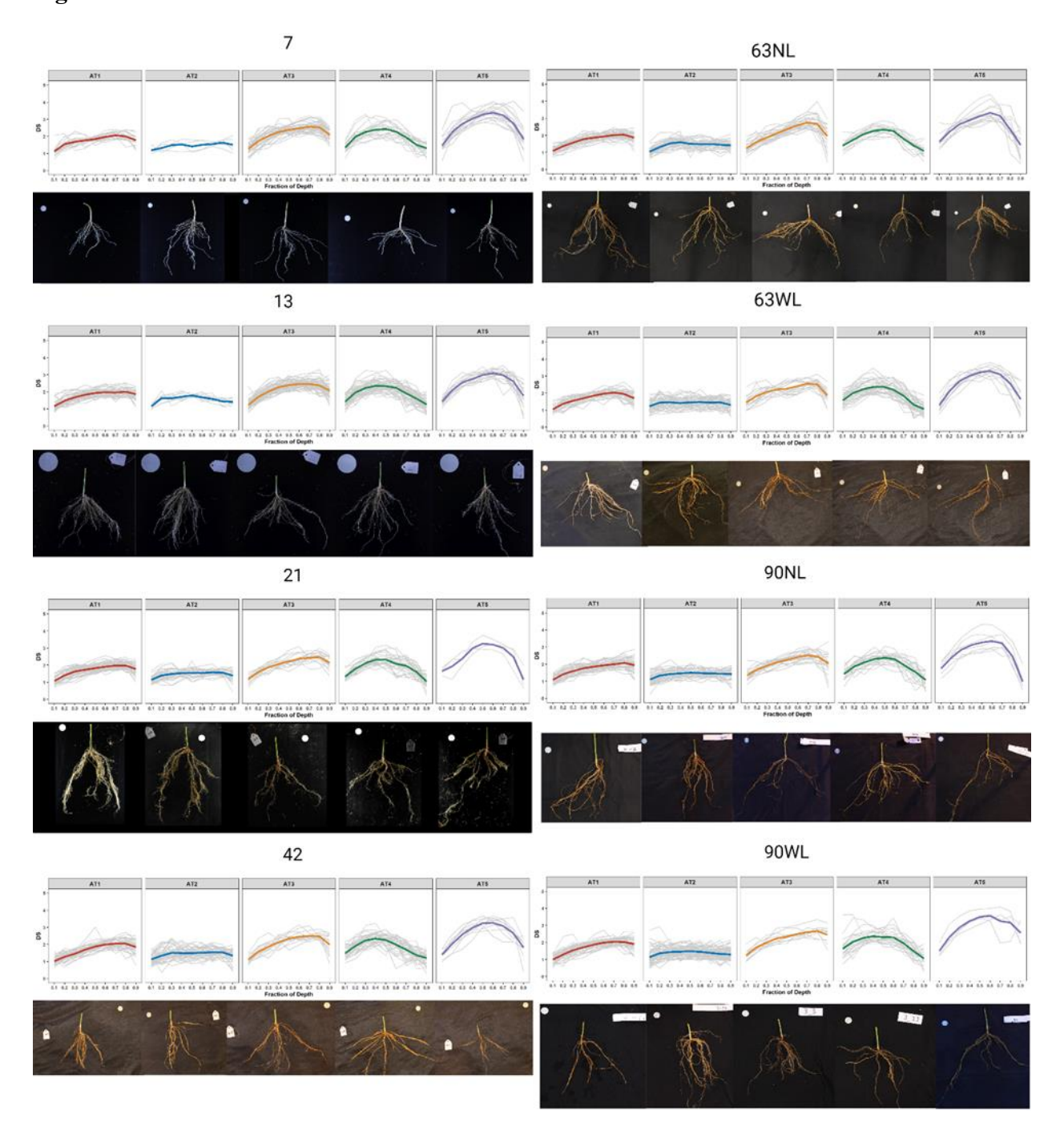


Figure 3.1: Five root architecture types of SEQ7 were observed across developmental stages and conditions. The observed growth stages were: 7 days after sowing (DAS) (n=100), 13 DAS (n=170), 21 DAS (n=127), 42 DAS (n=138), 63 DAS under both water-limited (WL) (n=145) and non-limiting (NL) (n=123) conditions, and 90 DAS under both WL (n=133) and NL (n=143)

conditions. We have graphed the mean DS curve corresponding to each root architecture type, with a representative root image displayed beneath. The reference marker in the root images measured 11.50 mm at 7 DAS and 50.90 mm at 13 DAS. For the remaining images, the marker measured 24.26 mm.

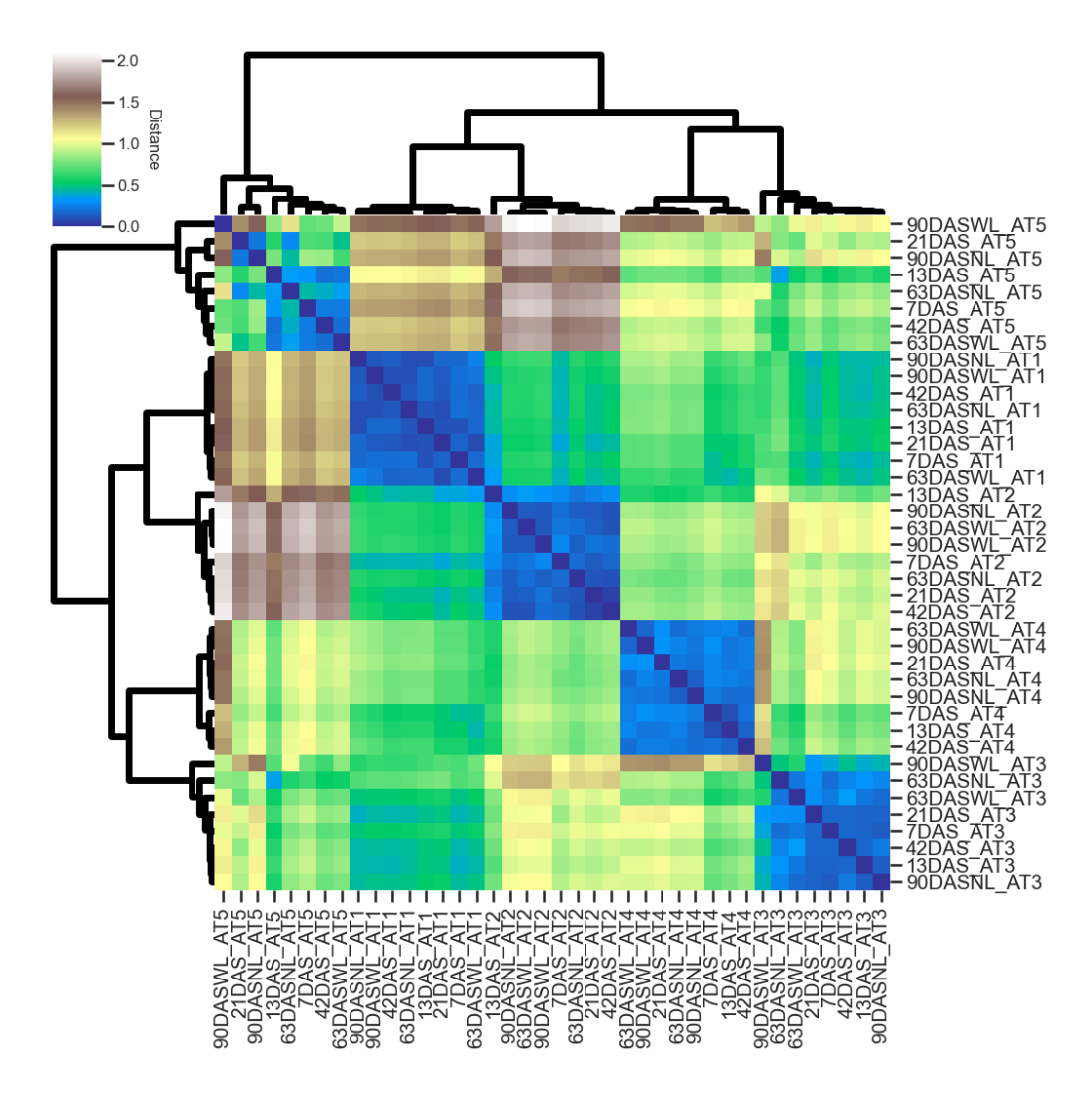


Figure 3.2: The heatmap of Fréchet distance matrix confirmed that while AT1 through AT5 were distinct, each showed consistent internal similarity across varying growth stages and conditions. The heatmap of Fréchet distance matrix between the mean curve of each root architecture type across different growth stages: 7 days after sowing (DAS),13 DAS, 21 DAS, 42 DAS, 63 DAS under both water-limited (WL) and non-limiting (NL) conditions, and 90 DAS under both WL and NL conditions. Each pixel's color in the heatmap corresponds to the Fréchet distance between two root architecture types, with blue representing higher similarity and brown denoting greater dissimilarity. The dendrograms on the axes represent the hierarchical clustering of the clusters based on their Fréchet distances.

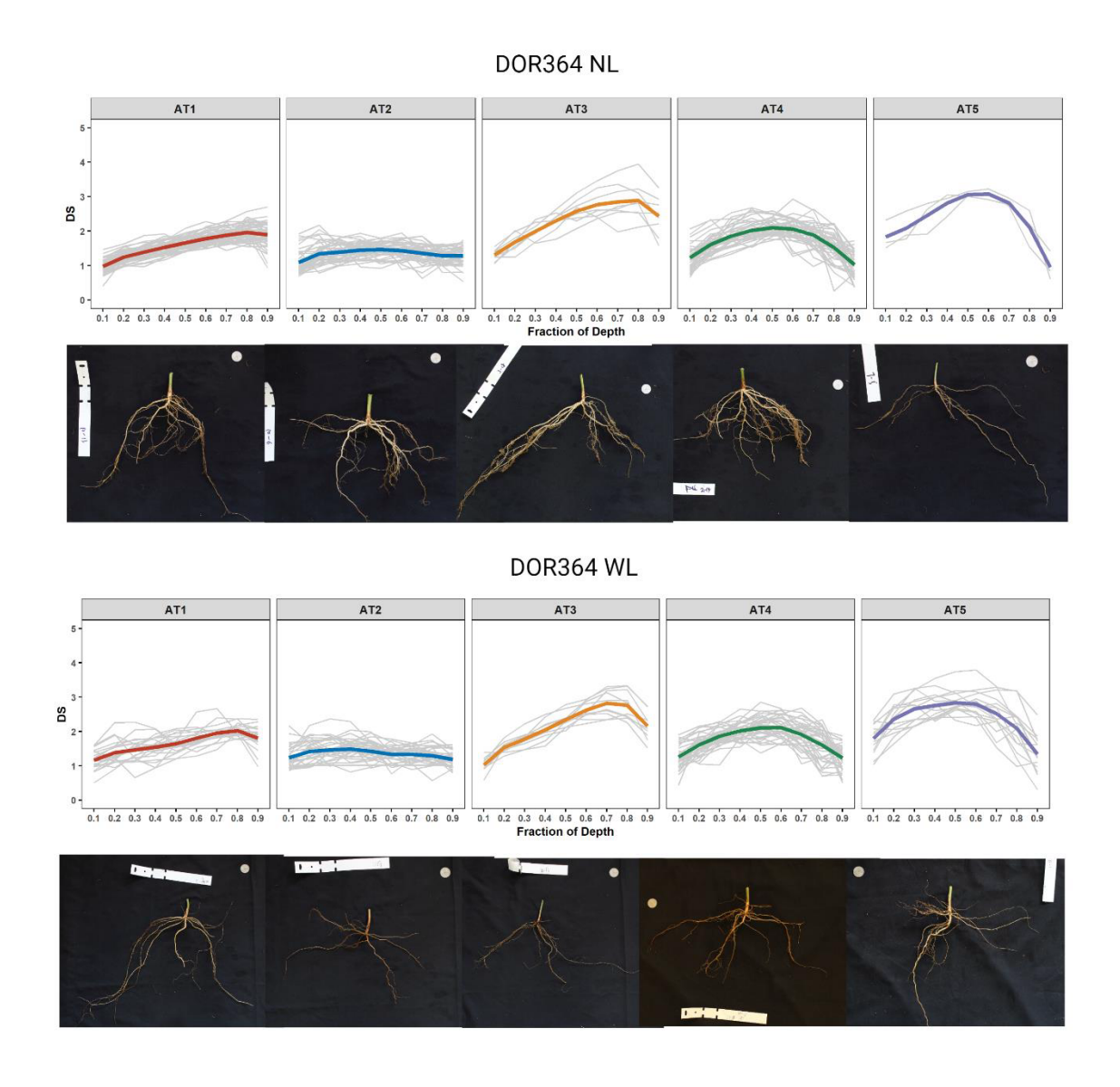


Figure 3.3: Five root architecture types of DOR364 were observed at mature stage (R8-R9, 84 days of sowing) under nonlimiting (NL, n=143) and water-limited (WL, n=118) conditions. We have graphed the mean DS curve corresponding to each root architecture type, with a representative root image displayed beneath. The reference marker in the root images measured 24.26 mm.

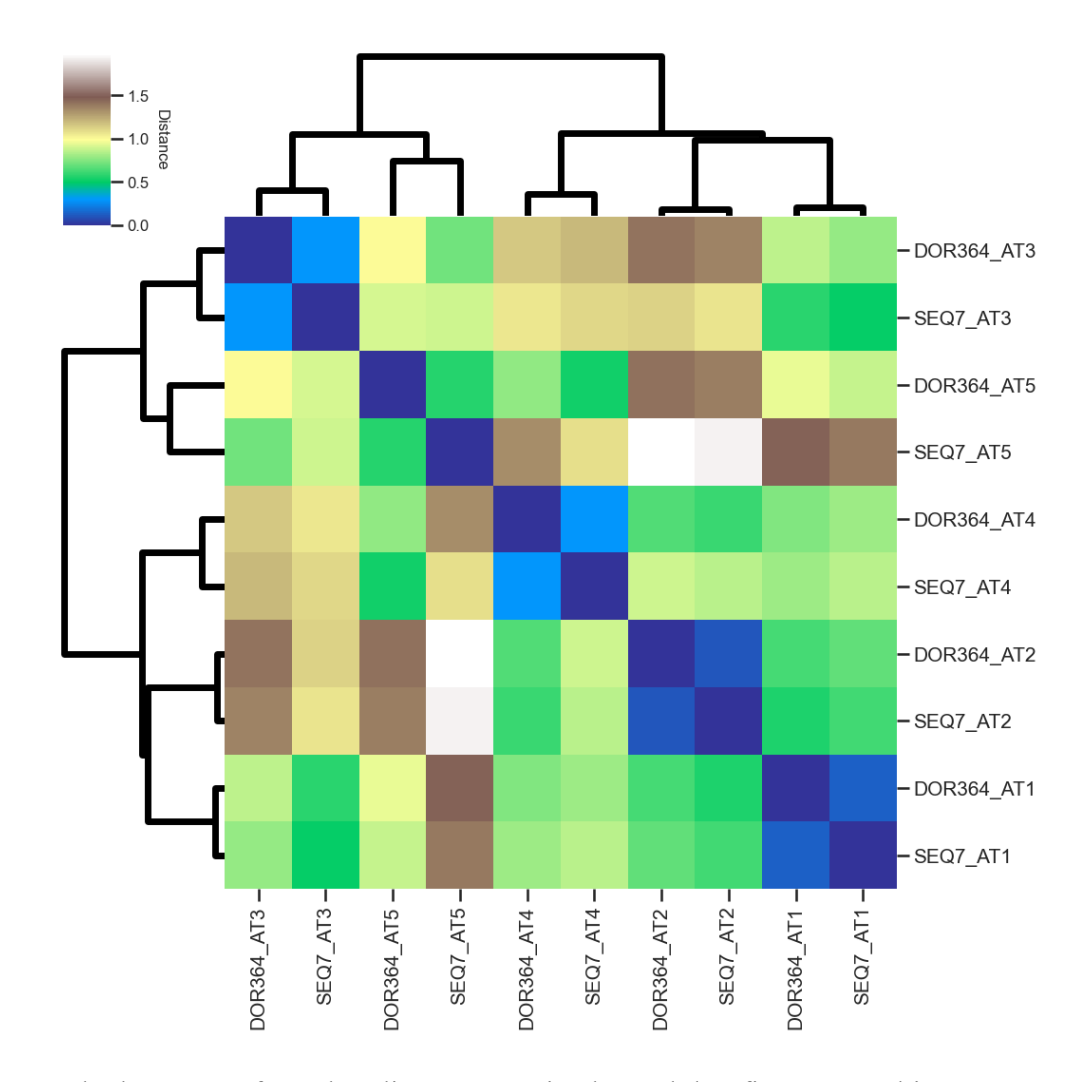


Figure 3.4 The heatmap of Fréchet distance matrix showed that five root architecture types were similar between SEQ7 and DOR364 at mature stages (R8-R9). The heatmap of Fréchet distance matrix between the mean curve of each root architecture type of SEQ7 and DOR364 at mature stages (R8-R9). Each pixel's color in the heatmap corresponds to the Fréchet distance between two root architecture types, with blue representing higher similarity and brown denoting greater dissimilarity. The dendrograms on the axes represent the hierarchical clustering of the clusters based on their Fréchet distances.

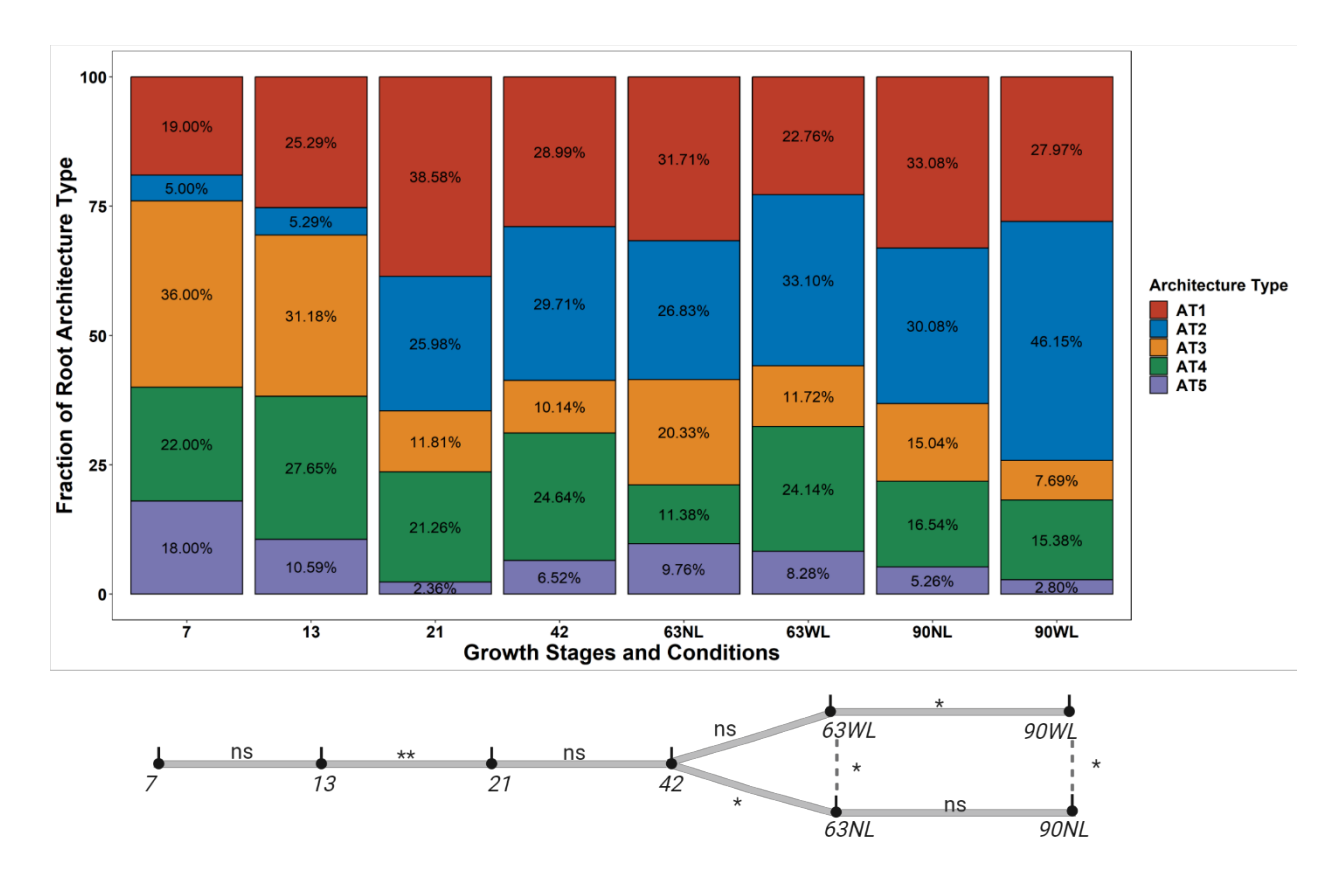


Figure 3.5: The composition of root architecture types of SEQ7 changed over growth stages and conditions. This figure represents the composition of root architecture type of SEQ7 at various growth stages and conditions, including 7 days after sowing (DAS) (n=100), 13 DAS (n=170), 21 DAS (n=127), 42 DAS (n=138), 63 DAS under both water-limited (WL) (n=145) and non-limiting (NL) (n=123) conditions, and 90 DAS under both WL (n=143) and NL (n=133) conditions. We used the chi-square test of homogeneity to compare the different composition of root architecture types between two growth stages or condition. The statistical significance is denoted as follows: ** $P \le 0.01$, * $P \le 0.05$ and ns: not significant.

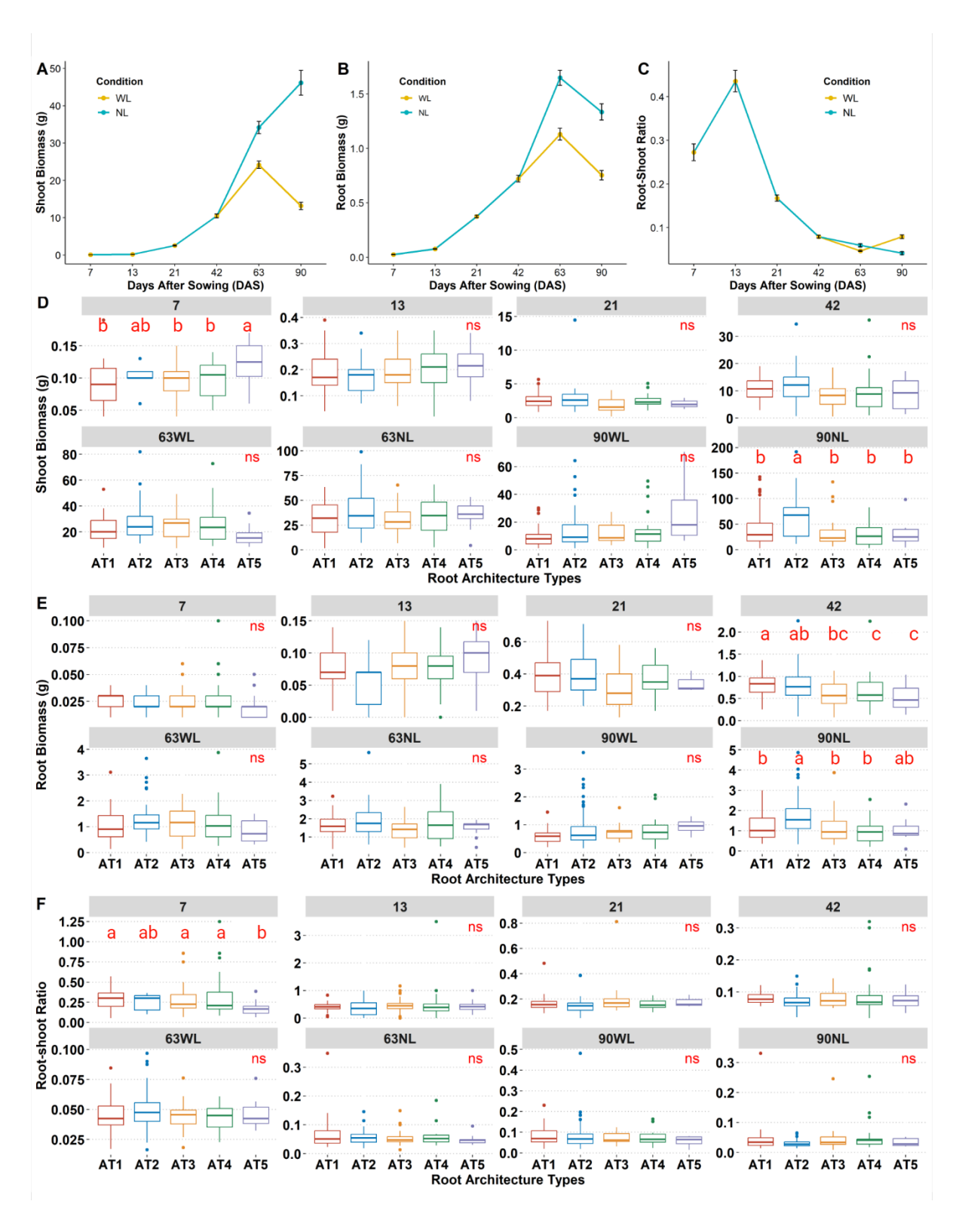


Figure 3.6: Shoot biomass, root biomass and root-shoot ratio were mostly not correlated with root architecture types (AT) but with growth stages. Line plots show the mean and standard error

of shoot biomass (A), root biomass (B), and root-shoot ratio (C) at 7 days after sowing (DAS) (n=100), 13 DAS (n=170), 21 DAS (n=127), 42 DAS (n=138), 63 DAS under both water-limited (WL) (n=145) and non-limiting (NL) (n=123) conditions, and 90 DAS under both WL (n=143) and NL (n=133). Boxplots depict the median of shoot biomass (D), root biomass (E) and root-shoot ratio (F) for each AT bounded by the first and third quantile within each growth stage. We applied Kruskal-Wallis's test and pairwise Wilcoxon rank sum test to identify any significant differences in these traits among ATs. Different letters label ATs with significant differences, with significance threshold set as P < 0.05. The notation ns refers not significant.

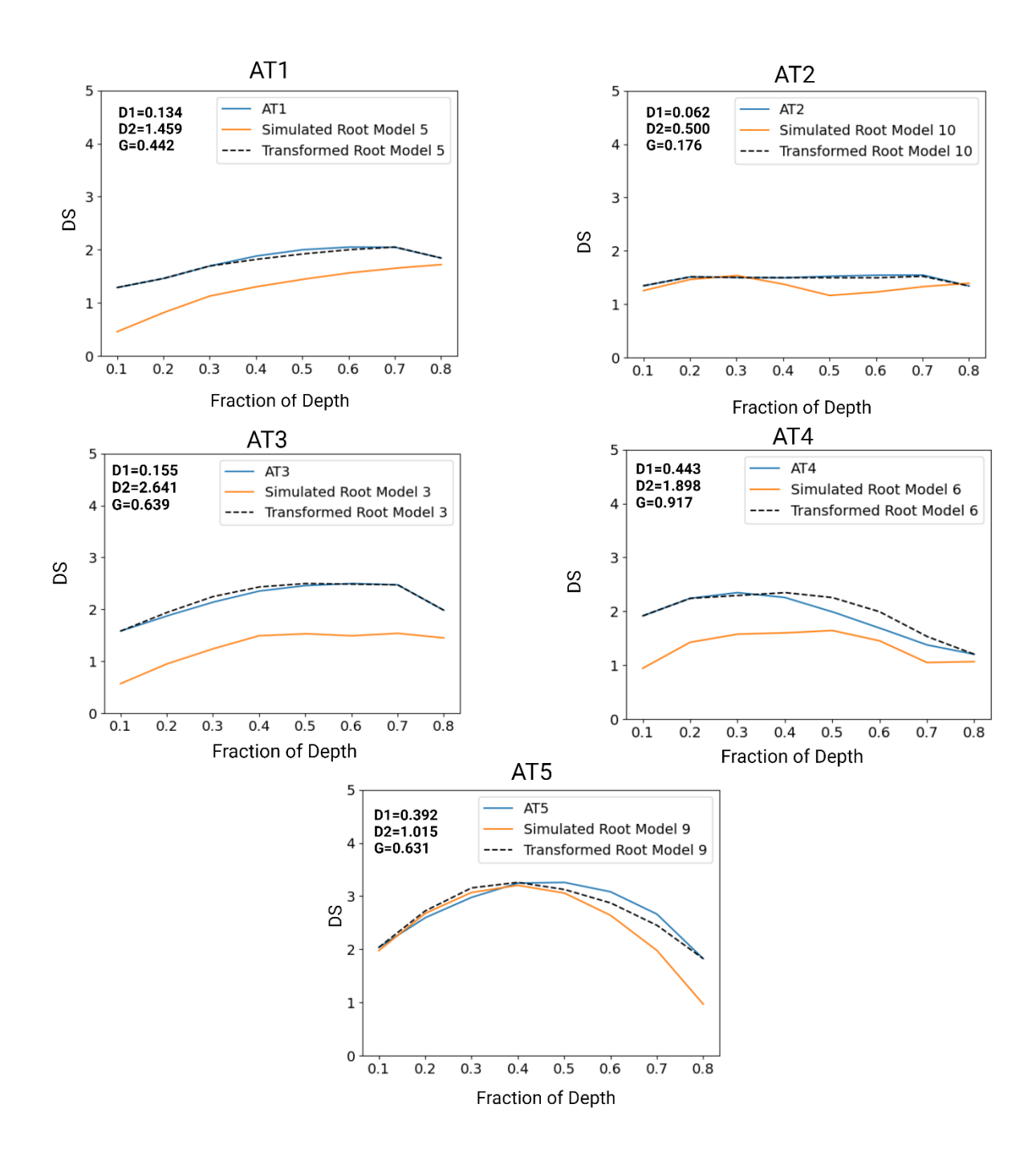


Figure 3.7: The closest matched simulated root architecture model with root architecture types observed at 42 days of sowing (DAS). The blue line indicates the 80% depth of the DS curve from observed root architecture types at 42 DAS, while the orange line represents the DS curve of the corresponding simulated model. The dashed line represents the transformed curve of the

simulated root architecture model post-elastic registration. Refer to Figure S3.5 for detailed simulated root architecture model. D1 was calculated as the Euclidean distance between the transformed DS curve of simulated root architecture and the mean DS curve the observed root architecture type, representing as a measure of alignment accuracy. D2 was calculated as the Euclidean distance between the original and transformed DS curves of the simulated root architecture, thereby quantifying the extent of the transformation. D1, D2 and geometric mean of D1 and D2 were reported in each plot.

Appendix B

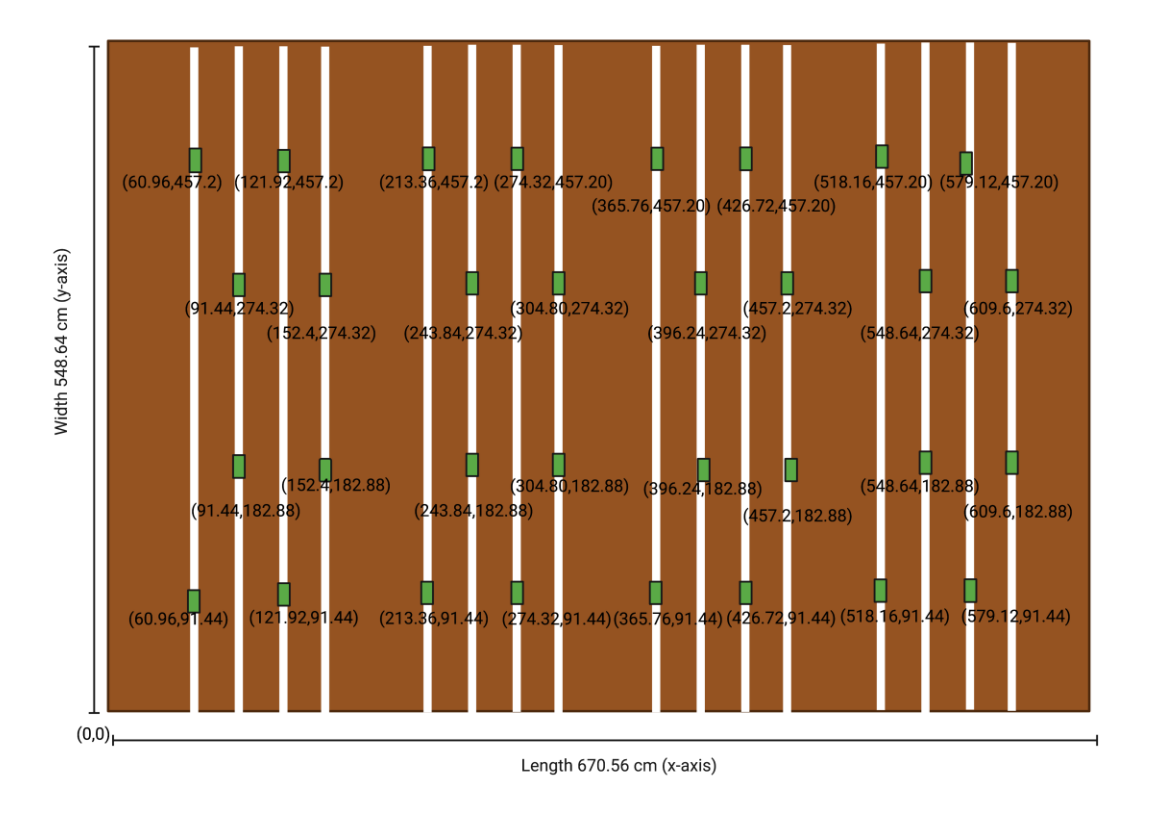


Figure S3.1: Top view schematic of the mesocosm system. We marked a total of 64 sensors (the green rectangle) with location coordinates on the x-y plane. For each location, we installed two sensors at 15.24 cm and 38.10 cm depth. The white bars represent the irrigation pipes. The entire mesocosm is divided into 4 irrigation plots.

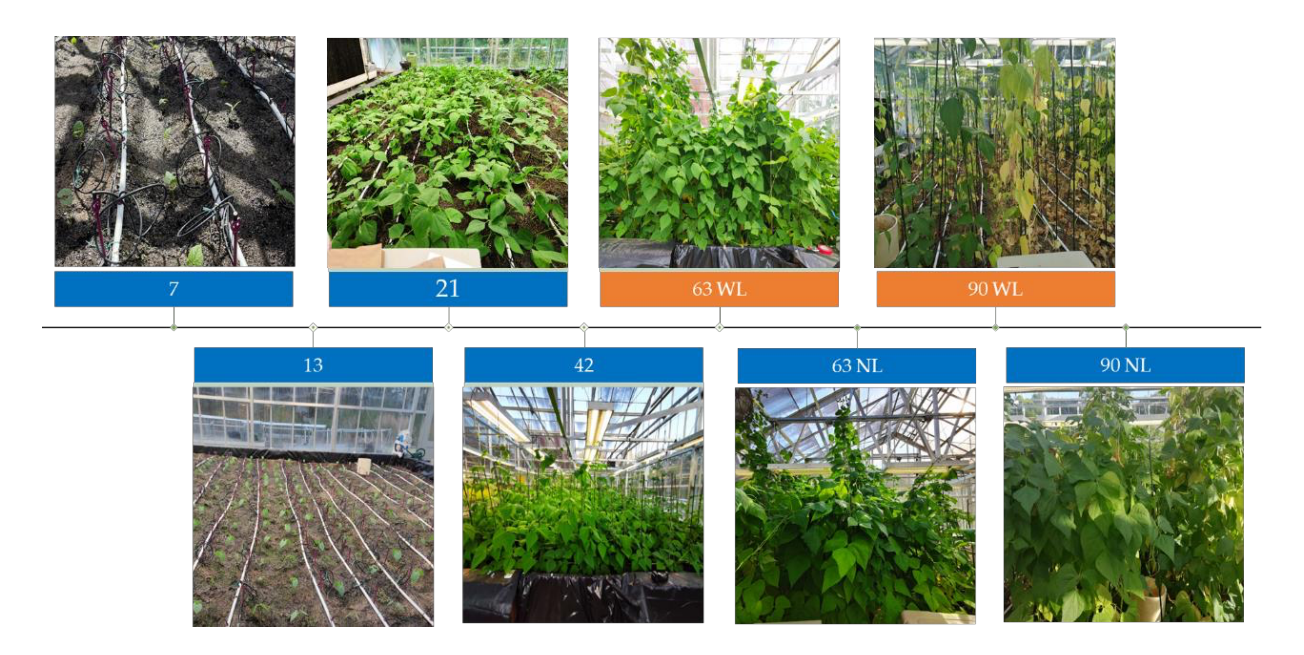


Figure S3.2: The time-series experiment of SEQ7 in the mesocosm system. We planted SEQ7 in completely random design for 7, 13, 21, 42 days after sowing (DAS) and 63 DAS and 90 DAS under water-limited (WL) and non-limiting (NL) conditions.

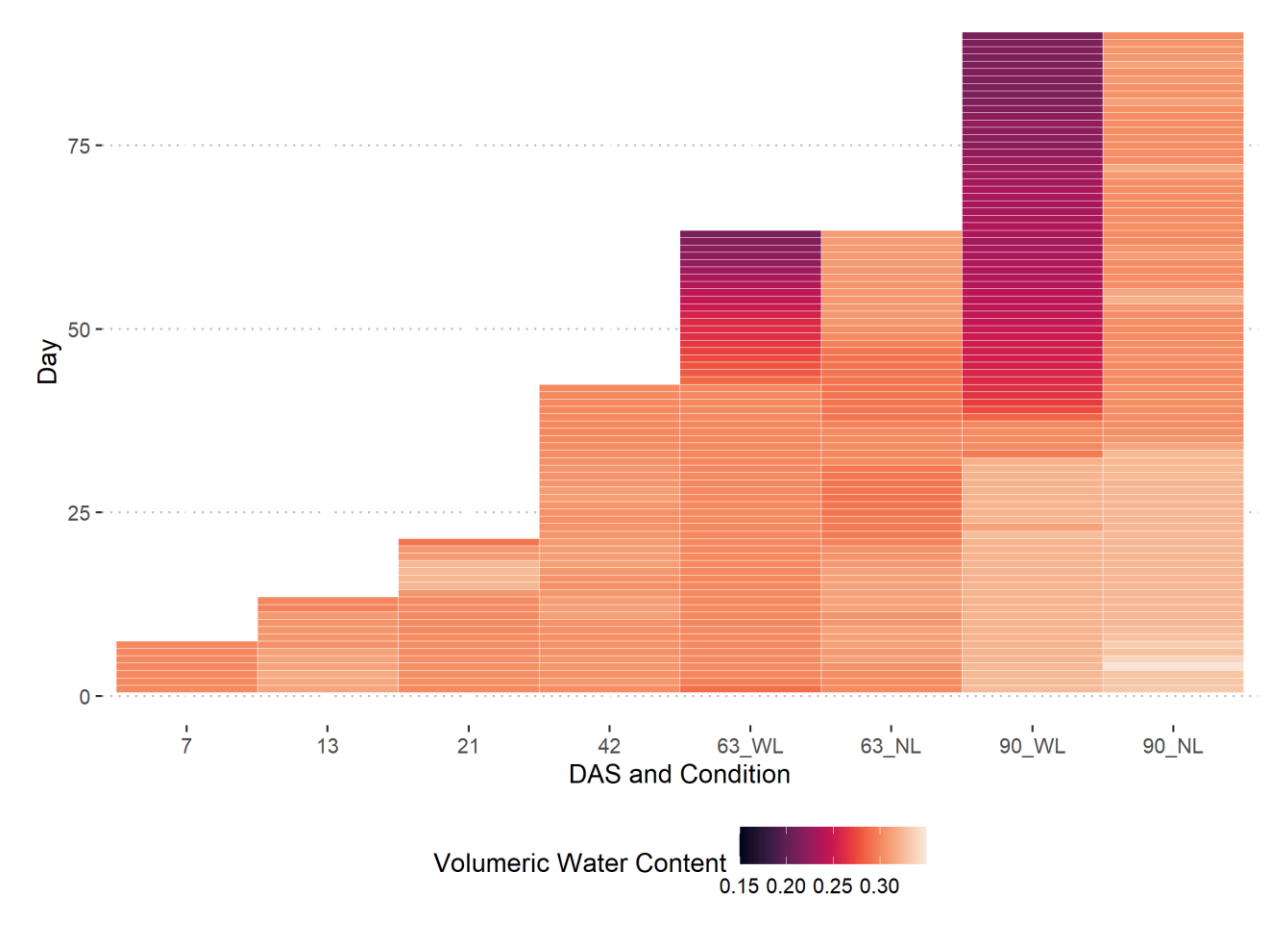


Figure S3.3: The daily mean volumetric water content (vwc) across all growth stages and conditions. In this figure, the color key indicates the vwc values, with darker color representing lower vwc, and lighter color corresponding to higher vwc. "NL" denotes for non-limiting conditions, while "WL" denotes water-limited conditions. "DAS" is an abbreviation for days of sowing.

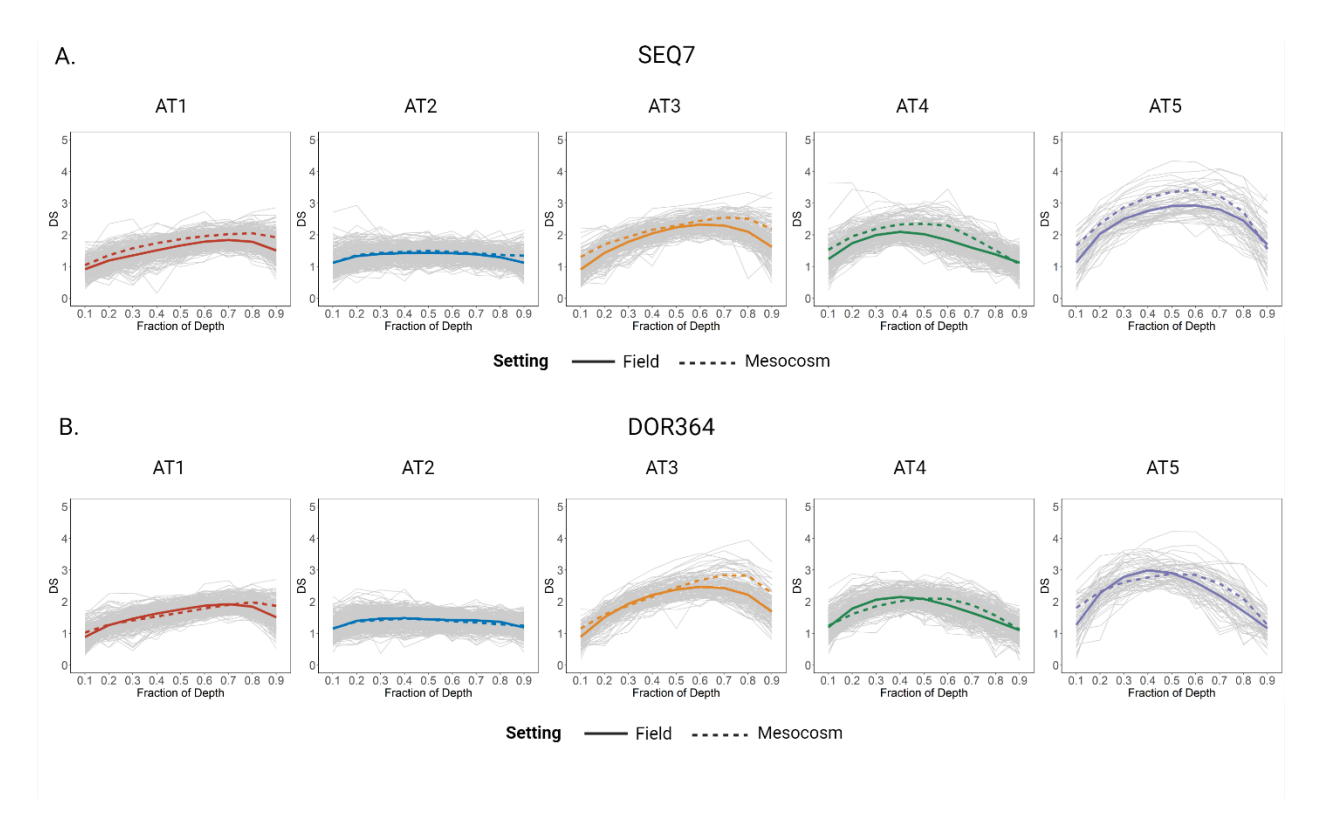


Figure S3.4: The five root architecture types of SEQ7 (Panel A) and DOR364 (Panel B) are presented from both field and mesocosm settings. The mean DS curves for each root architecture type are shown in the figure. Solid lines represent the root architecture types of both SEQ7 and DOR364 at the mature stage, 70 days after sowing (DAS), in the field, while dashed lines correspond to the mature stage root architecture types of DOR364 at 84 DAS and SEQ7 at 90 DAS in the mesocosm system.

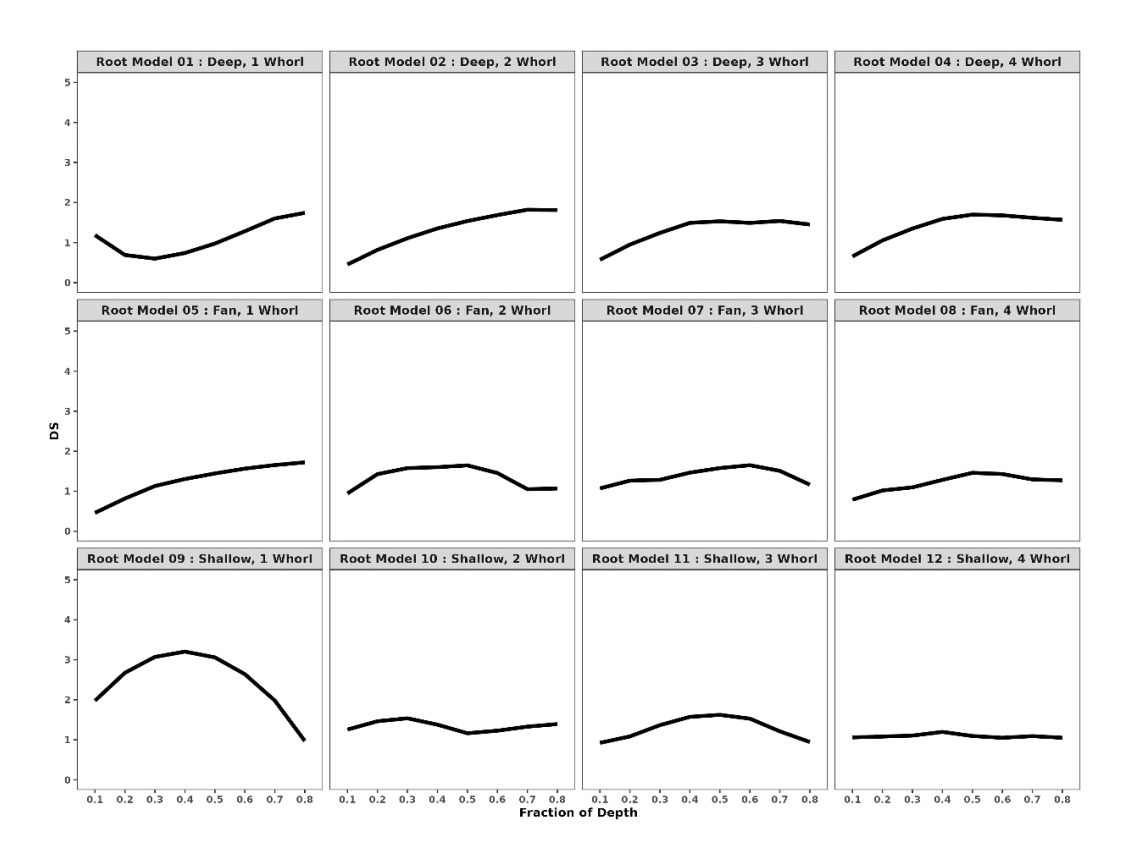


Figure S3.5: DS curves derived from 12 simulated root architecture models¹. These models varied in 3 root angles (Shallow, Fan, Deep) and 4 basal whorl numbers. We processed images of these models in DIRT to generate the DS curves. Note: Only 80% of the DS values were depicted²¹.

Table S3.1: Sample sizes across different root architecture types of SEQ7 during various growth stages and DOR364 at mature stage under each water condition. "NL" denotes for non-limiting conditions, while "WL" denotes water-limited conditions. "DAS" is an abbreviation for days of sowing.

DAS	AT1	AT2	AT3	AT4	AT5	Total
SEQ7_7	19	5	36	22	18	100
SEQ7_13	43	9	53	47	18	170
SEQ7_21	49	33	15	27	3	127
SEQ7_42	40	41	14	34	9	138
SEQ7_63NL	39	33	25	14	12	123
SEQ7_63WL	33	48	17	35	12	145
SEQ7_90NL	44	40	20	22	7	133
SEQ7_90WL	40	66	11	22	4	143
DOR364_84NL	51	42	8	39	3	143
DOR364_84WL	21	35	10	37	15	118

Table S3.2: The mean DS curve of SEQ7 is listed across growth stages and conditions. In the "AT" column, the first number represents the days after sowing. "NL" denotes for non-limiting condition, while "WL" denotes water-limited conditions. "AT" refers to the root architecture type.

AT	DS10	DS20	DS30	DS40	DS50	DS60	DS70	DS80	DS90
7 AT1	1.135	1.553	1.687	1.762	1.847	1.981	2.069	2.000	1.778
7 AT2	1.196	1.326	1.489	1.533	1.419	1.510	1.555	1.634	1.510
7_AT3	1.274	1.735	2.042	2.264	2.393	2.481	2.571	2.530	2.083
7 AT4	1.346	1.986	2.263	2.398	2.429	2.278	1.940	1.516	1.312
7 AT5	1.466	2.260	2.745	3.046	3.282	3.396	3.242	2.772	1.843
13 AT1	1.160	1.478	1.686	1.827	1.935	1.974	1.964	2.012	1.861
13_AT2	1.151	1.636	1.630	1.718	1.790	1.682	1.585	1.445	1.415
13_AT3	1.235	1.710	2.030	2.279	2.393	2.460	2.459	2.376	2.065
13_AT4	1.425	1.970	2.228	2.363	2.336	2.239	1.914	1.604	1.263
13_AT5	1.435	2.098	2.567	2.760	2.993	3.090	2.975	2.614	1.756
21_AT1	1.080	1.405	1.634	1.732	1.832	1.914	1.989	1.986	1.777
21_AT2	1.148	1.397	1.486	1.539	1.543	1.550	1.586	1.560	1.390
21_AT3	1.185	1.603	1.883	2.084	2.223	2.388	2.437	2.482	2.143
21_AT4	1.332	1.790	2.127	2.326	2.329	2.088	1.961	1.614	1.043
21_AT5	1.654	1.940	2.389	2.998	3.263	3.203	3.015	2.498	1.159
42_AT1	1.028	1.289	1.459	1.695	1.882	2.001	2.051	2.049	1.845
42_AT2	1.128	1.346	1.513	1.500	1.495	1.525	1.545	1.548	1.342
42_AT3	1.113	1.583	1.873	2.139	2.353	2.459	2.499	2.474	1.984
42_AT4	1.479	1.916	2.241	2.348	2.257	1.993	1.691	1.378	1.204
42_AT5	1.402	2.036	2.594	2.977	3.245	3.259	3.083	2.663	1.825
63NL_AT1	1.094	1.365	1.580	1.777	1.867	1.939	2.015	2.045	1.860
63NL_AT2	1.038	1.309	1.530	1.604	1.504	1.493	1.486	1.446	1.413
63NL_AT3	1.241	1.611	1.870	2.112	2.351	2.577	2.758	2.679	1.957
63NL_AT4	1.388	1.731	2.056	2.266	2.339	2.263	1.801	1.396	1.090
63NL_AT5	1.632	2.214	2.664	2.886	3.135	3.332	3.141	2.332	1.428
63WL_AT1	1.047	1.375	1.555	1.701	1.849	1.973	2.031	1.949	1.697
63WL_AT2	1.226	1.444	1.464	1.415	1.459	1.474	1.444	1.455	1.301
63WL_AT3	1.447	1.821	2.057	2.212	2.255	2.402	2.558	2.515	1.861
63WL_AT4	1.573	2.002	2.228	2.362	2.378	2.198	1.840	1.320	1.068
63WL_AT5	1.294	2.120	2.706	3.023	3.211	3.298	3.091	2.550	1.641
90WL_AT1	1.004	1.296	1.555	1.719	1.874	1.990	2.046	2.031	1.904
90WL_AT2	1.138	1.367	1.440	1.463	1.490	1.459	1.390	1.326	1.301
90WL_AT3	1.244	1.714	1.992	2.234	2.342	2.493	2.597	2.673	2.454
90WL_AT4	1.634	2.037	2.272	2.365	2.321	2.301	1.951	1.482	1.063
90WL_AT5	1.504	2.325	2.898	3.266	3.497	3.565	3.251	3.165	2.568
90NL_AT1	1.094	1.412	1.604	1.765	1.858	1.935	2.006	2.076	1.943
90NL_AT2	1.103	1.346	1.421	1.469	1.509	1.480	1.456	1.445	1.423
90NL_AT3	1.340	1.697	1.914	2.120	2.267	2.417	2.521	2.421	2.035
90NL_AT4	1.428	1.873	2.112	2.301	2.374	2.284	1.907	1.541	1.084
90NL_AT5	1.750	2.377	2.859	3.127	3.268	3.355	3.215	2.463	0.985

Table S3.3: The value of mean DS curve of DOR364 is listed under non-limiting (NL) and water-limited (WL) conditions.

AT	DS10	DS20	DS30	DS40	DS50	DS60	DS70	DS80	DS90
NL_AT1	0.977	1.241	1.391	1.530	1.660	1.785	1.881	1.963	1.896
NL_AT2	1.094	1.342	1.392	1.448	1.461	1.428	1.357	1.285	1.288
NL_AT3	1.307	1.681	1.997	2.302	2.583	2.764	2.847	2.892	2.429
NL_AT4	1.228	1.615	1.852	2.020	2.098	2.061	1.892	1.518	1.022
NL_AT5	1.834	2.079	2.446	2.813	3.062	3.073	2.813	2.110	0.955
WL_AT1	1.162	1.381	1.466	1.549	1.646	1.803	1.954	2.028	1.808
WL_AT2	1.235	1.414	1.464	1.485	1.427	1.332	1.334	1.296	1.190
WL_AT3	1.029	1.534	1.782	2.050	2.344	2.617	2.825	2.767	2.154
WL_AT4	1.261	1.609	1.863	2.014	2.109	2.118	1.916	1.599	1.231
WL AT5	1.799	2.359	2.661	2.755	2.839	2.797	2.523	2.088	1.339

Table S3.4: Chi-square test of homogeneity for comparing compositions of root architecture types between growth stages and conditions. "NL" denotes for non-limiting conditions, while "WL" denotes water-limited conditions.

Comparisons	Chi-Squared	P value
7 vs 13	4.920958	0.295504
13 vs 21	46.20348	2.23E-09
21 vs 42	5.165034	0.270779
42 vs 63NL	11.91929	0.017962
63NL vs 90NL	4.237401	0.374829
42 vs 63WL	1.783128	0.775568
63WL vs 90WL	11.75064	0.019305
90WL vs 90NL	9.649268	0.046769
63WL vs 63NL	12.077	0.016788

Table S3.5: The summary statistics for shoot biomass, root biomass and shoot/root ratio of SEQ7 over growth stages and conditions. "NL" denotes for non-limiting conditions, while "WL" denotes water-limited conditions.

Shoot Biomass					
Growth stage and conditions	Mean	Standard Deviation	Standard Error	Median	Interquartile range
7	0.103	0.031	0.003	0.100	0.040
13	0.196	0.072	0.005	0.190	0.090
21	2.552	1.471	0.131	2.420	1.345
42	10.486	5.903	0.502	10.180	7.573
63NL	34.157	18.274	1.648	33.550	26.370
63WL	24.152	12.073	1.003	22.200	14.220
90NL	46.127	38.375	3.328	31.720	50.840
90WL	13.166	12.165	1.017	9.130	11.285
Root Biomass					
Growth stage and	Mean	Standard	Standard	Median	Interquartile
conditions		Deviation	Error		range
7	0.025	0.014	0.001	0.020	0.010
13	0.076	0.034	0.003	0.080	0.040
21	0.375	0.124	0.011	0.360	0.165
42	0.721	0.352	0.030	0.723	0.445
63NL	1.647	0.756	0.068	1.580	0.850
63WL	1.130	0.648	0.054	1.043	0.770
90NL	1.334	0.867	0.075	1.143	1.060
90WL	0.753	0.522	0.044	0.613	0.400
Root-Shoot Ratio					
Growth stage and conditions	Mean	Standard Deviation	Standard Error	Median	Interquartile range
7	0.272	0.192	0.019	0.222	0.167
13	0.436	0.318	0.024	0.412	0.200
21	0.167	0.080	0.007	0.155	0.051
42	0.079	0.037	0.003	0.070	0.029
63NL	0.059	0.039	0.004	0.048	0.029
63WL	0.046	0.015	0.001	0.045	0.015
90NL	0.041	0.041	0.004	0.032	0.020
90WL	0.079	0.051	0.004	0.067	0.044

Table S3.6: Geometric mean values of D1 and D2 for each alignment of the mean DS curve at 42 DAS for observed root architecture types and simulated root architecture models¹²¹. Note: D1 represents the Euclidean distance between the transformed curve and the mean DS curve, indicating alignment accuracy after transformation. D2 denotes the Euclidean distance between the original simulated DS curve and its post-elastic registration transformation.

AT	Simulated Root Architecture Model	D1	D2	Geometric Mean
1	1	0.954	1.329	1.126
_1	2	0.161	1.336	0.464
1	3	0.289	1.599	0.680
1	4	0.307	1.254	0.620
1	5	0.134	1.459	0.442
1	6	0.542	1.559	0.920
1	7	0.247	1.251	0.556
1	8	0.247	1.688	0.646
1	9	0.382	2.547	0.986
1	10	0.580	1.567	0.953
1	11	0.206	1.498	0.555
1	12	0.248	2.022	0.708
2	1	0.207	1.434	0.544
2	2	0.159	1.266	0.448
2 2	3	0.133	0.930	0.352
2	4	0.161	0.870	0.374
2	5	0.137	1.207	0.407
2	6	0.162	0.627	0.318
2	7	0.161	0.425	0.261
2	8	0.161	0.828	0.365
2	9	0.176	3.372	0.770
2	10	0.062	0.500	0.176
2	11	0.176	0.727	0.357
2	12	0.211	0.992	0.458
3	1	1.193	2.233	1.632
3	2	0.220	2.374	0.722
3	3	0.155	2.641	0.639
3	4	0.275	2.207	0.780
3	5	0.178	2.558	0.674
3	6	0.580	2.443	1.191
3	7	0.378	2.323	0.937

Table S 3.6 (continued)

3	8	0.246	2.659	0.809
3 3	9	0.553	1.699	0.969
3 3	10	0.795	2.415	1.385
	11	0.255	2.473	0.794
3	12	0.484	2.909	1.187
4	1	1.106	2.977	1.814
4	2	1.225	2.652	1.803
4	3	1.145	2.574	1.717
4	4	0.764	2.197	1.295
4	5	1.225	2.735	1.831
4	6	0.443	1.898	0.917
4	7	0.929	2.046	1.379
4	8	0.764	2.525	1.389
4	9	0.533	1.691	0.949
4	10	0.779	1.424	1.053
4	11	0.798	2.062	1.283
4	12	0.470	2.421	1.067
5 5	1	1.555	3.762	2.419
	2	0.925	3.891	1.897
5 5	3	0.429	4.387	1.372
	4	0.305	3.795	1.075
5	5	0.743	4.251	1.778
5	6	0.329	4.121	1.165
5	7	0.562	3.941	1.489
5	8	0.374	4.300	1.268
5	9	0.392	1.015	0.631
5 5 5 5 5 5 5 5	10	1.521	3.299	2.240
5	11	0.492	3.819	1.371
5	12	0.780	4.173	1.804

CHAPTER 4

EVALUATION OF POPULATION FITNESS OF COMMON BEAN MONOCULTURE AND MIXTURE

Introduction

In agricultural systems, understanding plant-plant interactions is crucial for optimizing crop yield and resource use. Two primary theories—resource partitioning and kin selection—provide a framework for understanding these interactions, but often yield contradictory predictions. Resource partitioning theory assumes that individuals of the same species or genotype generally exhibit similar phenotypes and, hence, have similar resource needs^{1–3}. This could intensify competition within the same species or genotype compared to competition between different species or genotypes, and potentially lead to decreased overall fitness in populations comprised of closely related genotypes⁴. At the same time, physiological and agronomic experiments have demonstrated that avoidance between genetically distinct plants can result in increased combined yield^{5–7}. This improvement often occurs because these plants have differing traits and resource requirements, allowing for more effective resource capture. An example of such enhanced yield through polycultures is the intercropping of squash, common bean and maize, which utilize differences in root architecture and spatial root segregation for synergistic resource acquisition⁸.

Conversely, kin selection theory argues that plants are capable of recognizing the identity of their neighbors, modulating their competitive behavior based on the genetic relatedness of neighboring plants^{9–11}. Interactions with genetically similar individuals may lead to reduced

competition and, consequently, increased group fitness, suggesting that populations of closely related genotypes could exhibit higher overall fitness than genetically distinct populations¹². Supporting this theory, ecological studies have shown that closely related plants showed less competitive traits, such as decreased root allocation, less branch density and lower nutrient and water uptake, among themselves compared to distantly related ones^{9,13–15}. Molecular data further supports the kin selection theory. A study on rice genotypes grown in transparent gel media revealed less competition and larger distance between roots of related genotypes scavenging for a limiting nutrition resource¹⁶.

Both the niche partition and kin selection theories have limitations. The niche partition theory has an underlying assumption that genetically similar individuals have similar phenotype and resource use, thus may overlook the intra-genotypic or intra-species variation. The observations presented in Chapter 2 and Chapter 3 challenge this assumption, revealing that a single common bean genotype has five distinct root architecture types with different associated functions.

Empirical research supporting kin selection in plants often concludes that kin groups exhibit less competitive traits and higher group fitness compared to non-kin groups^{9,17–19}. However, the observed higher fitness in kin groups could be alternatively explained by variation in plant size within non-kin groups²⁰. Specifically, Jensen's inequality suggests that, when plant size and fitness measured by seed number follow a decelerating function and the plants in non-kin groups have large size asymmetry, non-kin groups will have lower group fitness than those in kin groups²⁰.

Chapter 4 focuses on the population fitness outcomes of three agricultural planting scenarios: monocultures of common bean genotypes SEQ7 and DOR364, and a mixture of both.

Following on Chapters 2 and 3 that suggest a pre-determined root architecture diversity with associated function, we ask how a single genotype can benefit from multiple root architecture types. The primary objective of this chapter is to investigate the fitness outcomes in these three planting scenarios, particularly when plants interact with genetically similar or varied neighbors. This chapter further examine the differences in belowground competition, as quantified by the root-shoot ratio—a measure of plant belowground competitive ability^{9,17,21}, between monocultures and mixtures under both water-limited (WL) and nutrient-limited (NL) conditions. The root-shoot ratio indicates how a plant allocates its resources between root and shoot growth. In environments where belowground resources (such as water and nutrients) are limited, plants may allocate more resources to root growth to enhance their competitive ability for these limiting resources²². The additional analysis includes the compositions of root architecture types between the monocultures and mixtures under both WL and NL conditions to understand how different genotypes adjust their root architecture types for resource uptake in different planting scenarios.

Materials and Methods

Plant growth condition and experimental design

Mixtures of DOR364 and SEQ7 under NL and WL conditions were planted in the mesocosm system at The University of Georgia Botany greenhouse in Athens, GA. Genotypes DOR364 and SEQ7 were planted in a chessboard pattern to ensure that each plant was surrounded by four neighbors of the other genotype. The specific growth media and dimension of the mesocosm system was detailed in Chapter 3. The experimental conditions, NL and WL, were implemented as previously described in Chapter 3. For the WL condition, we initially maintained the irrigation threshold at an average 30% volumetric water content (vwc), subsequently changed it to 20% vwc during the vine developmental stages, thereby limiting the

water supply for the remainder of the growth period. To represent monoculture in this study, we used data from the SEQ7 and DOR364 experiment described in Chapter 3, where both the SEQ7 and DOR364 genotypes were grown separately to full maturity. The daily average vwc for these three planting scenarios were plotted in the Figure S4.1: The daily mean volumetric water content (vwc) across planting scenarios. In this figure, the color key indicates the VWC values, with darker color representing lower VWC, and lighter color corresponding to higher VWC. "NL" denotes for non-limiting conditions, while "WL" denotes water-limited conditions. Mix refers to mixture and Mono refers monoculture. The mixture of SEQ7 and DOR364 was grown for 93 days, SEQ7 monoculture for 90 days, and DOR364 monoculture for 84 days. It is noted that DOR364 reached maturity earlier than SEQ7 (personal observation).

Trait measurement

We harvested the mixtures of DOR364 and SEQ7at 94 DAS when plants reached full maturity. The standard legume Shovelomics method²³ and the DIRT software^{24,25} was used to extract root architecture traits. Both shoot and root tissues were dried in an oven at 60 °C for a minimum of 72 hours before weighing them on a digital balance (Model CQT202, Readability 0.01g, Adam Equipment, Oxford, CT, USA). For the monoculture of SEQ7, we used the Seed Counter Android app²⁶ to quantify the seed number per plant for majority of samples. For samples not easily detected by the app, we manually counted the seeds. For both the monoculture of DOR364 and mixtures of DOR364 and SEQ7, the seed numbers were counted for each individual plant using the python package GridFree²⁷. We quantified the population's fitness by measuring the average number of seeds per plant across various planting scenarios and water conditions.

Statistical analysis

We applied the DIRT-Pop pipeline developed in Chapter 2 to cluster the root architecture types of mixtures of DOR364 and SEQ7. The clustering result for monocultures of SEQ7 and DOR364 were obtained from Chapter 3. Once root architecture types were assigned, we employed the Fréchet pairwise distance matrix across both monoculture and mixture for DOR364 and SEQ7. This analysis allowed us to correlate the identified root architecture types with the simulated root architecture models discussed in Chapter 3. Subsequent statistical analyses were conducted in R (v 4.2.0)²⁸ for testing any difference in the composition of root architecture types, seed number and root-shoot ratio between monoculture and mixture for each genotype and water condition. First, we used the pairwise Chi-square test of homogeneity to determine whether the composition of root architecture types was uniform under different planting scenarios and conditions. We then used the non-parametric Wilcoxon rank-sum test to test for significant differences in seed number per plant and root-shoot ratio between monoculture and mixture for each genotype and water condition.

Results

Mixtures of SEQ7 and DOR364 exhibited greater population fitness than monocultures, with distinct fitness responses observed within each genotype.

In assessing population fitness through average seed number per plant, the mixture of SEQ7 and DOR364 (mean=133.33, NL; mean=102.31, WL) had significantly higher fitness than SEQ7 monoculture (mean=68.95, NL; mean=24.68, WL) and DOR364 (mean=96.97, NL; mean=76.25, WL) under both water conditions (Wilcoxon rank-sum test, P <0.05; Figure 4.1 & Table S4.2). The fitness of DOR364 was significantly lower in mixture (mean=87.10, NL; mean=71.62, WL) than in monoculture (mean=96.97, NL; mean=76.25, WL) under both water

conditions (Wilcoxon rank-sum test, P <0.05; Figure 4.2 & Table S4.2). In contrast, while SEQ7 showed a significant increase in fitness in mixtures (mean=175.89, NL; mean=127.25, WL) compared to its fitness in monocultures (mean=68.95, NL; mean=24.68, WL) for both water conditions (Wilcoxon rank-sum test, P <0.05; Figure 4.2 & Table S4.2).

SEQ7 and DOR364 showed differences in change of root-shoot ratio and proportions of root architecture types in response to different planting scenarios.

In examining the root-shoot ratios of SEQ7 and DOR364 in monocultures and mixtures (Figure 4.4), DOR364 significantly increased root-shoot ratio in mixture and monoculture under both NL (mean=0.09, mixture; mean=0.049, monoculture) and WL (mean=0.09, mixture; mean=0.053, monoculture) conditions (Wilcoxon rank-sum test, P <0.05). SEQ7 maintained a similar root-shoot ratio between mixture and monoculture under NL conditions (mean=0.037, mixture; mean=0.040, monoculture) conditions. However, under WL conditions, SEQ7 demonstrated a significant decrease in root-shoot ratio in mixtures compared to monocultures (mean=0.038 in mixture; mean=0.079 in monoculture; Wilcoxon rank-sum test, P < 0.05).

Regarding the root architecture types, DOR364 showed a significant difference in the composition of root architecture types between monocultures and mixtures under NL conditions (Figure 4.6; Chi-square test: P < 0.05) but was not under WL (Figure 4.6; Chi-square test: P =0.273) conditions. Under both WL and NL conditions, DOR364 exhibited an increase in AT2 root architecture in mixtures by 9.53% and 8.56%, respectively (Figure 4.6). On the other hand, SEQ7 showed a significant shift in the composition of root architecture types between monocultures and mixtures under WL conditions (Figure 4.6; Chi-square test: P <0.05) but not under NL conditions (Figure 4.6; Chi-square test: P =0.257). Specifically, SEQ7 showed a

decrease in AT2 by 14.58% (WL) and 9.45% (NL) in mixtures, accompanied by a decline in AT3 by 18.92% (WL) and 9.45% (NL) in mixtures, respectively (Figure 4.6).

Using the linked root architecture model results in Chapter3, we grouped the root architecture types of DOR364 and SEQ7 into three main categories: deep (AT3), fan (AT1 and AT4), and shallow (AT2 and AT5). Under the NL condition, DOR364 increased proportion of shallow root category by 15.08%, slightly increased proportion of deep root category by 4.75%, while decreased proportion of fan root category by 19.83% in the mixture than monoculture (Figure 4.3 & Figure 4.7). While under the WL condition, DOR364 increased shallow root category by 1.86%, fan root category by 4.69%, but decreased deep root category by 6.55% in the mixture than the monoculture (Figure 4.3 & Figure 4.7). For SEQ7, under NL conditions, there was a decrease in shallow root category by 6.77%, a decrease in fan root category by 3.59%, and an increase in deep root category by 10.36% in mixtures compared to monocultures (Figure 4.3 & Figure 4.7). Under WL conditions, the pattern intensified, with decreases in shallow (8.33%) and fan (10.54%) root category, coupled with a significant increase in deep root category by 18.87% (Figure 4.3 & Figure 4.7).

Discussion

In this chapter, the differential root allocation strategies and architectural changes exhibited by SEQ7 and DOR364 when grown as monoculture versus mixture offer insights into the complexity of plant competition dynamics and their implications in agriculture. SEQ7 exhibited a tendency to either maintain or reduce its root biomass allocation in mixture compared to monoculture under both NL and WL conditions (Figure 4.3 & Table S4.2). In contrast, DOR364 consistently increased its root biomass allocation in mixture compared to monoculture under both conditions (Figure 4.3 & Table S4.2). Interestingly, the corresponding population

fitness of DOR364 decreased by 10.17% under the NL and 6.04% under the WL condition in mixture compared to monoculture, while the population fitness of SEQ7 increased dramatically by 155.10% under the NL condition and 415.60% under the WL condition in mixture than monoculture. Together, the combined population fitness of the mixture SEQ7 and DOR364 were significantly higher than its monocultures DOR364 and SEQ7 (Table S 4.2, Table S 4.3, Figure 4.1). This could be attributed to the average seed number per plant of SEQ7 increasing more substantially than the decrease observed in DOR364's average seed number per plant, thus enhancing the overall fitness of the mixture over monocultures. These findings suggest that although DOR364 allocates more resources to root biomass in competition, this strategy does not confer a fitness advantage. The increased root proliferation maybe a cost of competition, as increased root biomass can be a trade-off with aboveground biomass, consequently fitness^{13,21}. On the other hand, SEQ7, with its less or similar root allocation between monocultures and mixtures under both water condition, have a significant fitness benefit.

Another notable observation was a difference in the composition of root architecture types of DOR364 and SEQ7, when plants were grown in monoculture or mixture. Overall, when grown with DOR364, SEQ7 predominantly shifted towards producing a higher proportion of deep root phenotype under both water conditions, notably doubling the proportion under WL conditions. In contrast, when growing with SEQ7, DOR364 tended to produce more shallow root phenotype under the NL condition and reduced its deep root phenotype proportion under the WL condition. These findings suggest both genotypes, SEQ7 and DOR364, appear to employ strategies to avoid acquisition for same soil resources, with DOR364 focusing on topsoil and SEQ7 targeting subsoil resources when in mixture. This differentiation in resource utilization

suggests a form of niche partitioning, allowing both to coexist by avoiding direct competition in the soil layers.

To summarize, when in mixture, DOR364 increased root allocation, investing more in root growth for competition than in monoculture when interacting with its own kind. The increased root allocations in mixture in line with kin selection theory prediction, which anticipate intensified competition in mixture^{9,19}. However, the more investment root growth for competition may represent a fitness trade-off for DOR364. In comparison, SEQ7 either maintained or decreased root allocation in the presence of DOR364, which is more consistent with niche partitioning theory prediction. Architecturally, DOR364 and SEQ7 showed complementary root architecture categories to avoid competition. Specifically, SEQ7 increased frequency of deep root architecture phenotype potentially advantageous for water acquisition, particularly under stress conditions. This shift in root architecture type within SEQ7's population, as opposed to a mere change in allocation, contribute to its higher fitness levels when competing with DOR364. Chapter 3 also showed root architectural change was independent of root allocation change, may not be a cost of fitness, implying that changing the fraction of root architecture types could be a more effective strategy for competing with other plants than changing how resources are allocated to roots. The differential responses of DOR364 and SEQ7, suggest that neither kin selection nor niche partitioning theories can fully account for the complexity of plant root interactions. The fitness outcomes of plant interactions also depend on the specific genotypes involved^{6,12,29–31}. Differences in genotypes regarding quantitative traits such as plant size, growth rate, and allocation can lead to variations in competitive abilities. The fitness outcomes of monoculture and mixture can range from positive to neutral or even

negative³². This variability suggests a continuum of fitness outcome influenced by both kin selection and niche differentiation, rather than dichotomy.

Acknowledgements

We extend our sincere gratitude to Sydney Page for her efforts in collecting the biomass data of the DOR364 monoculture experiment, to Huang Chen for his assistance in root harvest and biomass and seed data collection for the mixture experiment, and to Michael Boyd and Gregory Cousins for their expertise in pest control and greenhouse management.

Reference

- Ashton, I. W., Miller, A. E., Bowman, W. D. & Suding, K. N. Niche complementarity due to plasticity in resource use: plant partitioning of chemical N forms. *Ecology* 91, 3252–3260 (2010).
- 2. Fajardo, A. & McIntire, E. J. B. Under strong niche overlap conspecifics do not compete but help each other to survive: facilitation at the intraspecific level. *J. Ecol.* **99**, 642–650 (2011).
- 3. Silvertown, J. Plant coexistence and the niche. Trends Ecol. Evol. 19, 605–611 (2004).
- 4. Macarthur, R. & Levins, R. The Limiting Similarity, Convergence, and Divergence of Coexisting Species. *Am. Nat.* **101**, 377–385 (1967).
- 5. Brooker, R. W. *et al.* Improving intercropping: a synthesis of research in agronomy, plant physiology and ecology. *New Phytol.* **206**, 107–117 (2015).
- 6. Demie, D. T. *et al.* Mixture × Genotype Effects in Cereal/Legume Intercropping. *Front. Plant Sci.* **13**, (2022).
- 7. Li, L., Tilman, D., Lambers, H. & Zhang, F. S. Plant diversity and overyielding: Insights from belowground facilitation of intercropping in agriculture. *New Phytol.* **203**, 63–69 (2014).
- 8. Zhang, C., Postma, J. A., York, L. M. & Lynch, J. P. Root foraging elicits niche complementarity-dependent yield advantage in the ancient 'three sisters' (maize/bean/squash) polyculture. *Ann. Bot.* **114**, 1719–1733 (2014).
- 9. Dudley, S. A. & File, A. L. Kin recognition in an annual plant. *Biol. Lett.* **3**, 435–438 (2007).
- Bais, H. P. Shedding light on kin recognition response in plants. *New Phytol.* 205, 4–6 (2015).

- 11. Yang, X.-F., Li, L.-L., Xu, Y. & Kong, C.-H. Kin recognition in rice (*Oryza sativa*) lines. *New Phytol.* **220**, 567–578 (2018).
- 12. West, S. A., Pen, I. & Griffin, A. S. Cooperation and competition between relatives. *Science* **296**, 72–75 (2002).
- 13. Semchenko, M., Saar, S. & Lepik, A. Plant root exudates mediate neighbour recognition and trigger complex behavioural changes. *New Phytol.* **204**, 631–637 (2014).
- 14. Zhang, L., Liu, Q., Tian, Y., Xu, X. & Ouyang, H. Kin selection or resource partitioning for growing with siblings: implications from measurements of nitrogen uptake. *Plant Soil* **398**, 79–86 (2016).
- Takigahira, H. & Yamawo, A. Competitive responses based on kin-discrimination underlie variations in leaf functional traits in Japanese beech (*Fagus crenata*) seedlings. *Evol. Ecol.* 33, 521–531 (2019).
- 16. Fang, S. *et al.* Genotypic recognition and spatial responses by rice roots. *Proc. Natl. Acad. Sci. U. S. A.* **110**, 2670–2675 (2013).
- 17. Murphy, G. P. & Dudley, S. A. Kin recognition: Competition and cooperation in Impatiens (*Balsaminaceae*). *Am. J. Bot.* **96**, 1990–1996 (2009).
- 18. Biernaskie, J. M. Evidence for competition and cooperation among climbing plants. *Proc. R. Soc. B Biol. Sci.* **278**, 1989–1996 (2011).
- 19. Bhatt, M. V., Khandelwal, A. & Dudley, S. A. Kin recognition, not competitive interactions, predicts root allocation in young *Cakile edentula* seedling pairs. *New Phytol.* **189**, 1135–1142 (2011).
- 20. Simonsen, A. K., Chow, T. & Stinchcombe, J. R. Reduced plant competition among kin can be explained by Jensen's inequality. *Ecol. Evol.* **4**, 4454–4466 (2014).

- 21. O'Brien, E. E., Gersani, M. & Brown, J. S. Root proliferation and seed yield in response to spatial heterogeneity of below-ground competition. *New Phytol.* **168**, 401–412 (2005).
- 22. Aerts, R., Boot, R. G. A. & van der Aart, P. J. M. The relation between above- and belowground biomass allocation patterns and competitive ability. *Oecologia* **87**, 551–559 (1991).
- 23. Burridge, J., Jochua, C. N., Bucksch, A. & Lynch, J. P. Legume shovelomics: High-Throughput phenotyping of common bean (*Phaseolus vulgaris* L.) and cowpea (*Vigna unguiculata* subsp, *unguiculata*) root architecture in the field. *Field Crops Res.* **192**, 21–32 (2016).
- 24. Das, A. *et al.* Digital imaging of root traits (DIRT): A high-throughput computing and collaboration platform for field-based root phenomics. *Plant Methods* **11**, 1–12 (2015).
- 25. Bucksch, A. *et al.* Image-Based High-Throughput Field Phenotyping of Crop Roots. *Plant Physiol.* **166**, 470–486 (2014).
- 26. Komyshev, E., Genaev, M. & Afonnikov, D. Evaluation of the SeedCounter, A Mobile Application for Grain Phenotyping. *Front. Plant Sci.* **7**, (2017).
- 27. Hu, Y. & Zhang, Z. GridFree: a python package of image analysis for interactive grain counting and measuring. *Plant Physiol.* **186**, 2239–2252 (2021).
- 28. R Core Team. R: A Language and Environment for Statistical Computing. (2022).
- 29. Fridley, J. D. & Grime, J. P. Community and ecosystem effects of intraspecific genetic diversity in grassland microcosms of varying species diversity. *Ecology* **91**, 2272–2283 (2010).

- 30. Fridley, J. D., Grime, J. P. & Bilton, M. Genetic identity of interspecific neighbours mediates plant responses to competition and environmental variation in a species-rich grassland. *J. Ecol.* **95**, 908–915 (2007).
- 31. Yamawo, A. & Mukai, H. Outcome of interspecific competition depends on genotype of conspecific neighbours. *Oecologia* **193**, 415–423 (2020).
- 32. Ehlers, B. K. & Bilde, T. Inclusive fitness, asymmetric competition and kin selection in plants. *Oikos* **128**, 765–774 (2019).

Figures

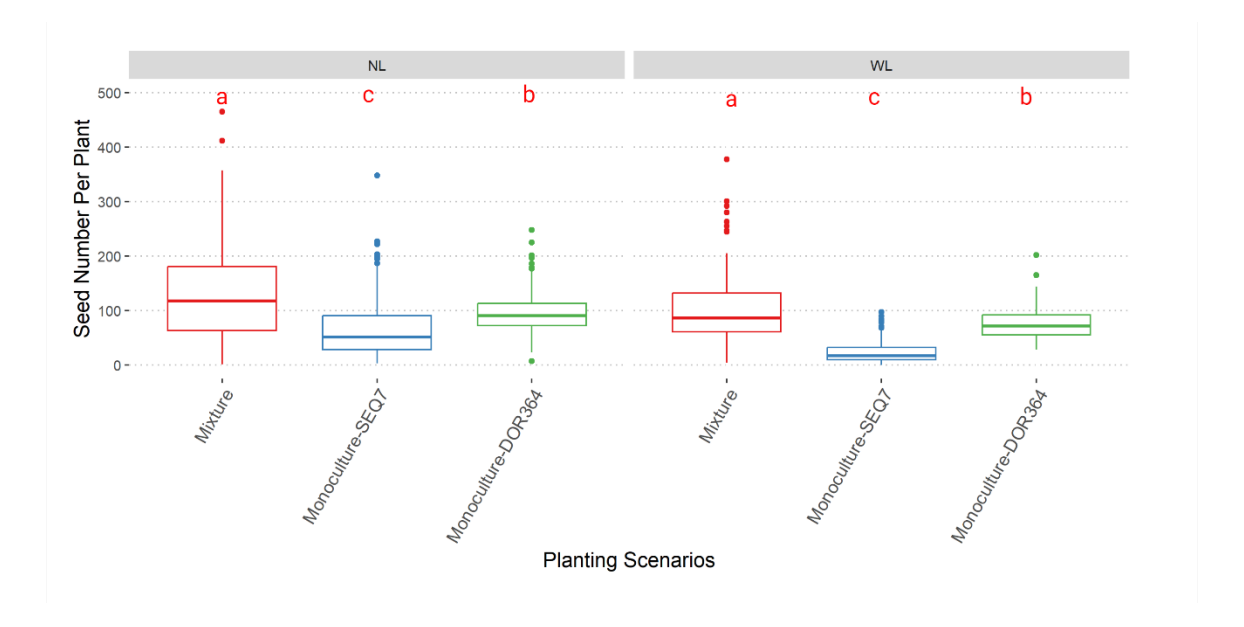


Figure 4.1: Seed number per plant of mixture of DOR364 and SEQ7 were higher than monoculture of DOR364 and SEQ7. Boxplots depict the median of seed number per plant in each planting scenario bounded by the first and third quantile. We applied the pairwise Wilcoxon rank sum test to identify any significant differences in seed number among planting scenarios. Different letters label planting scenarios with significant differences, with significance threshold set as P < 0.05.

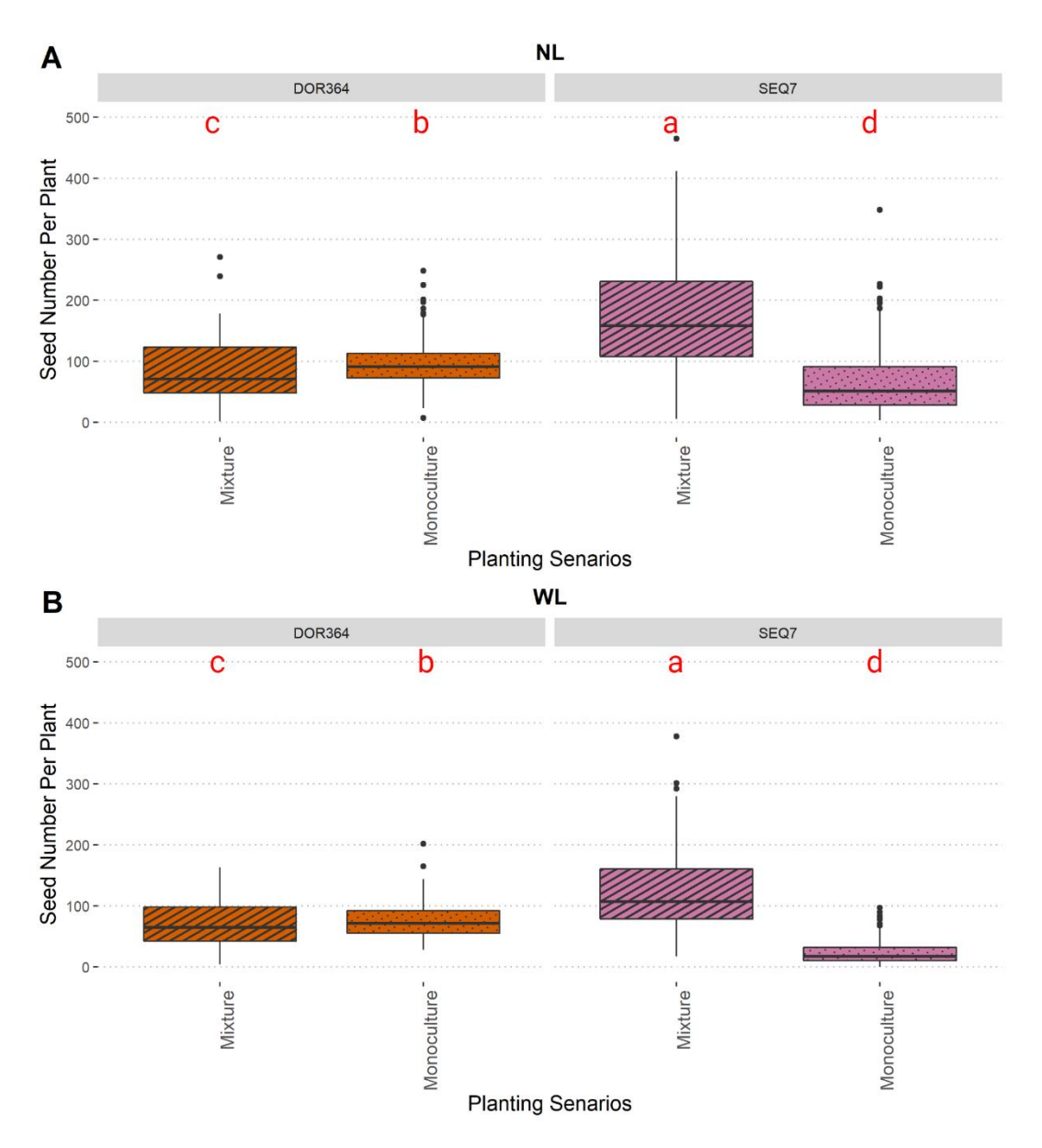


Figure 4.2: Seed number per plant of DOR364 (A) and SEQ7 (B) were different between mixture and monoculture planting scenarios under between non-limiting (NL) and water-limited (WL) conditions. Boxplots depict the median of seed number per plant by the first and third quantile between mixture and monoculture planting scenarios. We applied the Wilcoxon rank-sum test to identify any significant differences in seed number per plant between the planting scenarios under each condition. Different letters label planting scenarios with significant differences, with significance threshold set as P < 0.05.

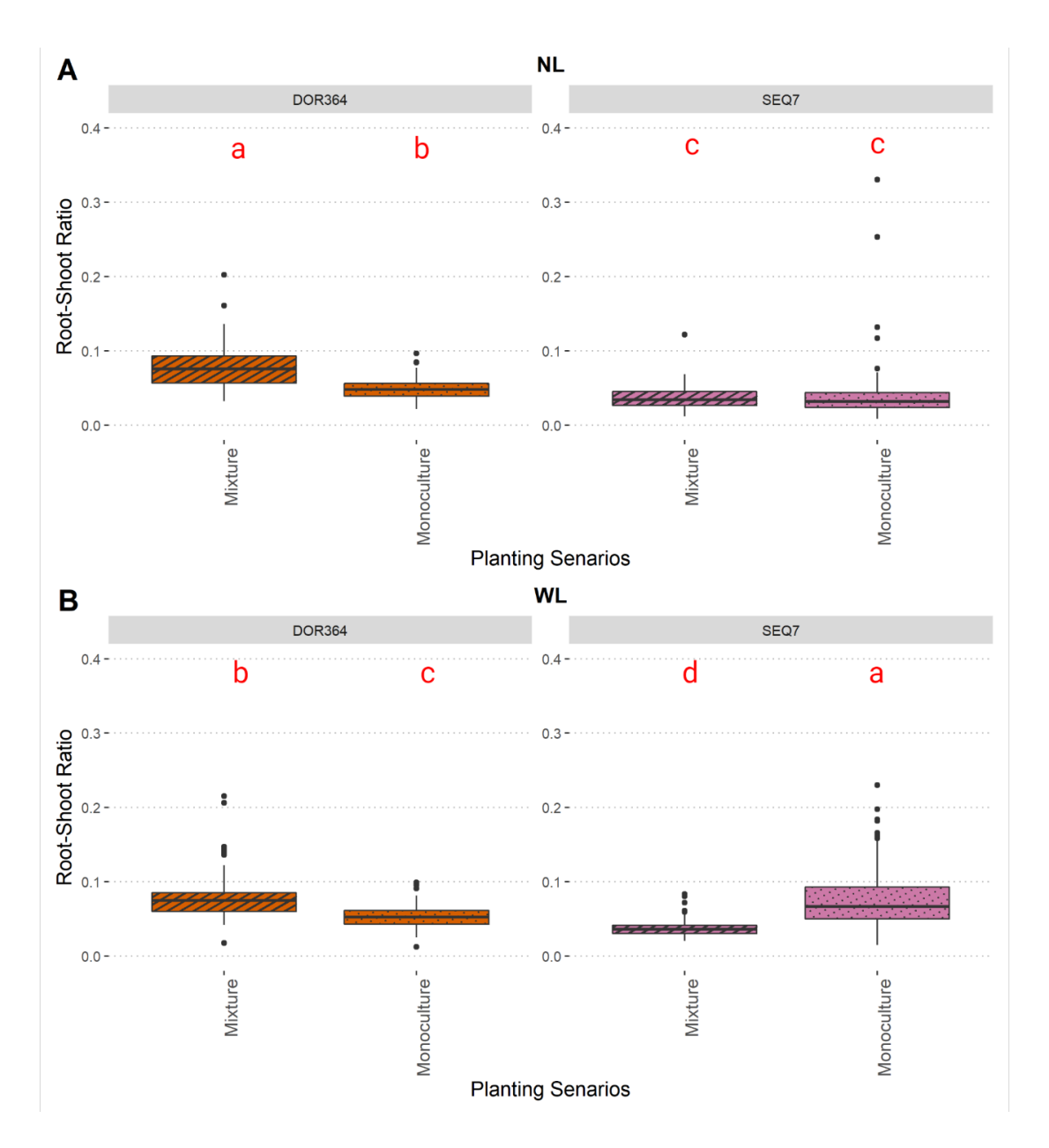


Figure 4.3: Comparison of root-shoot ratio of DOR364 (A) and SEQ7 (B) between mixture and monoculture planting scenarios under non-limiting (NL) and water-limited (WL) conditions. Boxplots depict the median of root-shoot ratio by the first and third quantile between mixture and monoculture planting scenarios. We applied the Wilcoxon rank-sum test to identify any significant differences in root-shoot ratio between the planting scenarios under each condition. Different letters label planting scenarios with significant differences, with significance threshold set as P < 0.05.

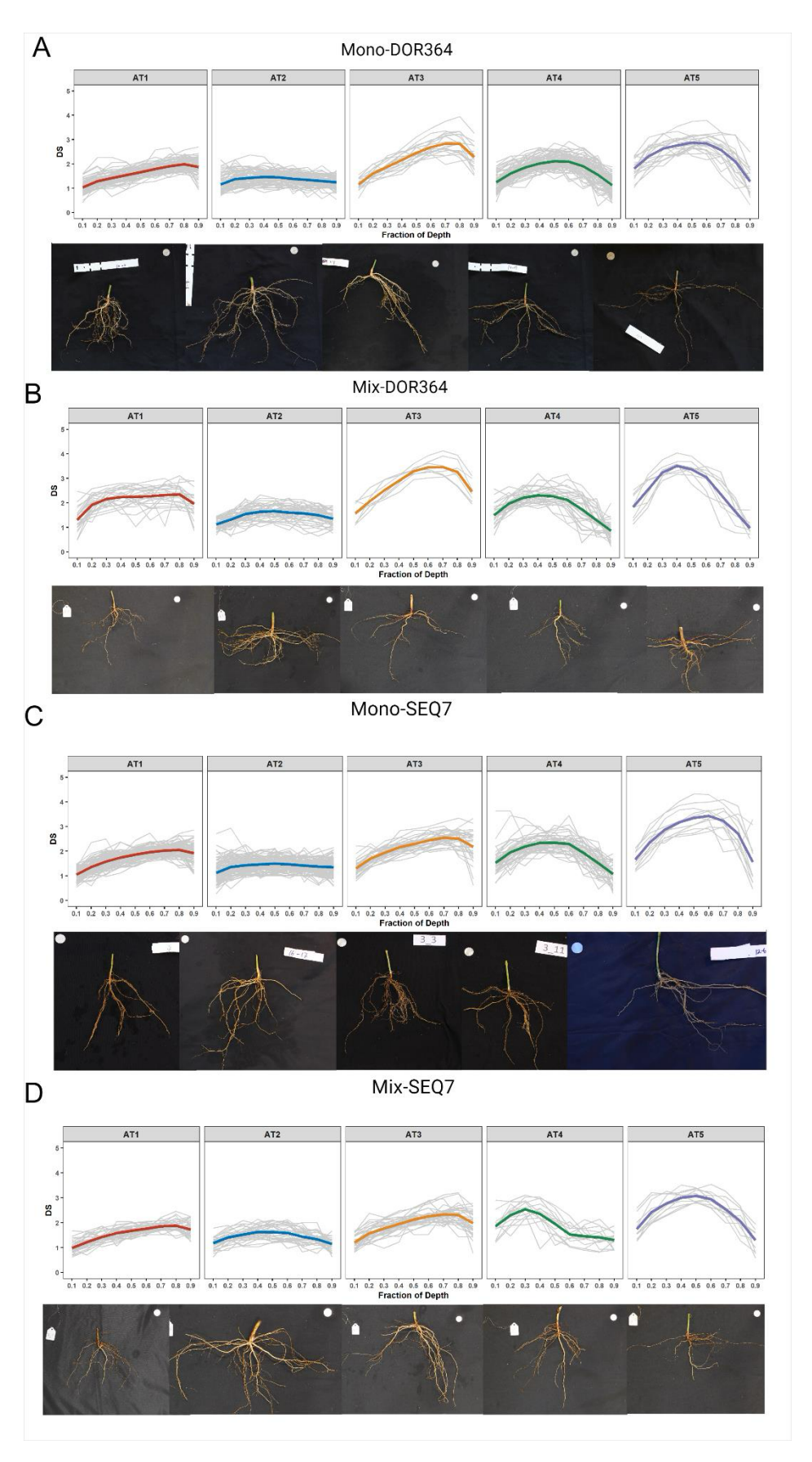


Figure 4.4: Five root architecture types of SEQ7 and DOR364 were observed across planting scenarios (monoculture and mixture). We have graphed the mean DS curve corresponding to each root architecture type: DOR364 in monoculture (Panel A, n=261; DOR364 in mixture (Panel B, n=110); SEQ7 in monoculture (Panel C, n=276)); SEQ7 in mixture (Panel D, n=127). with a representative root image displayed beneath. The diameter of reference marker in the root images measured 24.26 mm.

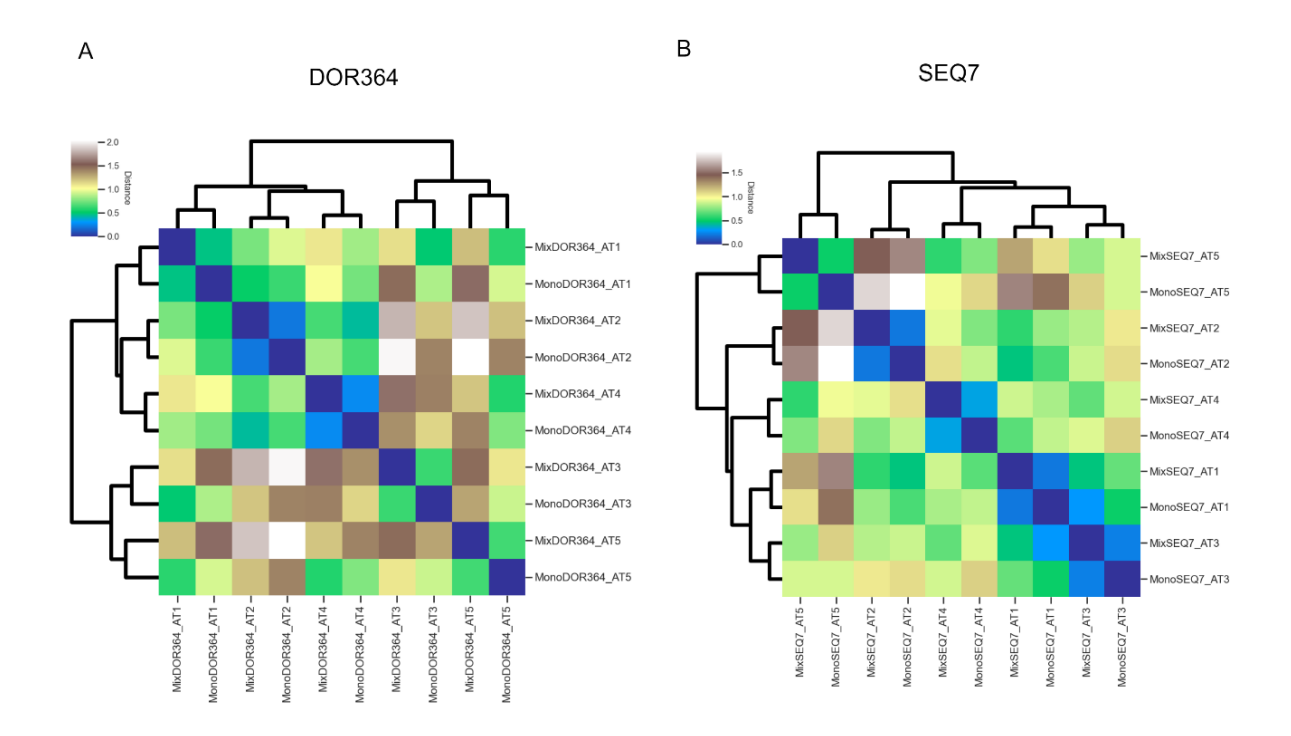


Figure 4.5: The heatmap of Fréchet distance matrix confirmed that while AT1 through AT5 were distinct, each showed consistent internal similarity across both monoculture and mixture for DOR364 (panel A) and SEQ7 (panel B). The heatmap depicts the Fréchet distances between the mean curves of each root architecture type in different planting scenarios. Each pixel's color in the heatmap corresponds to the Fréchet distance between two root architecture types, with blue representing higher similarity and brown denoting greater dissimilarity. The dendrograms on the axes represent the hierarchical clustering of the clusters based on their Fréchet distances.

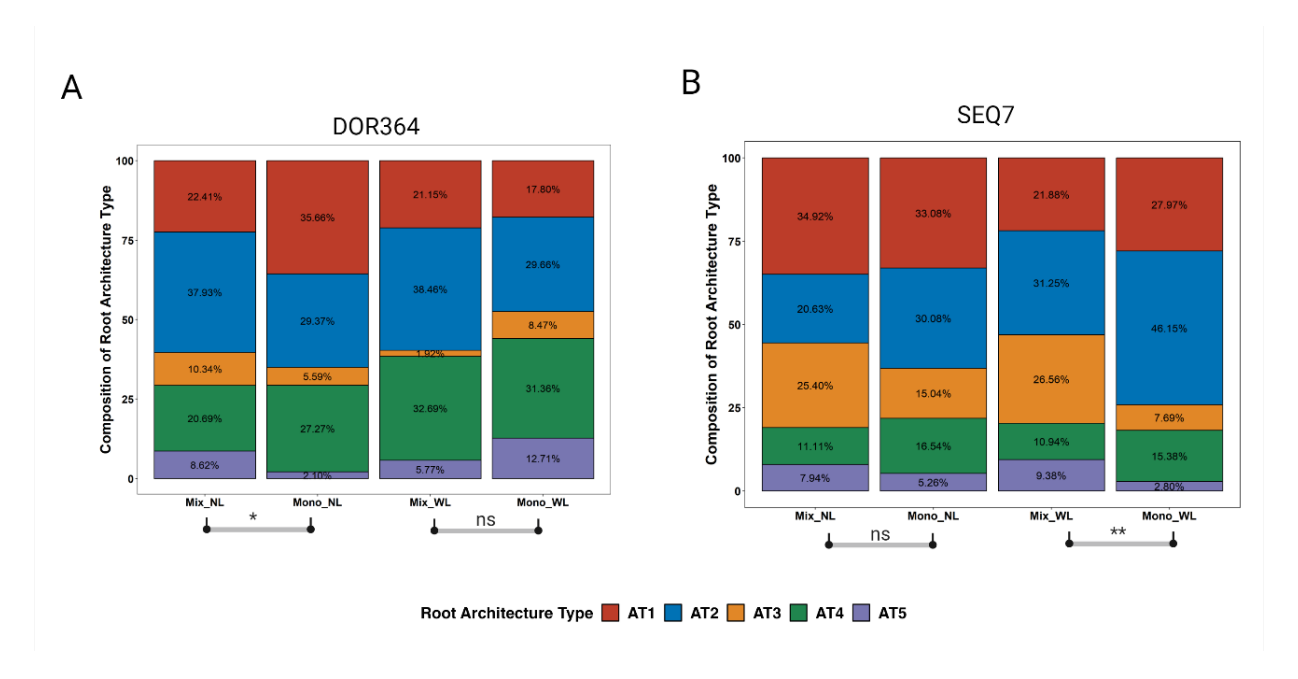


Figure 4.6: The composition of root architecture types of DOR364 (panel A) and SEQ7 (panel B) between planting scenarios (Mix: mixture and Mono: monoculture) and conditions (WL: Waterlimited and NL: Non-limiting). The sample size for each planting scenario and condition of each genotype were detailed in Table S4.1. We used the chi-square test of homogeneity to compare the different distribution of root architecture types between planting scenarios for each genotype. The statistical significance is denoted as follows: ** $P \le 0.01$, * $P \le 0.05$, • P < 0.1 and ns: not significant.

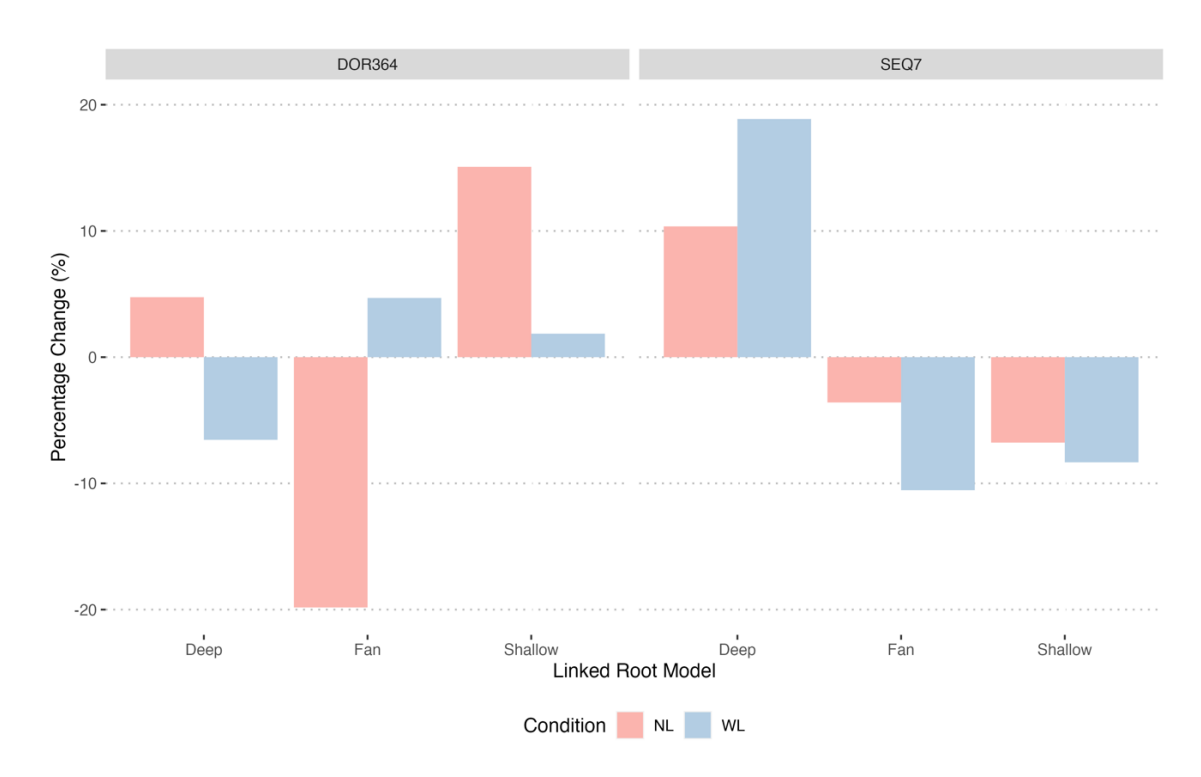


Figure 4.7: Percentage change in root architecture categories for SEQ7 and DOR364 when comparing mixtures to monocultures. Root architecture types were categorized based on Chapter 3's findings into three main models: Deep (AT3 with 3 whorls), Fan (AT1 with 1 whorl, AT4 with 2 whorls), and Shallow (AT2 with 2 whorls, AT5 with 1 whorl). The percentage changes were determined by subtracting the proportions of each root architecture type in mixtures to those in monocultures.

Appendix C

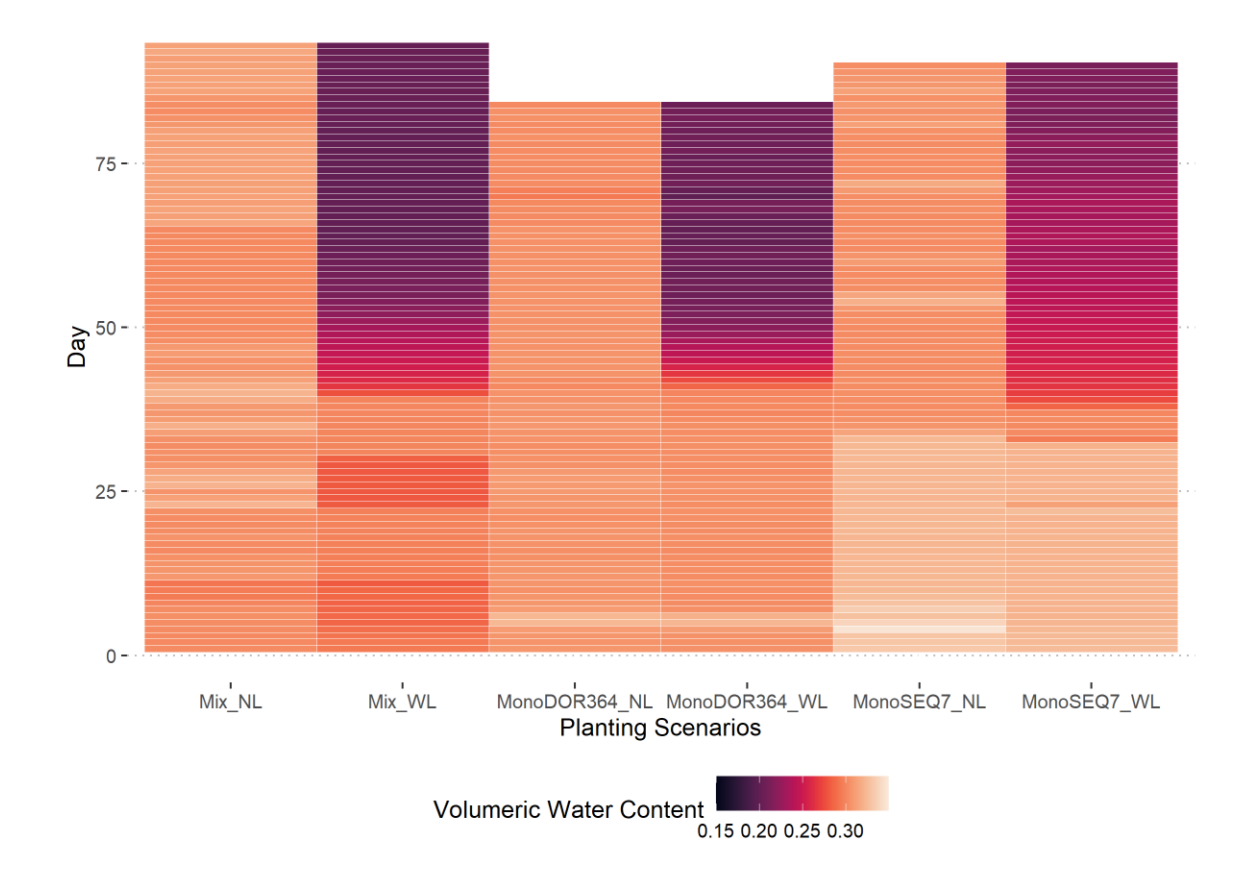


Figure S4.1: The daily mean volumetric water content (vwc) across planting scenarios. In this figure, the color key indicates the VWC values, with darker color representing lower VWC, and lighter color corresponding to higher VWC. "NL" denotes for non-limiting conditions, while "WL" denotes water-limited conditions. Mix refers to mixture and Mono refers monoculture. The mixture of SEQ7 and DOR364 was grown for 93 days, SEQ7 monoculture for 90 days, and DOR364 monoculture for 84 days. It is noted that DOR364 reached maturity earlier than SEQ7 (personal observation).

Table S4.1: Sample sizes across different root architecture types of DOR364 and SEQ7 under various planting scenarios and conditions. 'NL' represents non-limiting conditions, while 'WL' represents water-limited conditions. 'Mix' means mixture and 'Mono' means monoculture.

	AT1	AT2	AT3	AT4	AT5	Total
Mix_NL_DOR364	13	22	6	12	5	58
Mix_WL_DOR364	11	20	1	17	3	52
Mono_NL_DOR364	51	42	8	39	3	143
Mono_WL_DOR364	21	35	10	37	15	118
Mix_NL_SEQ7	22	13	16	7	5	63
Mix_WL_SEQ7	14	20	17	7	6	64
Mono_NL_SEQ7	44	40	20	22	7	133
Mono_WL_SEQ7	40	66	11	22	4	143

Table S4.2: The summary statistics of seed number per plant and root-shoot ratio of DOR364 and SEQ7 over planting scenarios and conditions. 'NL' denotes for non-limiting conditions, while 'WL' denotes water-limited conditions. Mixed denotes mixed-cropping, while Mono denotes mono-cropping.

Trait	Condition	Planting & Genotype	Mean	Median	Standard Error	Standard Deviation
Seed	NL	MixedDOR364	87.10	70.50	7.76	59.10
Number	NL	MixedSEQ7	175.89	158.00	12.96	102.89
Per Plant	NL	MonoDOR364	96.97	91.00	3.28	39.27
	NL	MonoSEQ7	68.95	51.00	4.97	57.30
	WL	MixedDOR364	71.62	65.00	5.47	39.42
	WL	MixedSEQ7	127.25	107.00	9.07	72.52
	WL	MonoDOR364	76.25	71.50	2.77	30.08
	WL	MonoSEQ7	24.68	17.00	1.79	21.46
Root-	NL	MixedDOR364	0.090	0.077	0.070	0.009
Shoot	NL	MixedSEQ7	0.037	0.034	0.016	0.002
Ratio	NL	MonoDOR364	0.049	0.048	0.013	0.001
	NL	MonoSEQ7	0.040	0.032	0.036	0.003
	WL	MixedDOR364	0.090	0.075	0.073	0.010
	WL	MixedSEQ7	0.038	0.036	0.013	0.002
	WL	MonoDOR364	0.053	0.052	0.014	0.001
	WL	MonoSEQ7	0.079	0.067	0.051	0.004

CHAPTER 5

SUMMARY

The central theme of this dissertation is the exploration of root architectural variation within plant populations. The common bean (*Phaseolus vulgaris* L.) was used as the model system to conduct studies in both field conditions and controlled environments. One aim was to confirm the existence of varied root architecture types within a single genotype across years and conditions and to understand how these types change in response to different water conditions and over the developmental stages. This dissertation also delved into the role these root architectural types play in plant competition and their subsequent impact on the fitness of the population in both monoculture and mixture, using two genotypes: DOR364 and SEQ7.

Chapter 2 challenged the current sampling strategy, which typically involves sampling only a few plants per genotype, and proposed that to capture the full extent of root architectural variation, researchers need to increase their sample size per genotype. In Chapter 2, we developed a computational pipeline, DIRT-Pop as a computational tool to analyze the root architectural variation of one genotype. This pipeline employs the DS-curve, a mathematical shape descriptor, to capture the entire root architecture. Applying this pipeline to a field dataset encompassing three common bean genotypes, DOR364, L8857 and SEQ7, under non-limiting (NL) and water-limited (WL) conditions, we have identified five distinct root architecture types across these genotypes and conditions. Additionally, five root architecture types of three genotypes have changed their composition in response to the most varying water conditions. Based on this finding, we hypothesize that plants might adopt specific belowground strategies

including modifications in the composition of root architecture types to acclimate to environmental changes without impacting their aboveground growth.

Chapter 3 introduced a newly developed mesocosm system that mimics field conditions with a sensor-controlled irrigation system, aiming to minimize environmental variations. By replicating the SEQ7 and DOR364 genotypes in this in a controlled mesocosm environment under WL and NL condition, we also observed the similar five root architecture types of SEQ7 and DOR364, suggesting that environmental variation in the field may not be the primary driver of these root architecture types. The results showed that the composition of these root architecture types within the SEQ7 population varied under different water conditions and developmental stages. This observation supports the hypothesis presented in Chapter 2 that plant populations may adjust their root architecture types as a strategy to acclimate in response to environmental changes. We also discussed that the changes in the composition of root architecture types during the early developmental stages could be triggered by seed reserve depletion and the beginning of root interaction. Further observations indicated that the shoot biomass, root biomass, and their root-to-shoot ratio did not significantly differ among the root architecture types, indicating that the change in root architecture could be independent of changes in biomass allocation. By linking identified root architecture types with existing public root simulation models, we hypothesized that each observed root architecture type may have a unique function in nitrogen and phosphorus uptake under the non-limiting condition.

In Chapters 2 and 3, we identified the presence of five root architecture types within a single genotype of the common bean, raising the questions about the fitness benefits of such diverse root architecture of one genotype when interacting with either with itself or with a different genotype as a neighbor. To address this, Chapter 4 further investigated how root

architecture types and biomass allocation impact fitness outcome in monoculture and mixture under WL and NL conditions, using SEQ7 and DOR364 genotypes. This exploration, through the lens of resource partitioning and kin selection theories, shed light on plant-plant interactions. The results showed that mixtures of these two genotypes had higher fitness compared to monocultures, primarily due to the significant fitness increase observed in SEQ7, in contrast to the fitness decrease in DOR364. Specifically, SEQ7 reduced root biomass allocation and increased the proportion of deep-root phenotypes in mixtures compared to monocultures, a strategy that significantly increased SEQ7's fitness. Conversely, DOR364 allocated more resources to root biomass and increased the proportion of shallow-root phenotypes in the mixture, which came at a cost to its short-term fitness. The different responses of DOR364 and SEQ7 in terms of root allocation and root architecture type, along with the observed fitness outcomes in monoculture and mixture, suggest that the two theories may not fully capture the complexities of root interactions. This indicates a need for further exploration into the mechanisms underlying these interactions and their consequences for plant fitness and ecosystem dynamics.

In the end, we would introduce the phenotypic spectrum framework (Figure 5.1) to study the diversity of crop roots. This framework serves as an extension to the existing phenotypic plasticity framework. The traditional phenotypic plasticity framework assume that a single genotype has a common root architecture (or ideotype) in a given environment. By measuring the mean of a particular root trait across various environments with significant differences, we can observe that the genotype exhibits phenotypic plasticity. However, the phenotypic spectrum framework assumes a single genotype can express a finite number of root architecture types within the same environmental context. This framework shifts the focus from assessing mean

trait variations to examining the ratios of distinct root architecture types within a genotype. A significant shift in these ratios across different environments is interpreted as the genotype's acclimatation strategy to environmental changes. The phenotypic spectrum categorizes phenotypic variation into several types, that goes beyond mere average trait analyses. Such a perspective allows for a more comprehensive understanding of how genotypes adapt to environmental challenges.

However, there are several limitations and future directions that can help us better understand root architectural variation and their implication in agriculture. Below are some examples of what these limitations and possible areas of exploration could be.

First, the DS curve used in DIRT-Pop Pipeline only measure the change of normalized root width over the rooting depth, which does not include information about lateral root branch density, number of basal roots and so on. The introduction of a new shape descriptor from the Dirt3D platform, which calculates area accumulation over depth without normalization, presents a promising avenue for better categorizing root architecture types¹. Further development of descriptors that capture details like root branch patterns could enrich our understanding of these root architectural variation, potentially revealing a broader spectrum of root architecture types identified for crop roots.

Second, Chapter 3 used the published root architecture models to infer the nutrient uptake function of each root architecture type. These simulated root architecture models were generated using the average parameters (number of basal whorls, top root angle, lateral root branch density) from several samples per genotype and no variation in adventitious shoot². Thus, the simulation model may not reflect the range of diverse root architecture type observed in the real world setting. As previously mentioned, the shape descriptor employed in the Dirt-Pop pipeline lacks

information regarding the number of basal roots and the density of lateral root branching. Consequently, the DS curves of some of simulated root architecture models appear similar, which may hinder the nutrient uptake function prediction. To improve inferring nutrient uptake function of root architecture types from the root architecture models, it is necessary to develop root architecture models and shape descriptors that more represent the real-world root systems. Given that root architecture types may be linked to specific nutrient uptake functions, such differences could influence the nutrient contents in seeds. We sent a subset of seeds from the SEQ7 genotype at 90 DAS under both water conditions was sent to the University of Georgia Extension Ag & Environmental Services Lab for macronutrients (Calcium, Ca; Sulfur, S; Nitrogen, N; Phosphorus, P; Magnesium, Mg; Potassium, K) and micronutrients (Boron, B; Copper, Cu; Iron, Fe; Manganese, Mn; Molybdenum, Mo; Chlorine, Cl) analysis. A preliminary analysis of macronutrients and micronutrients in the seed content data for each root architecture type within SEQ7 revealed distinctive patterns (Figure 5.2). However, due to the small sample size, the differences in seed content across root architecture types were not statistically significant (Figure 5.3). Nonetheless, this observation offers a potential direction for future research, particularly in exploring how root architecture might influence seed nutrient content. As demonstrated in Chapters 2 and 3, root architecture types were not correlated with aboveground biomass, suggesting that enhancing crop nutrient profiles through root architecture could offer a sustainable solution to improve food quality without the trade-off of reduced productivity.

Chapter 4 presented the different responses of DOR364 and SEQ7 in terms of root allocation and root architecture type, along with the observed fitness outcomes in monoculture and mixture of these two genotypes. SEQ7 showed more root avoidance in mixture than

monoculture, while DOR364 showed more root avoidance in monoculture than in mixture. This indicates a genotypic variation in adopting strategies of avoidance or competition when in response to in monoculture or mixed with a different genotype. According to the niche partition theory, intercropping different genotypes or species to exploit differences in spatial segregation and resource uptake, thereby avoid direct competition, achieving higher yields. For instance, successfully intercropping legumes with cereals demonstrates how niche partitioning can enhance grain production through more complete resource utilization in nitrogen³. However, not all intercropping systems guarantee yield or fitness benefits; this depends on the specific species or genotypes involved, the sowing ratio, and the growing conditions⁴. In contrast, kin selection theory advocates for the breeding of less competitive genotypes in monoculture, based on the plant's ability to recognize the identity of their neighbors and reduce competition with their closely related kin^{5,6}.

The variability in genotype responses underscores the importance of context-specific strategies, suggesting that the success of such approaches, either in intercropping of multiple crop species or genotypes or in breeding for less competitive traits in monoculture, will depend on careful consideration of genetic compatibility, environmental conditions, and crop management practices. Future research should aim to further elucidate the genetic basis of plant avoidance and competition, providing a more nuanced understanding of plant behavior that can inform the development of more resilient and productive agricultural systems.

Reference

1. Liu, S., Barrow, C. S., Hanlon, M., Lynch, J. P. & Bucksch, A. DIRT/3D: 3D root phenotyping for field-grown maize (Zea mays). *Plant Physiology* **187**, 739–757 (2021).

- 2. Rangarajan, H., Postma, J. A. & Lynch, J. P. Co-optimization of axial root phenotypes for nitrogen and phosphorus acquisition in common bean. *Ann. Bot.* **122**, 485–499 (2018).
- 3. Vandermeer, J. H. *The Ecology of Intercropping*. (Cambridge University Press, 1992).
- 4. Brooker, R. W. *et al.* Improving intercropping: a synthesis of research in agronomy, plant physiology and ecology. *New Phytol.* **206**, 107–117 (2015).
- 5. Dudley, S. A. & File, A. L. Kin recognition in an annual plant. *Biol. Lett.* **3**, 435–438 (2007).
- 6. Murphy, G. P. & Dudley, S. A. Kin recognition: Competition and cooperation in Impatiens (*Balsaminaceae*). *Am. J. Bot.* **96**, 1990–1996 (2009).

Figures

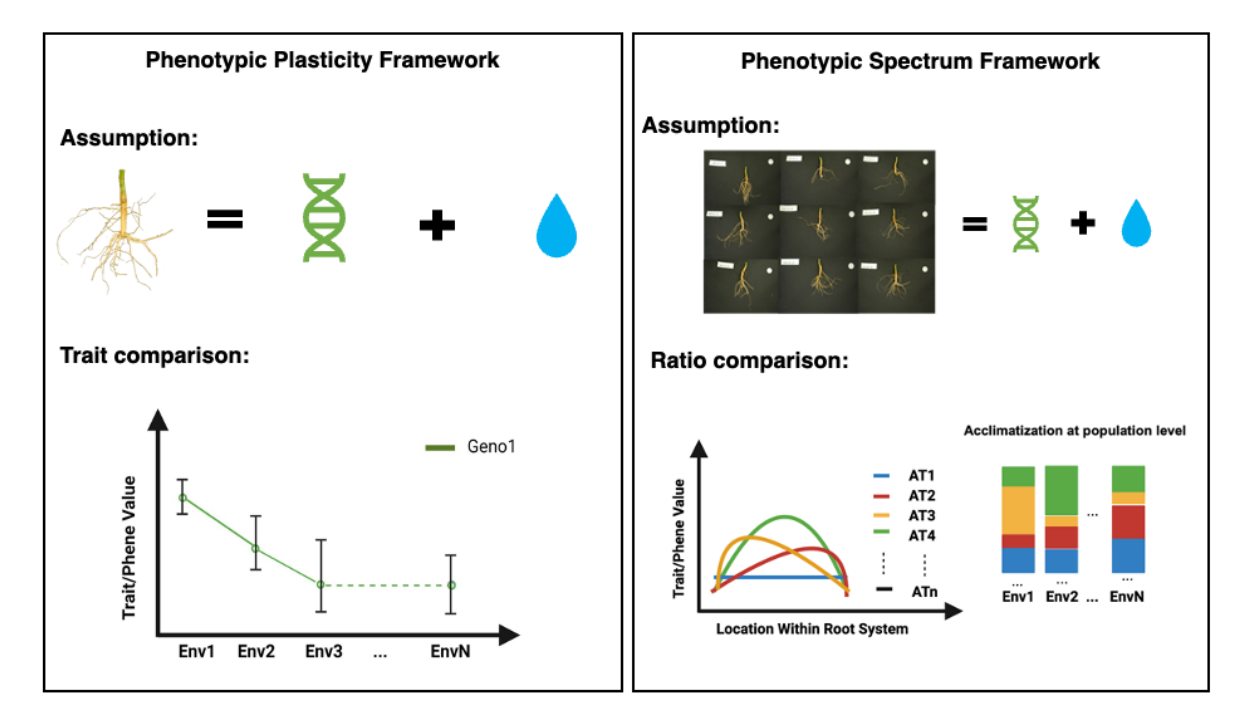


Figure 5.1: The comparison of phenotypic plasticity framework and phenotypic spectrum framework. The phenotypic plasticity framework assume that a single genotype has a common root architecture (or ideotype) in a given environment. By measuring the mean of a particular root trait across various environments with significant differences indicating the genotype exhibits phenotypic plasticity. The phenotypic spectrum framework assumes a single genotype can express a finite number of root architecture types within the same environmental context, by examining the ratios of distinct root architecture types within a genotype, a significant shift in these ratios across different environments is interpreted as the genotype's acclimatation strategy to environmental changes.

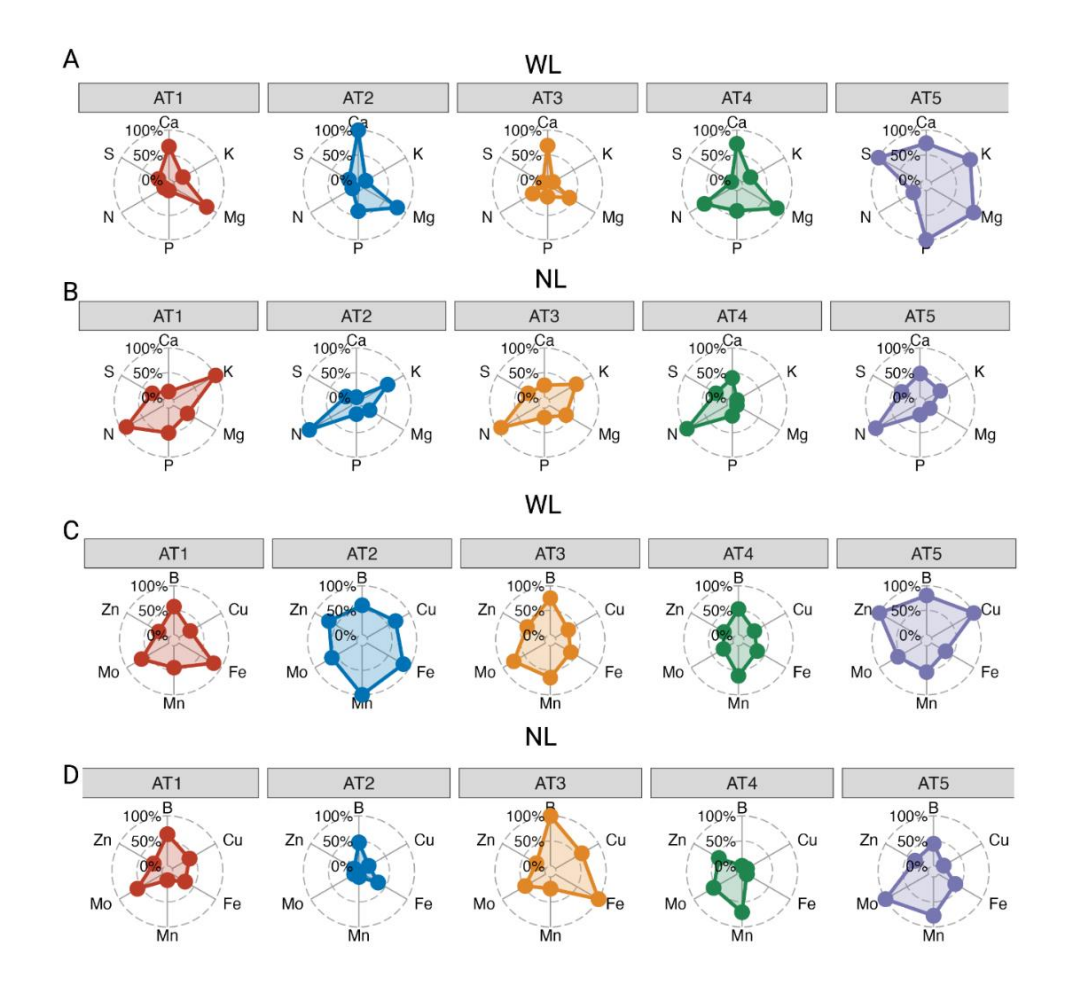


Figure 5.2: Radar plots illustrating the different patterns of both macronutrients and micronutrients in seeds among root architecture types of SEQ7 under water-limited (WL) and non-limiting (NL) conditions. In each plot, the dots indicate average normalized values, scaled from 0 to 100%. Panels (A, B) represent the patterns for macronutrients (Calcium, Ca; Sulfur, S; Nitrogen, N; Phosphorus, P; Magnesium, Mg; Potassium, K), whereas panels (C, D) represent the patterns for micronutrients (Boron, B; Copper, Cu; Iron, Fe; Manganese, Mn; Molybdenum, Mo; Zinc, Zn) under WL and NL conditions, respectively.

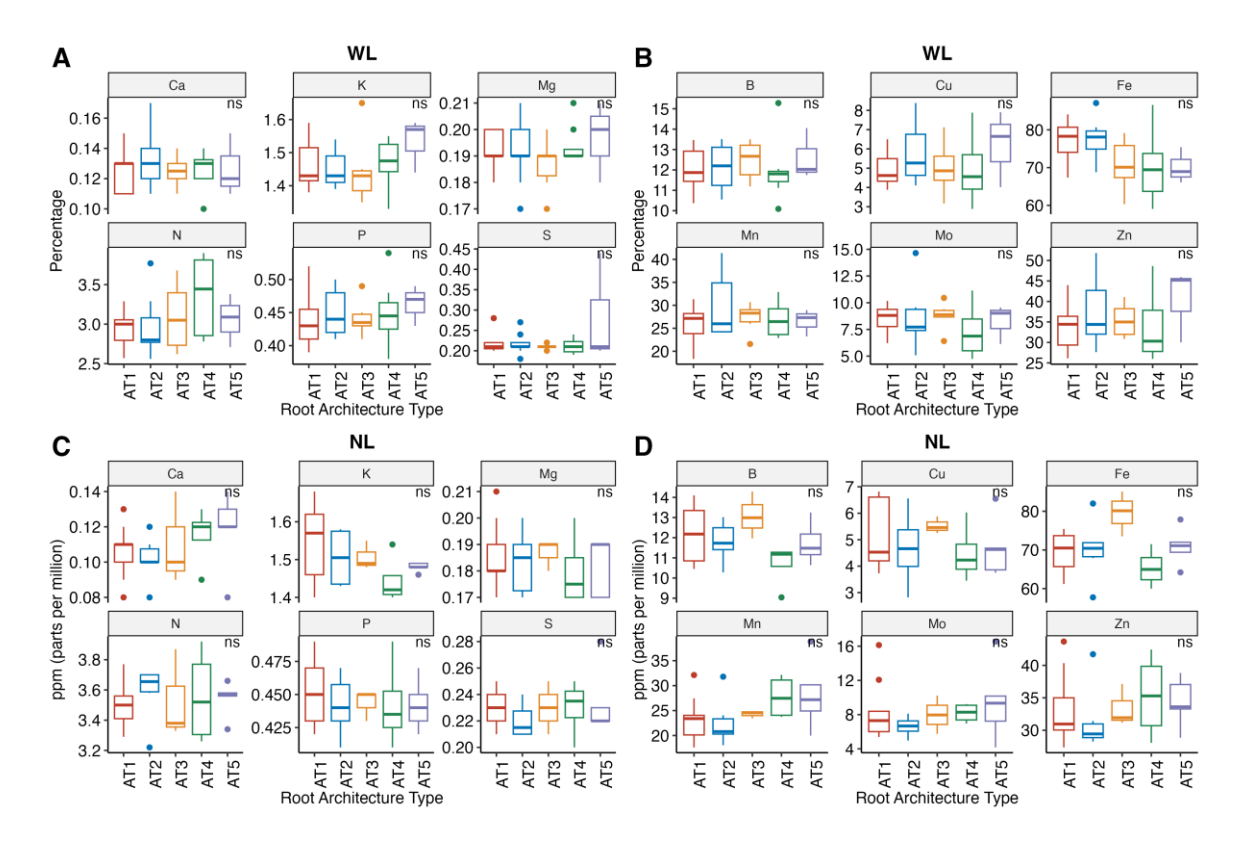


Figure 5.3: Boxplot of both macronutrients and micronutrients in seeds among root architecture types (ATs) of SEQ7 under water-limited (WL) and non-limiting (NL) conditions. Panels (A, C) show comparison of macronutrients (Calcium, Ca; Sulfur, S; Nitrogen, N; Phosphorus, P; Magnesium, Mg; Potassium, K), whereas panels (B, D) show the patterns for micronutrients (Boron, B; Copper, Cu; Iron, Fe; Manganese, Mn; Molybdenum, Mo; Chlorine, Cl) among root architecture types under WL and NL conditions, respectively. We applied Kruskal-Wallis's test to identify any significant differences in these nutrients among ATs. Different letters label ATs with significant differences, with significance threshold set as P < 0.05. The notation ns refers not significant. Sample sizes for WL conditions were: AT1 (n=7), AT2 (n=9), AT3 (n=3), AT4 (n=7), AT5 (n=3). For NL conditions, they were: AT1 (n=8), AT2 (n=6), AT3 (n=4), AT4 (n=6), AT5 (n=4).